

LIQUID POOL GEOMETRY AND LIQUID MIXING IN  
THE CONTINUOUS CASTING OF STEEL

by

STEWART K. MORTON

A THESIS SUBMITTED IN PARTIAL FULFILMENT OF  
THE REQUIREMENTS FOR THE DEGREE OF  
MASTER OF APPLIED SCIENCE

in the Department  
of  
METALLURGY

We accept this thesis as conforming to the  
standard required from candidates for the  
degree of MASTER OF APPLIED SCIENCE

THE UNIVERSITY OF BRITISH COLUMBIA

May, 1971

In presenting this thesis in partial fulfilment of the requirements for an advanced degree at the University of British Columbia, I agree that the Library shall make it freely available for reference and study.

I further agree that permission for extensive copying of this thesis for scholarly purposes may be granted by the Head of my Department or by his representatives. It is understood that copying or publication of this thesis for financial gain shall not be allowed without my written permission.

Department of Metallurgy

The University of British Columbia  
Vancouver 8, Canada

Date July 8, 1971

## ABSTRACT

Observations have been made of the liquid pool depth and profile in the continuous casting of steel at the Western Canada Steel Co. and at the Premier Works of the Steel Company of Canada. This was done by two techniques. In the first, radioactive gold was added to the mold during a normal casting, and subsequently determining the distribution of gold in the casting by autoradiography. In the second method, tungsten pellets containing a small  $^{60}\text{Co}$  wire were dropped into the steel during ~~the~~ casting in order to obtain direct measurements of the pool depth. The results of the pool profiles and liquid flow patterns as a function of casting conditions will be presented and compared to theoretical predictions based on heat flow considerations.

## TABLE OF CONTENTS

ABSTRACT .....	ii
TABLE OF CONTENTS .....	iii
ACKNOWLEDGEMENT .....	vii
1. Introduction .....	1
1.1. General comments .....	1
1.2. Previous work .....	5
1.2.1. Heat transfer - experimental .....	5
1.2.2. Heat transfer - theoretical .....	7
1.2.2.1. Hills model - analytical solution .....	8
1.2.2.2. Mizikar model - numerical solution .....	11
1.2.3. Fluid flow and liquid mixing - theoretical ..	14
1.2.4. Fluid flow and the liquid pool - experimental	16
1.2.5. Objectives of present work .....	18
2. Methods .....	20
2.1. Continuous casting operation .....	20
2.2. Radioactive tracer techniques .....	23
3. Observations .....	30
3.1. Radioactive tracer experiments .....	30
3.1.1. General comments .....	30
3.1.2. Experiment #1 .....	33
3.1.2.1. Pool profile .....	33
3.1.2.2. Liquid mixing .....	36
3.1.2.3. Structure .....	36
3.1.3. Experiment #2 .....	39

3.1.3.1. Pool profile .....	39
3.1.3.2. Liquid mixing .....	42
3.1.3.3. Structure .....	42
3.1.4. Experiment #3 .....	46
3.1.4.1. General comments .....	46
3.1.4.2. Pool profile .....	46
3.1.4.3. Structure .....	54
3.1.5. Experiments #4, 5 .....	56
3.1.5.1. Pool depths .....	56
3.1.6. Experiment #6 .....	56
3.1.6.1. General comments .....	56
3.1.6.2. Pool profile and depth .....	57
3.1.7. Experiment #7 .....	59
3.1.7.1. General comments .....	59
3.1.7.2. Pool profile and depth .....	59
3.1.8. Experiment #8 (Stelco) .....	66
3.1.8.1. General comments .....	66
3.1.8.2. Pool profile .....	67
3.1.8.3. Structure .....	71
3.1.9. Experiment #9 .....	79
3.1.9.1. General comments .....	80
3.1.9.2. Pool profile .....	80
3.1.10. Experiment #10 .....	84
3.1.10.1 General comments .....	84
3.1.10.2. Pool depths .....	84

3.1.11.	Experiment #11 .....	85
3.1.11.1.	General comments .....	85
3.1.11.2.	Pool profile .....	85
3.1.11.3.	Structure .....	87
3.2.	Comparison of theoretical and experimental liquid pool profiles .....	87
4.	Discussion .....	93
4.1.	Pool depths .....	93
4.1.1.	From Au <sup>198</sup> profiles .....	93
4.1.2.	From tungsten pellets .....	94
4.2.	Pool geometry .....	95
4.2.1.	Inside the mold .....	95
4.2.1.1.	In the centre pool .....	95
4.2.1.2.	In the north pool .....	96
4.2.2.	Below the mold .....	97
4.2.3.	Fluctuations in wall thickness .....	98
4.2.4.	Web depth .....	99
4.3.	Liquid mixing .....	101
4.3.1.	Between pools in the Weybridge mold .....	101
4.3.2.	In the north pool .....	101
4.3.3.	In the centre pool .....	102
4.3.4.	Comparison of theoretical and experimental tracer concentration profiles .....	106
4.4.	Structure .....	111
4.4.1.	Columnar zone .....	111
4.4.1.1.	Weybridge mold .....	111

4.4.1.2. Single strand mold (Stelco) .....	111
4.4.2. Equiaxed zone .....	113
4.4.2.1. Weybridge mold .....	113
4.4.2.2. Single strand mold (Stelco) .....	113
4.4.3. Origin of equiaxed zone .....	113
4.4.4. V-segregation pattern .....	115
4.4.5. Porosity .....	115
4.4.6. Cracking .....	116
4.5. Theoretical and Experimental Pool Profiles .....	116
SUGGESTED FUTURE WORK .....	117
REFERENCES .....	118

ACKNOWLEDGEMENT

I would like to thank my research director, Dr. Fred Weinberg, for his assistance and guidance throughout the course of this work. I would also like to thank Dr. Keith Brimacombe for his work on heat transfer and for his assistance in carrying out the experiments.

The interest and cooperation of Western Canada Steel Limited and the Steel Company of Canada is gratefully acknowledged.

## 1. Introduction

### 1.1. General Comments.

The continuous casting process is used industrially on a large scale in the production of a wide range of steels, including carbon, low alloy, and stainless steels. The reasons for the increasing use of the process are both economic and metallurgical. Economically it is advantageous to cast the hot metal directly into a semi-finished product such as slabs, billets, blooms or rounds for use in subsequent hot rolling or forging operations. This results in a greater yield, lower unit labour cost, high production rate, and the elimination of several steps in reduction. In addition, the process is flexible and is capable of producing various sizes of sections for different products. Metallurgically, the process has both advantages and disadvantages. In general, better quality billets are produced by continuous casting than by static casting since the higher cooling rates used in continuous casting produce a more homogeneous, fine-grained billet, which is relatively free of porosity. However, special problems are encountered that have not been entirely eliminated.

The casting techniques produce unique conditions of fluid flow and solidification that yield a casting with its own characteristic structure and segregation. The amount of segregation varies from one casting machine to another and from one heat to another. The macro- and micro-segregation leads to interdendritic cracking which occasionally results in liquid metal breakouts or causes internal or external flaws in the billet. The dendritic structure and segregation also cause centreline porosity, generally present to some extent in continuously cast steel.

Another defect in continuously cast steel is the presence of non-metallic inclusions. These inclusions come from four sources. A certain amount comes from slag retained in the metal from the furnace refining operations. Erosion of refractories used in holding vessel linings and nozzles contribute a significant amount. Re-oxidation of the metal as it is poured into the mold produces still more of the non-metallics. Finally, the products of deoxidants added in the mold, such as aluminum, are retained as inclusions.

The casting operation is difficult to carry out at maximum efficiency. To be most economic, high production rates are desirable and therefore high casting speeds should be used. However, the maximum casting speeds attainable in practice are much below the theoretical maximum, based on the strength of the solid shell holding the liquid in the pool in the centre. If rates are increased, the frequency of liquid metal breakouts in-

creases rapidly, keeping the highest practical speeds to about one-half of the theoretical limit. Even on casting machines operating at relatively low speeds breakouts and bulges of the strand still occur occasionally. An example, from Western Canada Steel, of a bulge and breakout occurring simultaneously is shown in Fig. (1).

The limitation on casting speed also limits the size of heats that can be poured, since there is no further heating of the steel after it is tapped from the furnace. In general, the upper limit of pouring time is one hour, after which the temperature of the steel has dropped to too low a value to be cast properly. This limits the size of heat that can be used for a given number and size of billets cast simultaneously. Initially, small heats of 20 to 30 tons were poured to produce small billets suitable for subsequent forming operations. Now large blooms ( up to 12" x 12" ) and slabs ( up to 7" x 48" ) are cast from 200 ton heats for a range of mild and high quality steels and a wide range of shapes.

Research in continuous casting was aimed at improving the operational efficiency of the process and the quality of the product. This work has been directed primarily towards three areas: (1) the development of mathematical heat transfer models, (2) an analysis of the solidification processes and the structures of the billets, and (3) a study of the geometry of the liquid pool in the billet and the extent and pattern of fluid flow in the pool. The results of these investigations are summarized below.

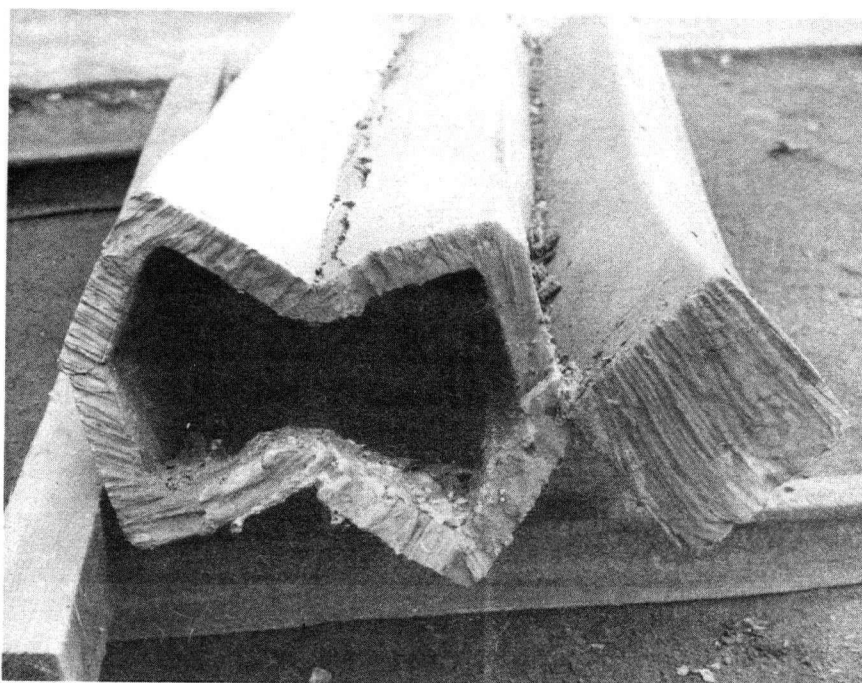


Fig. (1). Bulge in centre and outside strand  
at Western Canada Steel.

## 1.2. Previous work.

### 1.2.1. Heat Transfer - Experimental.

Heat transfer in continuous casting molds was first investigated by Krainer and Tarmann<sup>1</sup>. They recognized that the critical factor controlling the rate of thickening of the steel shell adjacent to the mold was the heat transfer across the metal-mold interface. The heat transfer coefficient across this interface is not known since the nature of the contact between the strand and the mold is uncertain. Also, the heat transfer coefficient is not constant along the length of the mold because of the contraction of the steel as it cools. In order to estimate the heat transfer across the interface at various positions in the mold, Krainer and Tarmann<sup>1</sup> embedded thermocouples in an operating continuous casting mold and monitored the temperature of the mold walls during casting. From this data they calculated the heat flux at different levels in the mold and were then able to estimate the heat transfer coefficient across the interface. They found that the coefficient was a maximum near the top of the mold at  $300 \text{ Btu./ft.}^2\text{hr.}^\circ\text{F.}$  The coefficient decreased steadily from the top to the bottom of the mold, reaching a value of  $150 \text{ Btu./ft.}^2\text{hr.}^\circ\text{F.}$  at the bottom.

Savage and Pritchard<sup>2</sup> used a different technique to measure the heat flow and obtained essentially the same results as Krainer and Tarmann.<sup>1</sup> They filled a continuous casting mold with

steel and allowed it to solidify statically. The rate of heat removed by the mold cooling water was determined as a function of time from measurements of the flow rate and temperature rise of the water. This rate was then considered to be equivalent to the case where the mold is oscillated and the casting is continuously withdrawn. The initial rate of heat removal measured for the static casting is equated to the heat removal at the meniscus level of the continuous casting. As the static casting cools, it contracts and separates from the mold in an analogous manner to the steel shell in the continuous cast progressively further along the mold. Therefore, the time elapsed after pouring in the static case is equivalent to mold length divided by the casting rate in continuous casting for the same mold.

$$t = \frac{L}{v}$$

where L = effective mold length

v = casting rate

t = time.

The experimental results for the static mold give a rate of heat transfer between the billet and the mold as a function of time, or, equivalently, of the distance below the meniscus. The rates found by Savage and Pritchard<sup>2</sup> are almost identical to those of Krainer and Tarmann<sup>1</sup>.

### 1.2.2. Heat Transfer - Theoretical.

The objective of a mathematical model of heat transfer in continuous casting is to relate mathematically the process variables, and to predict quantitatively the solidification rates and temperature profiles in a continuous casting operation. The mathematical models of heat transfer in the mold differ in their approach to the billet - mold interface and in their estimates of temperature gradients in the steel shell. The solutions to the heat transfer equations are either analytical (Savage,<sup>3</sup> Hills,<sup>4</sup> Pehlke,<sup>5</sup> Fahidy<sup>6</sup>) or numerical (Mizikar,<sup>7</sup> Donaldson and Hess,<sup>8</sup> Gautier et al.<sup>9</sup>). The analytical solutions, in general, require that certain properties such as thermal conductivity and specific heat remain constant in order to make the equations soluble. The numerical solutions, such as Mizikar's<sup>7</sup>, do not require this, but at some point in the analysis they must use experimental data obtained on a casting machine, and this imposes limitations on the usefulness of the results. Mizikar,<sup>7</sup> for example, obtains the heat transfer rates in the mold from the data of Krainer and Tarmann<sup>1</sup> and Savage and Pritchard.<sup>2</sup>

The thermal resistances to heat flow to be considered in the theory are: (i) the solid steel shell. (ii) the billet - mold interface. (iii) the mold walls. (iv) the mold wall - cooling water interface. Considering these factors plus the geometry and the temperatures involved, the difficulty in solving the problem becomes clear. The billet - mold interface is the

largest thermal resistance and controls the rate of heat extraction, but the nature of this interface is unknown. The billet and mold walls are constantly moving relative to each other, separated by a layer of rapeseed oil that burns and produces gases. In addition, there is a gap between the billet and the mold wall due to volume shrinkage on cooling, and it will be irregular because of surface irregularities on the mold and temperature variations. A further complication in the problem is that the temperature gradients in the steel shell and the liquid pool are not known and the thermophysical properties of the steel at these temperatures have not been accurately determined.

#### 1.2.2.1. Hills Model - Analytical Solution.

This model is confined to the region of the billet inside the mold. As discussed above, the problem in describing the heat flow in a continuous casting mold is in determining the nature of the billet - mold interface and the temperature gradients in the steel shell. Hills<sup>4</sup> simplifies the problem of the interface by using an effective heat transfer coefficient for heat flow from the billet surface to the mold cooling water. This coefficient is assumed to remain constant in the mold. Hills<sup>4</sup> develops equations which allow this heat transfer coefficient to be determined from the quantity of heat removed in the mold cooling water, and this is easily measured. However, the whole analysis depends on the validity of the assumption of a constant heat trans-

fer coefficient and Hills<sup>4</sup> justifies this by citing the results of Krainer and Tarmann<sup>1</sup> and Savage and Pritchard<sup>2</sup> which indicated that this coefficient did not vary much. In some heat transfer models there is considered to be a zone of intimate contact and a zone of separation between the billet and mold (eg. Gautier et al<sup>3</sup>), but in the view of this author the existence of a lubricant layer between the steel and mold and surface irregularities suggest that contact is intermittent throughout the mold and Hills'<sup>4</sup> assumption may be closer to reality. In any case, the value obtained for the effective heat transfer coefficient from Hills'<sup>4</sup> equations was found to be a good average of the values estimated by Krainer and Tarmann<sup>1</sup> and Savage and Pritchard<sup>2</sup>. Krainer and Tarmann<sup>1</sup> found the coefficient a maximum near the top and decreasing to about half this value towards the bottom of the mold.

For the temperature gradient in the solid steel shell, Hills uses the following equation:

$$\frac{\theta}{\theta_s} = a_0 + a_1 \left( \frac{y}{t} \right) + a_2 \left( \frac{y}{t} \right)^2 + a_3 \left( \frac{y}{t} \right)^3$$

where  $\theta$  = temperature

$\theta_s$  = "solidification temperature" (peritectic)

$a_0, a_1, \text{ etc.}$  = coefficients, which are a fcn. of distance

below meniscus

$y$  = distance perpendicular to mold face

$t$  = shell thickness.

This equation is solved for the coefficients by applying the boundary conditions and heat balance on a volume element of the shell. It should be noted that since the coefficients are functions of this vertical distance only, the temperature gradient in the shell can change as the steel moves down through the mold.

The assumptions Hills<sup>4</sup> must use to solve the heat balance are:

- (i) the effective heat transfer coefficient is constant in the mold.
- (ii) the thermophysical properties of the steel are constant (  $k$  ,  $C$  ,  $\rho$  ).
- (iii) reciprocation of the mold has no effect.
- (iv) casting speed is constant.
- (v) conduction of heat through the solid shell is significant only in the direction normal to the mold walls.

Then, having the temperature gradient and the effective heat transfer coefficient, Hills<sup>4</sup> solves the heat balance to give the following result:

$$t = (5.8 \times 10^{-6}) \left( \frac{\bar{q}}{q} \right)^{0.67} \frac{\chi^{0.08} x^{0.75}}{u^{0.83}}$$

where  $t$  = shell thickness (in.)

$\bar{q}$  = average heat flux through the mold to the cooling water (Btu./ft.<sup>2</sup>hr.).

$X$  = effective mold length (distance from meniscus to mold bottom) (ft.)

$x$  = distance below meniscus (ft.)

$u$  = casting speed (ft./hr.)

Therefore, to determine the profile of the solid steel shell in the mold, all one is required to know is the cooling water flow rate and temperature rise, the mold dimensions, and the casting speed.

#### 1.2.2.2. Mizikar model - Numerical Solution.

Mizikar<sup>7</sup> has developed a heat transfer model that applies to the entire solidification process. He divides the ~~billet~~<sup>cooling</sup> into three regions having different cooling rates, the region in the mold, the secondary cooling zone, and the radiant cooling zone. The control volume used allows the different conditions of heat transfer to be considered by changing the boundary conditions at the billet surface. In Hills'<sup>4</sup> model, the control volume was a section of the solid shell that was stationary with respect to the mold. In Mizikar's<sup>7</sup> model, this control volume is a slab extending from the outside of the billet to the centreline, and fixed with respect to the strand. The slab is divided into a series of slices, each one represented by a point at its centre ( a "node"). The heat transfer equations

for each slice are set up and the boundary conditions for the cooling zone concerned (ie. mold, secondary, or radiant cooling zone) are applied. At this point, it was necessary for Mizikar<sup>7</sup> to use the data of Krainer and Tarmann<sup>1</sup> and Savage and Pritchard<sup>2</sup> to describe the surface boundary conditions in the mold. This data gives the rate of heat removal in the mold as a function of distance below the meniscus. The heat balance is then solved by a series of iterations on the slices of the control volume as it moves down from the meniscus of the liquid metal. The solution obtained for the mold region is

$$d = 0.86\sqrt{t} - 0.03$$

where  $d$  = shell thickness (in.)

$t$  = time (min.)

$$\text{ie. } t = \frac{\text{distance below meniscus}}{\text{casting speed}}$$

The assumptions that were necessary to obtain the solution are:

- (i) heat transfer in the solid shell is significant only in the direction normal to the mold walls.
- (ii) the latent heat of fusion is accounted for by adjusting the specific heat over the solidification range.
- (iii) convective heat transfer in the liquid is accounted for by adjusting the thermal conductivity of the liquid metal.

This model offers the advantages of allowing for a variable heat

transfer coefficient between the billet and mold down the length of the mold and also a variable thermal conductivity, but it depends on specific data obtained from a particular mold for its solution. For example, the model may not be applicable if the cooling rate or lubricating practice for a given mold is changed since this would change the heat transfer coefficient.

In essentially the same way as Mizikar,<sup>7</sup> Donaldson and Hess<sup>8</sup> use measured heat flow rates in their analysis, but in this case they are applied to a mold that is considered to have two zones: one of good thermal contact and one of separation. The point at which separation occurs is calculated by the method proposed by Savage,<sup>3</sup> which requires that the modulus of elasticity of the steel be known at temperatures up to the melting point. It seems that at best this can be no more than a rough estimate and adds just one more uncertainty to the problem.

Gautier et al<sup>9</sup> also consider a two-zone mold, but they calculate the point of separation by another method. The heat flow equations in each zone are solved and the results compared to the measured heat removal by the mold cooling water. The zone of contact is then varied until the measured and calculated values correspond. This imposes a fixed set of casting conditions on the model and also requires the assumption of values for the heat transfer coefficients between the billet and mold. The model is therefore not strictly applicable to any casting operations other than the one

for which it was developed.

### 1.2.3. Fluid Flow and Liquid Mixing - Theoretical.

The only theoretical analysis of fluid flow and mixing in the liquid pool of a continuously cast strand was carried out by Szekely and Stanek.<sup>10</sup> They considered, in an idealized model, two of the techniques that may be used to determine the liquid flow patterns.

The first of these methods was the examination of the profiles of the solidus and liquidus ~~lines~~<sup>isotherms</sup> in the steel shell. This was done to determine if different conditions of fluid flow can produce significantly different profiles which may then be useful in estimating the flow patterns. The approach used was to calculate the profiles of the solidus and liquidus ~~lines~~<sup>isotherms</sup> using Mizikar's model of heat transfer, modified to allow for varying conditions of flow. Three conditions of liquid mixing were considered. (i) A high effective thermal conductivity of the liquid was assumed to take into account convective heat transfer due to fluid flow in the liquid. This follows the procedure used by Mizikar. (ii) Complete lateral mixing in the liquid. In this case the liquid has a zero lateral temperature gradient and the temperature is calculated from a heat balance. This is then applied to the heat transfer model. (iii) Potential flow. This flow pattern was allowed for in the heat transfer model by the addition of an appropriate convective heat transfer term.

The solidus and liquidus profiles for the three conditions of flow were calculated and compared and were found to be very similar, indicating that they are independent of the conditions of flow in the pool. Therefore it was concluded that the solid shell profiles are not useful in predicting the flow patterns in the liquid.

The second technique considered for determination of flow patterns was the addition of radioactive tracers to the pool. When a tracer material is added to the liquid metal and dissolved, its dispersion in the pool will be greatly influenced by the conditions of flow in the pool. Szekely and Stanek<sup>10</sup> derived expressions to predict the distribution of tracers in the steel under three idealized conditions of flow. These three conditions were: (i) complete mixing in the liquid. (ii) potential flow. (iii) eddy diffusion. These will be considered in turn.

(i) complete mixing.

For the case of complete mixing it was assumed that the tracer was added during a time interval  $\Delta t$  into the input stream. For this case Szekely and Stanek<sup>10</sup> derived equations which described the dispersion of the tracer in the liquid pool. Solutions of the equations give concentration profiles in the solidified billet showing both the liquid pool profile and the tracer concentration profiles at various positions in the cast billet.

(ii) potential flow.

Assuming potential flow in the liquid, the initial liquid region containing the tracer could be separated from an adjacent liquid region. In this case the interface outlined is not that of the solid-liquid interface obtained if the entire liquid pool was completely mixed. The calculations were based on an addition from the inlet stream which maintained the concentration of the stream at a fixed level over an interval of time.

(iii) eddy diffusion.

This model was used to predict the dispersion of a tracer under conditions of turbulent flow in the pool. The flow was described by an eddy diffusivity which was evaluated using Mizikar's<sup>7</sup> analysis. Tracer profiles in the final cast billet were calculated and plotted. The profiles were found to be very sensitive to the point of addition of the tracer material. Three different points of addition were tried in the calculations and gave three quite different profiles.

From the results of the three idealized models of flow and liquid mixing, Szekely and Stanek<sup>10</sup> conclude that radioactive tracers may provide a good method of determining the nature of the flow in the liquid pool.

1.2.4. Fluid Flow and the Liquid Pool - Experimental.

<sup>11</sup>  
Kohn has done a series of experiments to determine the shape and depth of the liquid pool using radioactive tracers. This was done by two techniques. In the first method he measured the pool

depth by dropping radioactive  $W^{184}$  pellets in the pool. The tungsten is 2.45 times the density of liquid steel and is only slightly soluble, so the pellet falls rapidly to the bottom of the pool. The final position of the pellet relative to the position of the meniscus at the time the pellet was dropped was determined by autoradiography, and the distance between the meniscus and the tungsten pellet indicated the pool depth. An alternative method to measure the pool depth was to drop lead shot in the pool and determine the distance between the meniscus and the farthest point reached by the lead as observed subsequently in the sectioned ingot. The results in this case were similar to those obtained with the tungsten pellets, but the lead was more difficult to locate unless it contained a dissolved tracer material. The pool depths determined by Kohn<sup>11</sup> using the tungsten and lead additions for billets 105 and 120 mm square (4.14 in. and 4.72 in. square) cast at from 1.75 to 2.28 m./min. (69 in./min. to 90 in./min.) were from 4.7 to 5.5 m. (15.5 ft. to 18 ft.). Increasing the casting speed by 25% from 1.83 to 2.28 m./min. produced an increase of only 14% (4.7 to 5.37m.) in the measured depth. The pool depth did not, therefore, increase in depth in direct proportion to the casting speed.

In a second tracer technique Kohn<sup>11</sup> added  $Au^{198}$  to the liquid pool. On addition, the gold dissolved and mixed in the liquid pool. By subsequently sectioning and autoradiographing sections of the ingot, Kohn<sup>11</sup> determined the distribution of  $Au^{198}$  in the billet. He found that the lower limit reached by the gold coincided with the

position of the tungsten pellet at the bottom of the pool. His observations of the distribution of gold in the liquid pool suggested the flow pattern of the liquid in the pool shown in Fig. (2).

Varga and Fodor,<sup>12</sup> in Hungary, have carried out experiments similar to those reported by Kohn,<sup>11</sup> but they used P<sup>32</sup> instead of Au<sup>198</sup>. They obtained pool depths of 12 ft. using tungsten pellets which contained a small Co<sup>60</sup> wire as markers of the bottom of the pool.

Gautier et al.<sup>9</sup> have continued the observations of Kohn,<sup>11</sup> adding Au<sup>198</sup> and W<sup>184</sup> to the liquid pool. Their results were generally similar to those reported by Kohn,<sup>11</sup> but with a slightly larger pool depth. For 105 mm. square billets cast at 1.83 m./min. they observed pool depths of 6.7 m. (20 ft.).

#### 1.2.5 Objectives of Present Work.

The purpose of the present investigation is to determine the liquid pool depths and profiles, fluid flow, and cast structure of continuously cast steel. This will be done in a commercial plant under normal operating conditions, as a function of the operating parameters. Observations will be made using radioactive tracer techniques. The results will be compared to those predicted by the theoretical analyses of wall thickness and fluid flow in the models discussed previously.

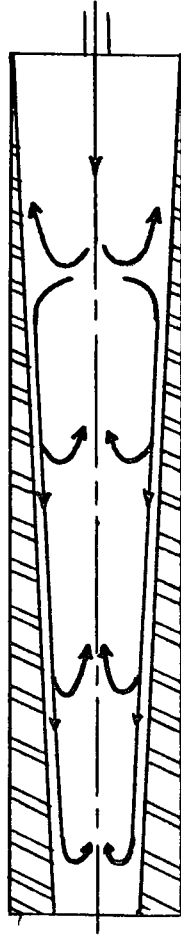


Fig. (2). Schematic diagram of flow patterns in the liquid pool, as suggested by Kohn.<sup>11</sup>

## 2. Methods

### 2.1. Continuous casting operation.

A series of experiments have been carried out on the continuous casting machine at Western Canada Steel and one at the Premier Steel Works of the Steel Company of Canada. A schematic diagram of the Western Canada Steel casting machine, which is similar to the one at the Premier Works, is given in Fig. (3). The 40 ton ladle of steel (A) from the furnace is raised from the melt shop floor to the casting platform, 50 ft. above ground level. The ladle is positioned over the preheated tundish (B) which is situated over the mold. The steel is bottom poured from the ladle to the tundish and from the tundish to the mold, (c). The machine operator controls the withdrawal rate of the strand and the flow of metal to the mold. A second operator controls the flow from the ladle to the tundish.

A stopper rod in the tundish is used to throttle the flow of metal to the mold and it is used either fully open or closed, giving an intermittent stream of metal to the mold. The mold itself is made of a cast copper-chromium alloy and is water cooled. The

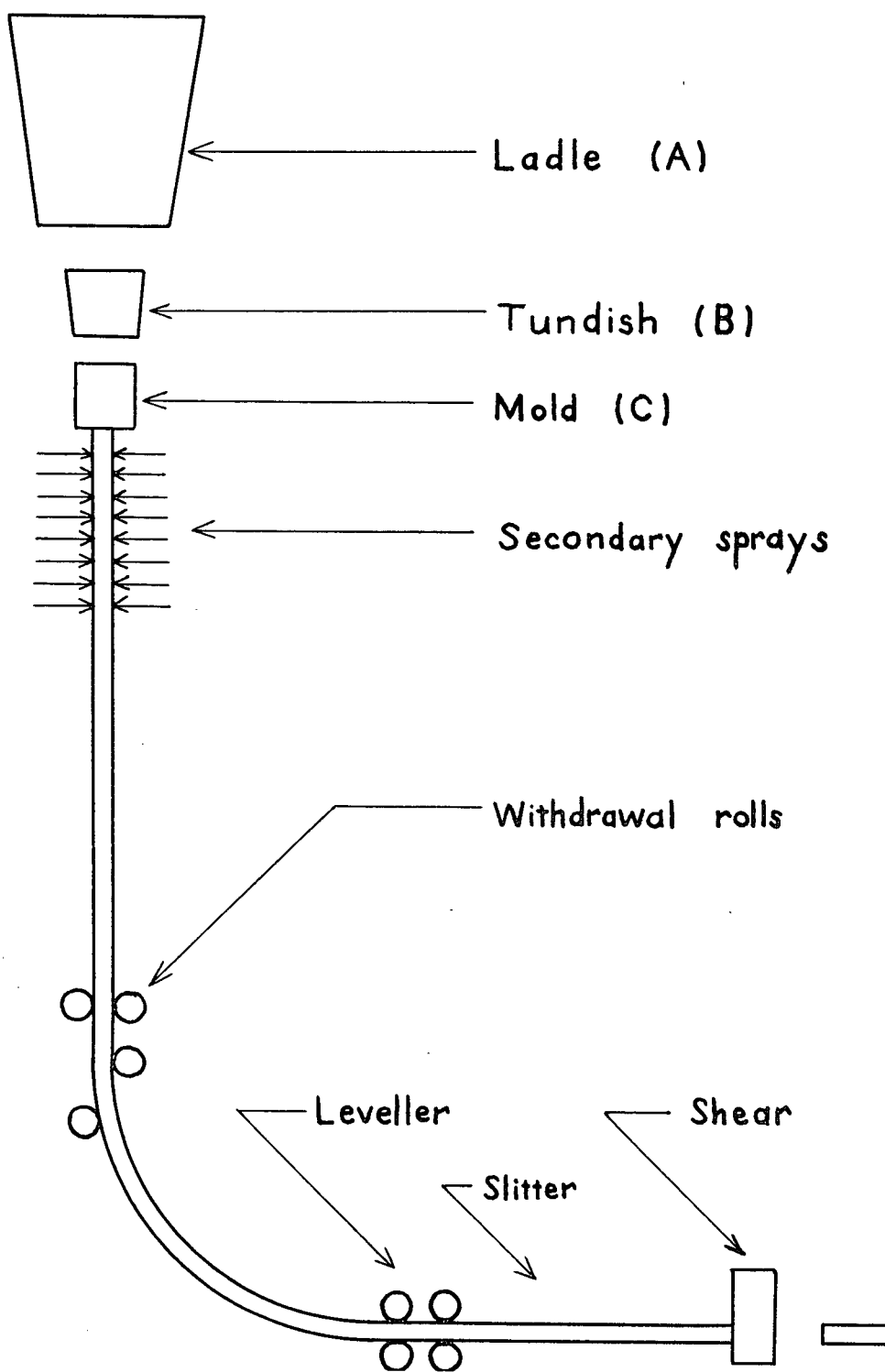


Fig. (3). Schematic diagram of the continuous casting machine at Western Canada Steel.

mold cooling water flows at a rate of approximately 1000 gal./min. The mold is of the Weybridge type and casts three billet sections simultaneously. Fig. (4) shows the cross sectional shape of the casting. The metal stream from the tundish enters the centre section and fills the two outer ones through the webs joining them. In the Western Canada Steel operation, the outside strands are termed the north and south strands and they will be referred to as such in this work.

During a cast, the mold is reciprocated through an amplitude of 1 in. moving both up and down at the same rate as the withdrawal rate of the billet. At the start of the casting of a heat, a dummy bar is inserted in the bottom of the mold and sealed with asbestos rope. As it is withdrawn, the dummy bar guides and supports the strand down as far as the withdrawal rolls which are located 30 ft. below the mold. When the withdrawal rolls grip the strand, the dummy bar is released and lowered out of the path of the billet.

As the steel emerges from the bottom of the mold, it moves directly into the spray chamber where it passes between banks of water sprays 12 ft. long. Following the spray chamber and withdrawal rolls, the strand is bent  $90^{\circ}$  through a radius of 21 ft. and levelled in a set of rolls at ground level. After levelling, the web joining the three sections is cut with acetylene torches, following which the strand is cut into lengths of from <sup>4</sup>~~2~~ to 14 ft., as required, by a mechanical shear. The entire casting process for

a 40 ton heat takes from 45 to 60 minutes to complete.

The Stelco casting operation is basically similar to the procedure used at Western Canada Steel except that a Weybridge mold is not used. In its place, a square sectioned copper mold is used which casts a single strand up to 6" in section. In the Stelco plant two strands are cast simultaneously from one tundish using two separate molds and two operators controlling the stream into each mold. The casting machine, as at Western Canada Steel, is built in a tower. The molds are 60 ft. above ground level and the strands are bent through a large arc, levelled, and cut to length. The section sizes, casting speeds, and grades of steel produced are similar to those at Western Canada Steel; as a result, comparing billets from each machine should give a reasonable comparison of the single strand and Weybridge processes.

## 2.2. Radioactive tracer techniques.

In this investigation, two radioactive tracer techniques were used. In the first, a small amount of  $\text{Au}^{198}$  was added to the liquid pool to be dissolved and mixed in the liquid, to delineate fluid flow in the pool and the solid shell profile. The second technique was to drop a tungsten pellet containing a radioactive material into the liquid pool to act as a marker in determining the pool depth.  $\text{Au}^{198}$  was selected for dissolving in the steel for several reasons:

- (i) The vapour pressure of liquid gold is low. As a result, the

possibility of gold vapour contaminating the casting area and the people working in it was minimized. Experimentally, no evidence was found to indicate that any gold vapour was produced. (ii) The short half-life of gold (2.6 days) ensures that any contamination resulting from cutting and sectioning operations will rapidly disappear. Even though the half-life is short, the activity was sufficient to obtain autoradiographs of all sections in a reasonable time. The activity at the time of addition was 200 mc. in 2 gm. of gold. (iii) The segregation coefficient of Au in steel is 0.5. Therefore, the gold segregates in the same manner as most of the alloying elements present in the steel.

The Au<sup>198</sup> was added to the liquid steel in the mold by means of a steel rod (Fig. 5) containing a small piece of gold wire. In some cases, the gold was added in a single piece to either the north or centre pool; generally it was added to both pools simultaneously. When added to both pools, approximately 1.5 gm. of the Au was used for the centre pool and 0.5 gm. or less for the north pool. The  $\frac{1}{4}$  inch rod used to add the gold melts off rapidly (in less than 5 seconds), releasing the liquid gold in the steel. The billets containing the gold tracer are located at the shear with a geiger counter and are marked and set aside.

After the billets had cooled, they were sectioned transversely and longitudinally to the billet axis. The longitudinal sections were cut on the centreline and parallel to the faces. The sections were then machined flat for autoradiography.

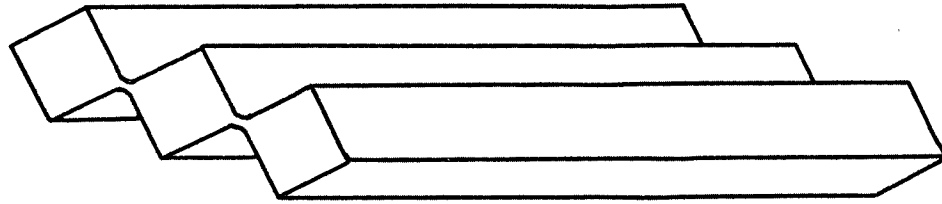


Fig. (4). Triple strand cast in the Weybridge mold at Western  
Canada Steel.

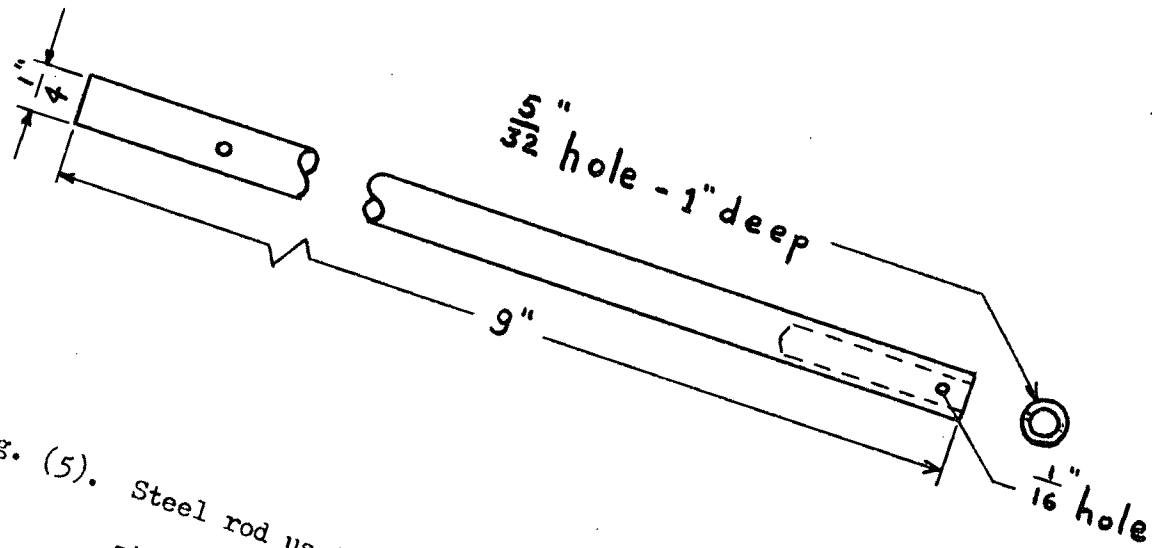


Fig. (5). Steel rod used to add  $Au^{198}$  tracer to the liquid  
steel in the mold.

Autoradiographs were made on two types of film. Ilford Ilfex x-ray film was used on all sections to show the general distribution of the tracer and the pool profiles. This is a coarse-grained double emulsion film that is fast and adequate for this purpose. Kodak Contrast Process Ortho film was used where higher resolution was required. This film is much slower than the x-ray film and requires about 10 times the exposure, but it has a fine-grained single emulsion that is able to resolve the details of the dendritic structure in the steel. Sections autoradiographed on this film were surface ground in order to show as much detail as possible.

The procedure used in making the autoradiographs on x-ray film is as follows. The film is placed on a piece of plate glass in a light tight box. The section to be autoradiographed is cleaned and placed on the film. The outline of the section is then made by briefly exposing the film around it to light. The steel and film are covered and left for the time of exposure, which may be from 15 min. to 1 week. After it is removed, the film is developed in Kodak developer D-19 or x-ray film developer. To make prints of these autoradiographs, the original films are first copied, and then these negatives are printed. The prints are then identical to the original autoradiographs, being dark in areas exposed by  $\text{Au}^{198}$  and light in areas not exposed.

The procedure used for the contrast process ortho film is similar, but the film is not exposed to outline the billet sections.

The second radioactive tracer technique used is similar to that of Varga and Fodor<sup>12</sup> and Kohn.<sup>11</sup> A small piece of  $\text{Co}^{60}$  wire, 1 mm. long and 1 mm. in diameter is placed in the centre of a  $\frac{1}{2}$  inch diameter,  $\frac{1}{2}$  inch long tungsten pellet which had been drilled out to accept the wire. The hole in the tungsten pellet is filled with a tungsten rod and sealed by heliarc welding.

The tungsten pellets are dropped into the liquid steel in the mold where they sink rapidly to the bottom of the pool. At the same time as the pellets are dropped, a 1 inch diameter steel bar is inserted in the corner of the mold and frozen into the steel shell. This marker is visible on the corner of the strand and marks the position of the meniscus at the time the pellets are added.

When the steel has cooled, the tungsten pellet can be located and the pool depth determined directly from the distance between the pellet and the marker. In most cases, the position of the pellet could be determined within one inch using only a hand monitor, but using a scintillation counter and a moveable slit mounted 8 inches from the steel, it can be located to within  $\frac{1}{2}$  cm., which is less than its own length. Fig. (6) shows a scan made of a billet section containing one of the pellets.

When the measurements are completed, the tungsten pellet is burned out of the steel with an acetylene torch and used over again. In the present observations the position of the pellet was observed in situ on a section perpendicular to the billet axis. In all cases, the

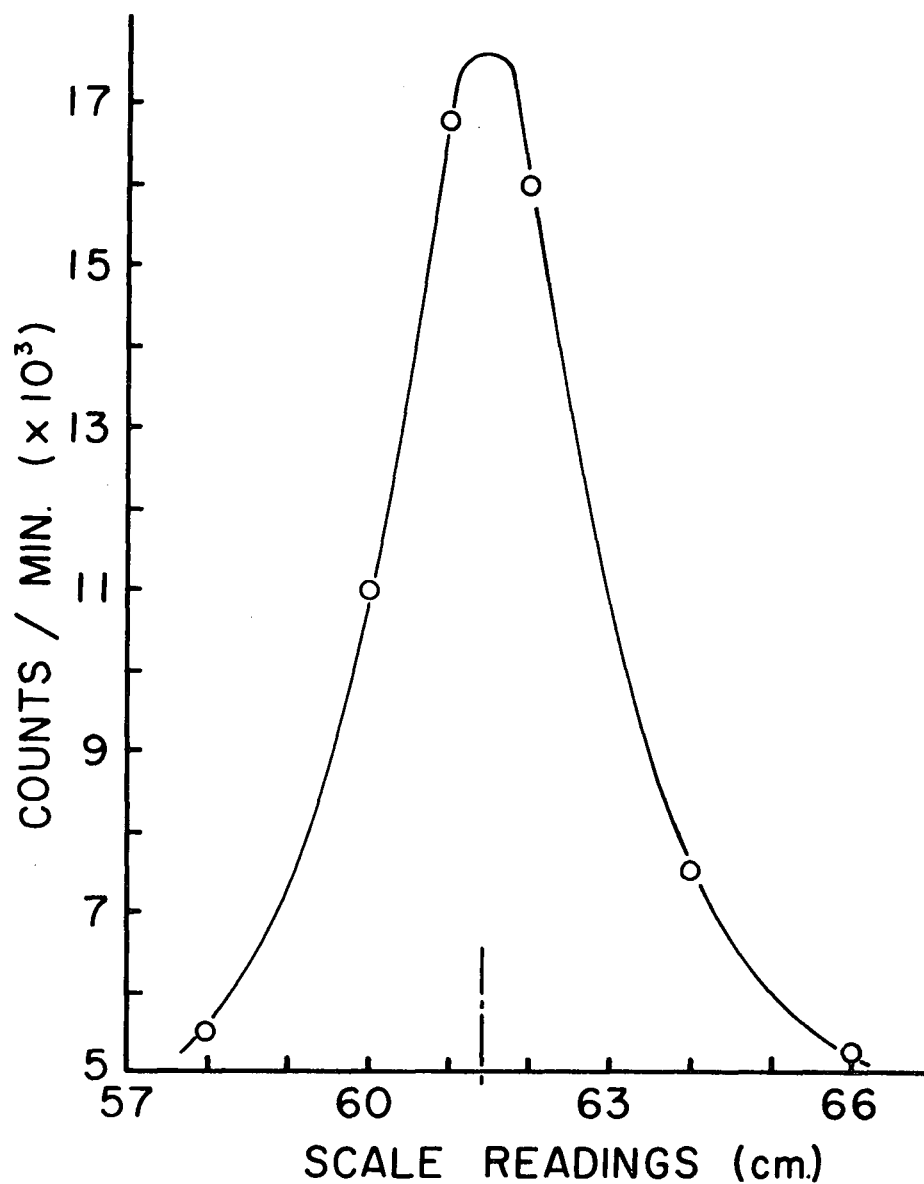


Fig. (6). Scintillation counter scan down a longitudinal section of a billet containing a tungsten pellet (and  $\text{Co}^{60}$  wire). Slit width =  $1/8$ ", detector mounted 8 in. from billet surface.

pellets were found on the centreline of the strand, indicating that the pellets had dropped to the bottom of the pool which was established to be coincident with the billet axis, and did not become attached to the pool sidewalls as it fell.

It was found that in the process of burning the pellets from the steel a certain amount of  $\text{Co}^{60}$  was lost. As a result, the last pellet made had the Co wire encased in a quartz capillary tube prior to being sealed in the tungsten. Using this technique, the loss of  $\text{Co}^{60}$  was greatly reduced.

The final position of the pellet at the bottom of the pool does not correspond to the position at which solidification is complete. The depth the pellet is able to fall is limited by the size of the pellet and the nature of the solid and the liquid at the bottom of the pool. Measurements obtained from the pellets are, however, useful in estimating the depths and the effects of changing the process variables on the depth.

In two of the experiments, billet sections that had been autoradiographed were scanned using a scintillation counter in order to show quantitatively the variation in  $\text{Au}^{198}$  concentration across the sections. This was done by mounting the detector of the counter behind lead bricks with a 1/16" slit located 8 inches from the steel surfaces. The sections were scanned transversely, with counts being made at 0.5 cm. intervals.

### 3. Observations

#### 3.1 Radioactive tracer experiments.

##### 3.1.1. General comments.

In the course of this work, eleven radioactive tracer experiments have been carried out. In the experiments at Western Canada Steel, Au<sup>198</sup> has been added to the north and centre pools separately to determine the influence of the incoming stream on fluid flow. Several experiments were done adding Au<sup>198</sup> to both pools simultaneously. It was found from the results of the separate additions that the addition to both pools was necessary to delineate the solid shell profile in the mold region.

Tungsten pellets were added to both the centre and north pools to determine the pool depths. This was done in one case for varying withdrawal rates to determine the effect of casting rate on the pool depth. Some of the experiments were done with the pellets alone, and in others the pellets were added simultaneously with the

Expt No.	(Au) Pool Depth		(W) Pool Depth		1st floor temp. °F	Centre pool temp. °F	North pool temp. °F	casting rate in/min	Δ T, mold water °F	mold water gal/min
	Centre	North	Centre	North						
1		30"						60		
2	7'				2920	2750	2742	60		
3	7'				2895	2720	2705	50	8.1	980
4			14'		2860	2725	2715	51	9.4	1030
5				13'	2885	2760	2750	60	7.4	960
6	3'			10'	2870	2720	2710	60	6.1	1040
7	3'		10'	9.5'	2880	2710	2710	60	6.6	1060
8					2880	2780		70	17	250
9			13'		2905	2750		65	5.8	1000
<del>10</del> 11					2885		2725	70	5.4	1000
<del>10</del>			5'		2770	2657		40	5.4	1120
			<del>14</del> 14.5					55	5.4	1120
			<del>14.5</del> 15.0					70	5.6	1120

Table 1. Casting data and pool depths.

Expt	C	Mn	P	S	Cu	Ni	Cr	Si	Mo	V	Sn
1	0.27	0.58	0.018	0.035	0.29	0.15	0.10	0.07	0.022	-	-
2	0.13	0.64	0.011	0.040	0.32	0.13	0.15	0.11	0.019	-	0.022
3	0.35	0.76	0.032	0.060	0.56	0.19	0.14	0.15	0.021	0.002	0.025
4	0.17	0.50	0.028	0.047	0.47	0.18	0.09	0.06	0.004	0.002	0.016
5	0.20	0.71	0.034	0.038	0.20	0.20	0.10	0.09	0.014	0.006	0.029
6	0.30	1.24	0.023	0.041	0.26	0.14	0.16	0.20	0.014	0.016	0.014
7	0.33	1.15	0.026	0.045	0.31	0.10	0.10	0.18	0.006	-	0.027
8	0.77	0.71	0.030	0.025	0.07	0.04	0.06	0.20	0.020	0.001	0.005
9	0.10	0.60	0.018	0.042	0.33	0.08	0.05	0.06	-	-	0.016
10	0.18	0.58	0.020	0.047	0.52	0.21	0.13	0.11	0.027	-	0.023
11	0.85	0.80	0.020	0.025	0.10	0.06	0.05	0.20	-	-	0.010

Table 2. Chemical analyses for experiments 1-11. (Wt. %).

Au<sup>198</sup> to obtain a comparison of the pool depth found by these two techniques.

The steel cast at the Stelco plant was a C1090 grade. A similar high carbon heat was examined at Western Canada Steel to establish that the difference in cast structure observed in the Stelco casting was due to a difference in mold design and not carbon content.

The data for the casting conditions in each experiment, and the results of the pool depth measurements are given in table 1. The composition of each heat is listed in table 2.

### 3.1.2. Experiment #1.

Tracers: Au<sup>198</sup> added to north pool only.

#### 3.1.2.1. Pool Profile.

A composite picture of the autoradiographs from the first experiment is shown in Fig.(7). The middle two columns in this figure show autoradiographs obtained from longitudinal sections of the centre and north strands. The outside columns are autoradiographs of transverse sections taken from the levels indicated. The bulk of the gold was found to be near the bottom of the liquid pool outlined in the autoradiographs.

In Fig. (7) it can be seen that the top of the liquid pool is well marked in the upper sections of the centre and north pools.

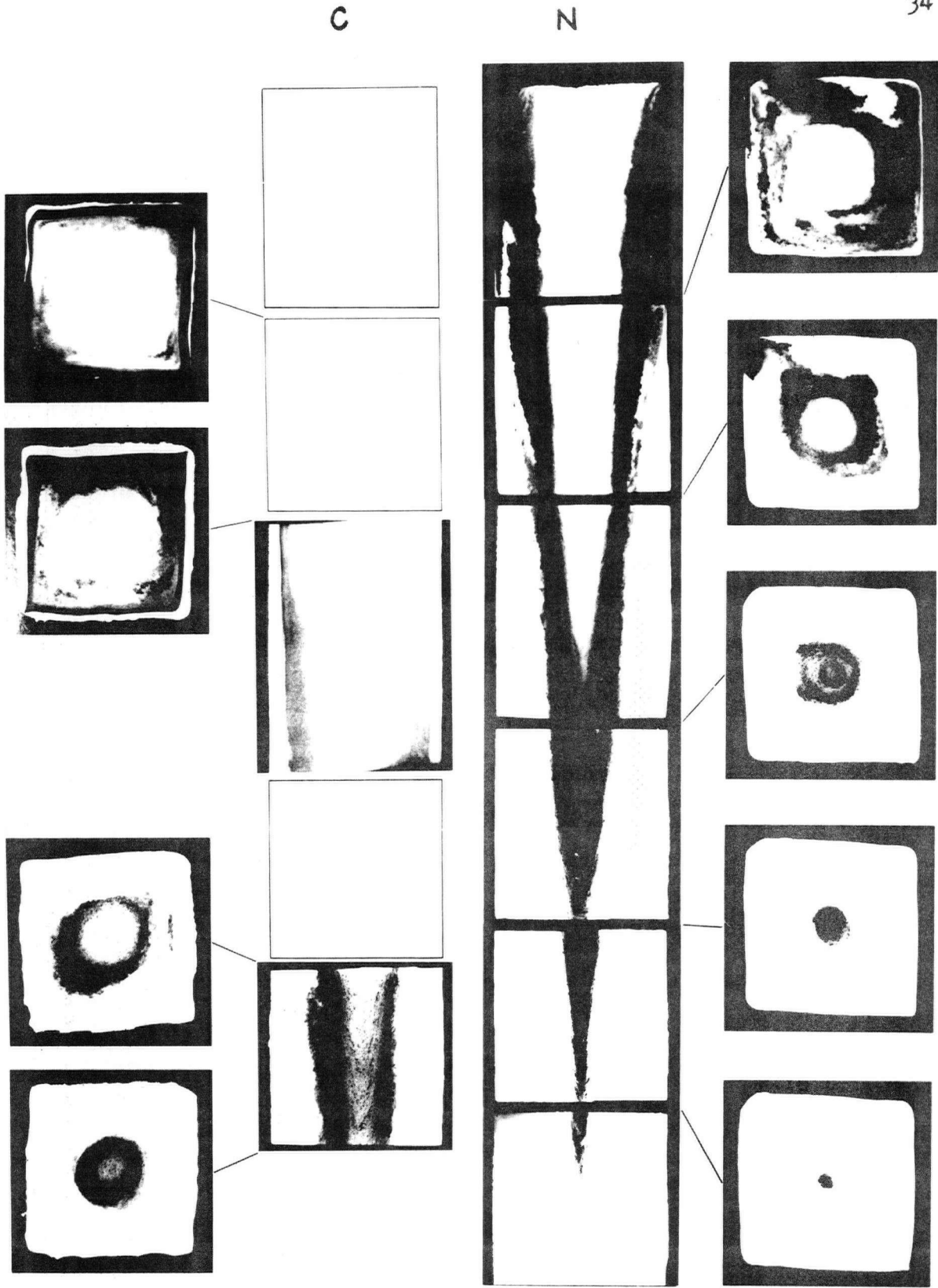


Fig. (7). Composite of autoradiograph from experiment #1, for centre and north pools. Transverse sections taken from levels indicated. 0.2X

The blackened areas extend to the extreme edges in the north pool, indicating that the Au<sup>198</sup> was mixing with liquid metal at the level of the meniscus. The topmost transverse sections in the two strands show a thin white area around the edges that is the initial solid shell formed at or near the meniscus. At this level it is very thin and irregular and is not continuous around the billet. The second transverse section in the centre strand outlines the solid shell at a depth 6" further down from the meniscus and here the shell has thickened to an average of about 5/16". Another 8" down the thickness has increased to about 1/2". Below this level, the solid liquid interface as defined by the tracer is not as sharp and clear as in the upper sections.

In the autoradiographs of the north strand the tracer describes a relatively short cone extending 30" below the meniscus. The profile from the centre pool are not complete but appears to show a much deeper pool than that in the north strand. The depth anticipated in the north pool based on estimates made by the Western Canada Steel staff was approximately 25 ft. This differed markedly from the depth of 3 ft. deduced from the autoradiographs of the north pool.

An interesting feature of the autoradiographs in Fig. (7) is that the central areas of the sections have relatively low concentrations of Au<sup>198</sup> while towards the outside the concentration increases to a maximum, ie. the film is lighter in the centre and gets progressively darker towards the outside. This effect is most noticeable in the first two transverse autoradiographs from the centre strand.

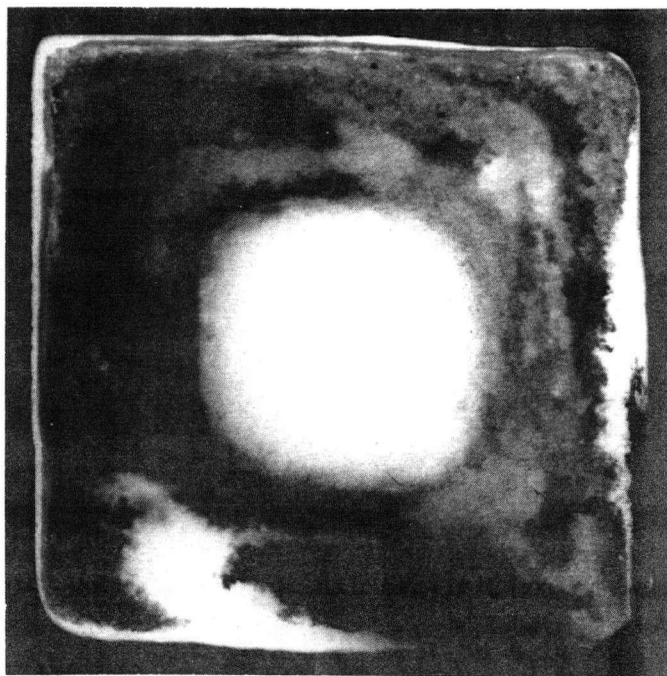
### 3.1.2.2. Liquid Mixing.

The Au<sup>198</sup> was added to the north pool only, but as the autoradiographs show, it is found not only in the north pool but in the centre and south pools, as well. An autoradiograph from the south pool is shown in Fig. (8), adjacent to one from the same level in the north strand. The correspondence between the two sections is good and in the centre and north strands in Fig. (7) the level of the meniscus compares closely. Therefore, the mixing between the strands must be quite rapid. The strand is moving at 1 in./sec. requiring mixing to occur in the order of a few seconds if the meniscus and pattern of the north and south pools are equivalent.

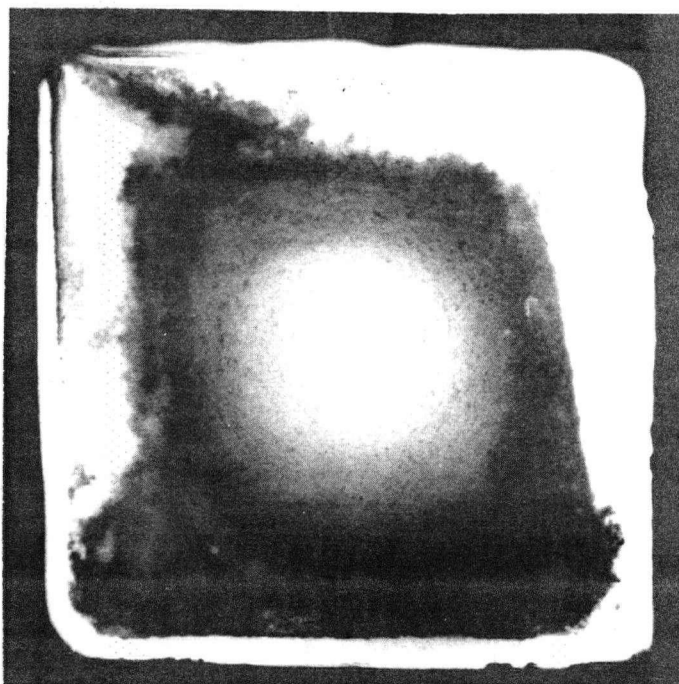
The mixing between the pools was unexpected for several reasons. First, the liquid steel is poured into the centre pot only and fills the outside areas through the narrow webs joining the three strands. One might therefore expect the steel to flow only from the centre pot to the outside. Furthermore, the level of steel in the centre pool can be seen to be approximately  $\frac{1}{2}$ " higher than that in the outside pools. Finally, the web is  $\frac{5}{8}$ " wide and should freeze over relatively rapidly, blocking any flow from the centre pool below the point in the mold where the web is closed. This would inhibit back flow from occurring.

### 3.1.2.3. Structure.

Fig. (9) shows an autoradiograph taken from near the



N



S

Fig. (8). Transverse autoradiographs taken from the same level in the north and south pools.

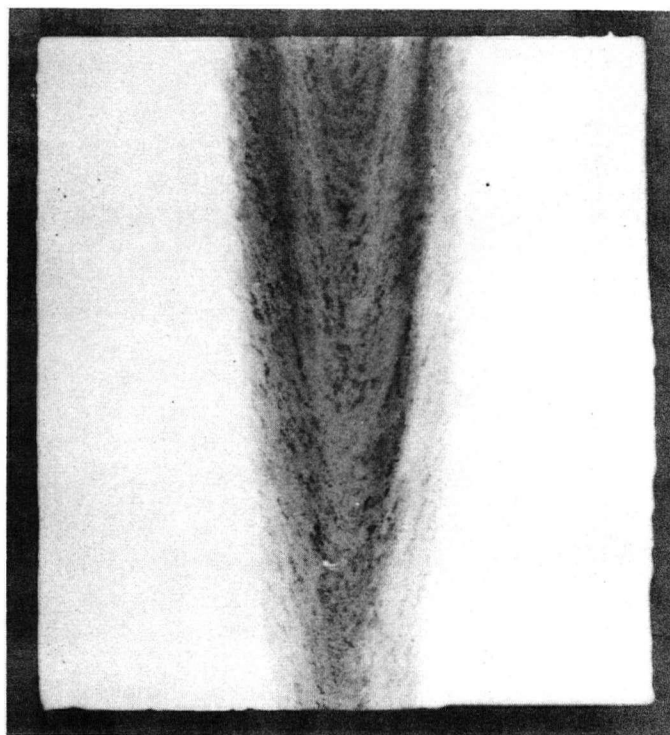


Fig. (9). Longitudinal section from north strand. (ie. section 4 in Fig. (7)).

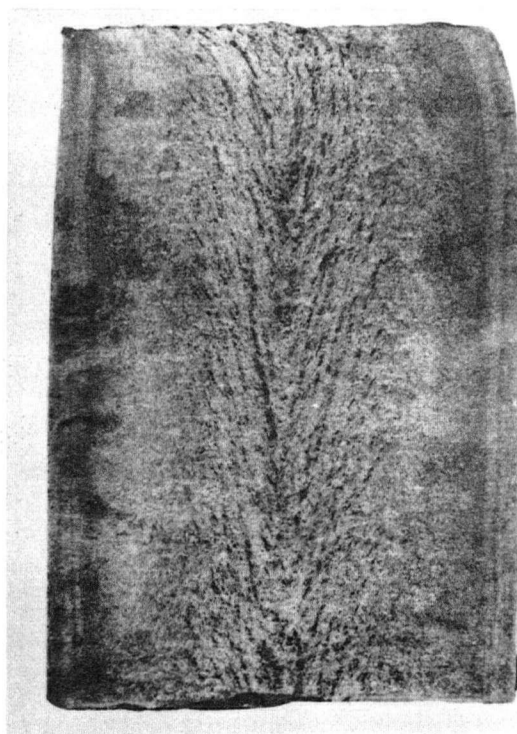


Fig. (10). Etched longitudinal section of a billet from Western Canada Steel.  
Etchant: 50% HCl.

bottom of the cone formed by the tracer in the north strand. The autoradiograph show the structure containing V-shaped patterns made up of dark spots. The resolution is not sufficient to determine the nature of the spots and whether they are caused by segregation or porosity. These spots are seen not only in the autoradiographs but in etched sections as well, such as that shown in Fig. (10).

### 3.1.3. Experiment #2.

Tracers: Au<sup>198</sup> in centre pool only.

#### 3.1.3.1. Pool Profile.

The second experiment carried out using Au<sup>198</sup> in the centre pool only. The autoradiographs obtained are shown in Fig. (11) and Fig. (12). It can be seen that the tracer did not show the level of the meniscus since the shell does not reduce to zero thickness, or the bottom of the pool since the activity gradually reduces to zero in an irregular manner. The Au<sup>198</sup> appears to have been carried down in the stream and been mixed fairly well in the lower parts of the pool, but has not been carried back up to the meniscus. The width of the zone containing the tracer widens toward the top of the sections in Fig. (11), but farther up the interface never reaches the mold walls. For example, Fig. (13) shows a transverse section taken 8 in. above the top section in Fig. (11). The zone blackened by the Au<sup>198</sup> is much narrower here than it is in lower sections. Also, it is different from the lower sections in that the centre of the section is

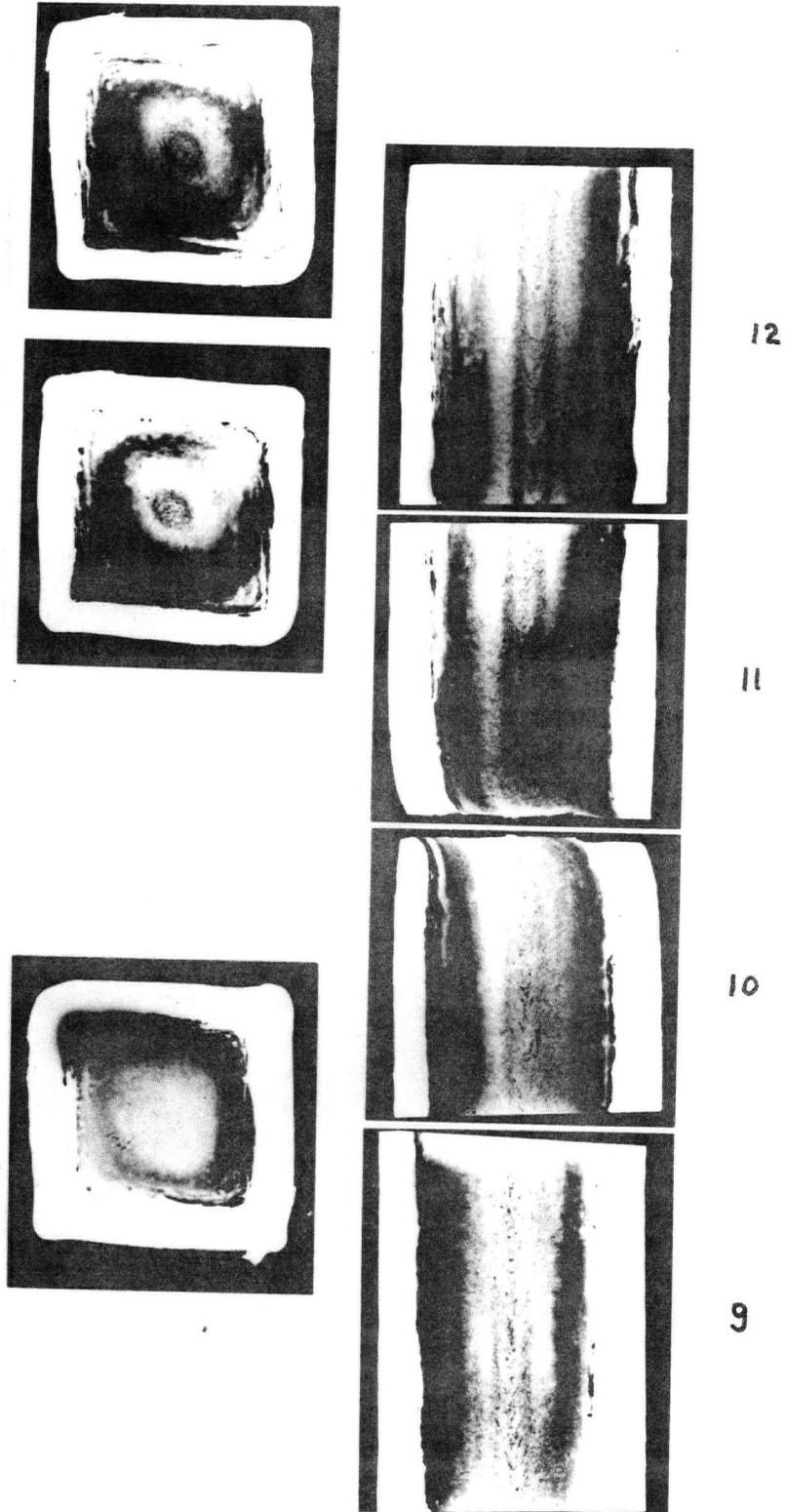


Fig. (11). Composite of autoradiographs from experiment #2.  
Transverse autoradiographs taken from positions  
indicated. 0.25x

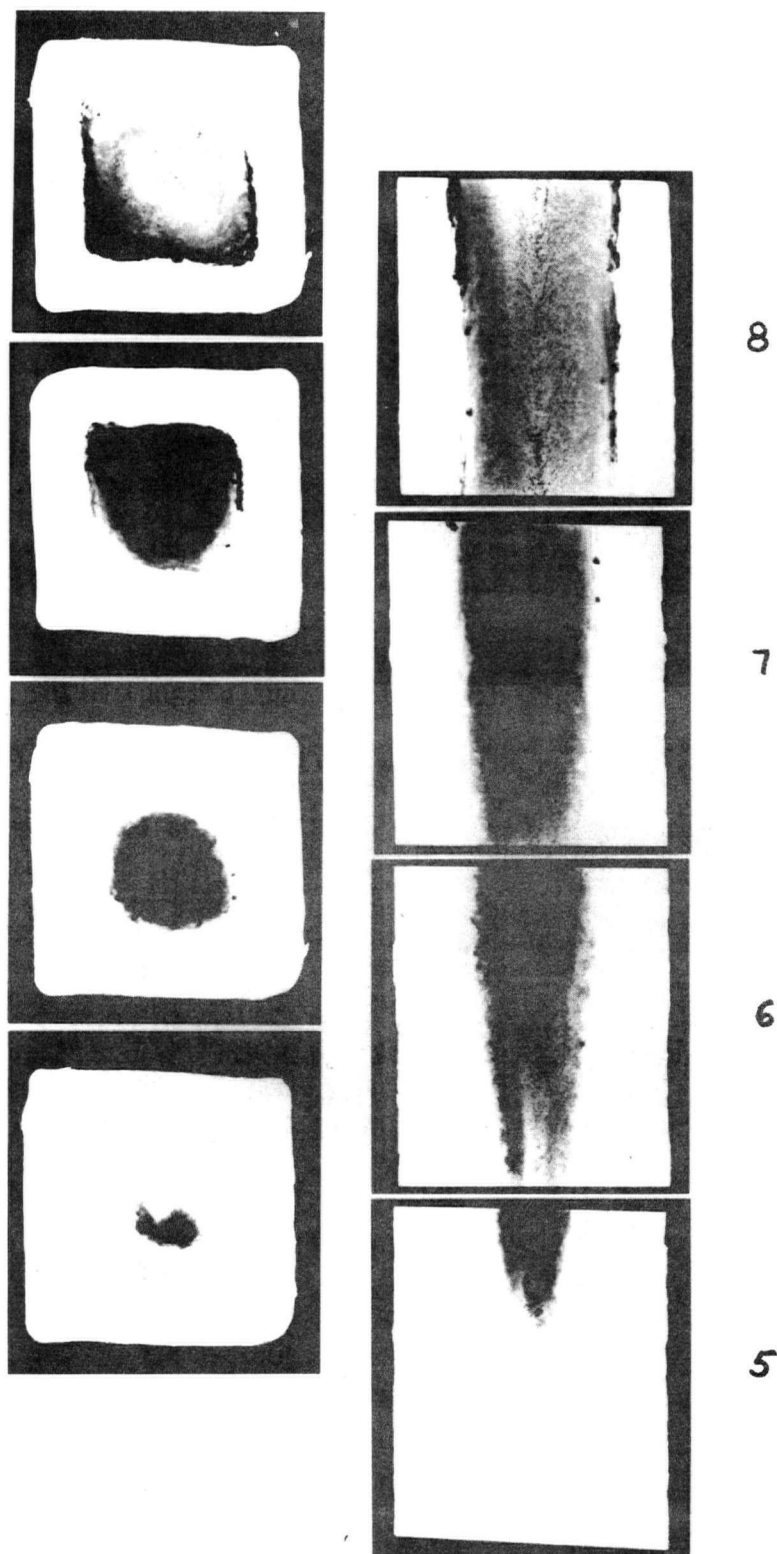


Fig. (12). Composite of autoradiographs from experiment #2.  
Sections 5-8 follow in sequence from (below) those  
in Fig. (11).

darkest, showing the greatest Au concentration. Towards the outside of the exposed area, the film gets progressively lighter showing a decreasing concentration of Au. In the sections in Fig. (11) the opposite to this effect is seen. The concentration is greatest at the outside of the exposed areas and diminishes towards the centre.

In the first four sections at the top of the part of the pool delineated by the tracer, in Fig. (11), the boundaries of the exposed areas are very sharp and well defined. These boundaries are not as well defined in the lower sections, shown in Fig. (12). In the last three longitudinal sections in Fig. (12) the edges of the exposed areas are very diffuse.

#### 3.1.3.2. Liquid Mixing.

In the first experiment, where the tracer was added to the north pool, the liquid was shown to mix between the three pools, but in this case the Au<sup>198</sup> has not done this. Apparently the gold has been carried down a considerable distance below the meniscus but has not mixed back to that level. Also, as shown in Fig. (12), the tracer has not mixed down to the bottom of the pool. The profile tapers down in the lower sections and in the last one the activity gradually decreases until it is no longer recorded on the film.

#### 3.1.3.3. Structure.

In this experiment, some of the sections were autoradio-

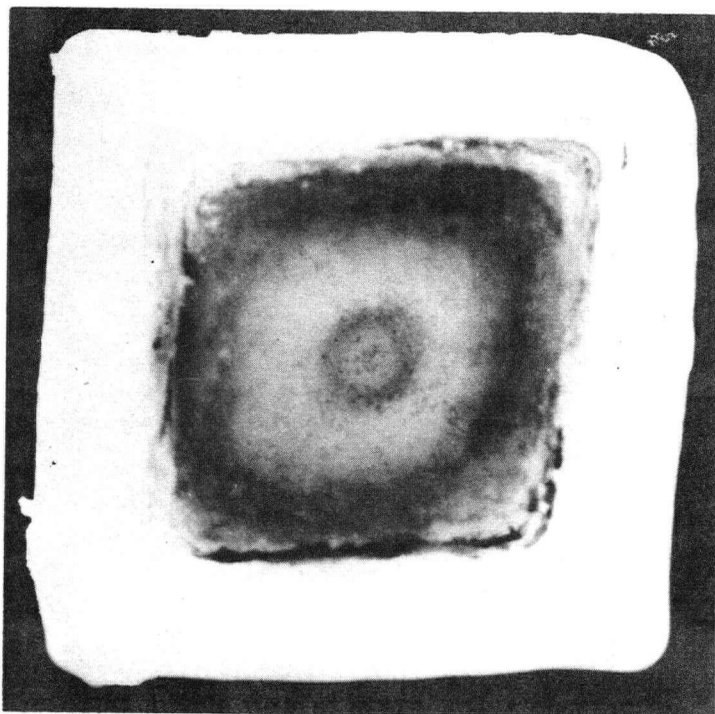


Fig. (13). Transverse section autoradiograph, taken 8 in.  
above section 12 in Fig. (11). 0.6 x

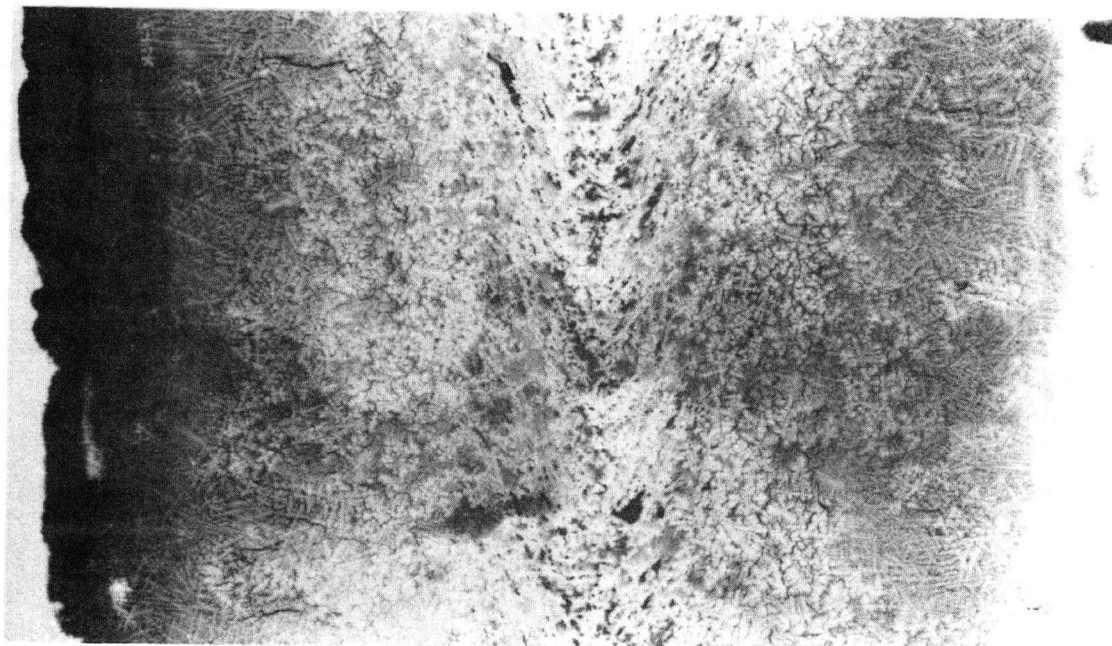


Fig. (14). Autoradiograph of longitudinal face, section 10  
in Fig. (11). 1.3 x

graphed on Contrast Process Ortho film. Examples of these are shown in Figs. (14), (15) and (16). The section numbers on these can be compared to the same sections exposed on x-ray film, in Figs. (11) and (12). Fig. (14) is an autoradiograph taken from section 10 of the centre strand. Only the central part of the section which contains the tracer is shown. The dendritic structure shows up very clearly and primary and secondary dentrite arms are resolved. Toward the outside of the section the autoradiograph shows the end of the columnar zone which extends approximately  $1\frac{1}{2}$  inches from the ingot surface. The dendrites, which are depleted in Au, shows up as light areas and the Au-rich interdendritic regions are dark. The pattern of black spots observed in experiment 1 are also found in this second one and in Fig. (14). They are resolved as pockets of Au-rich interdendritic liquid in the central equiaxed zone.

Fig. (15) shows another feature observed in several of the sections. Down one side of the centreline a series of dark lines can be seen running transversely across the section. These lines are about  $3/4$  in. long. The lines are dark and therefore must be caused by a concentration of gold or a crack in the steel. No cracks were observed on the ground surface, either from direct observation or with dye check or ultrasonic tests from which it was concluded that the lines are concentrations of gold formed during solidification. The lines show where interdendritic cracks have opened before solidification was complete, the cracks being filled with residual interdendritic liquid rich in Au.

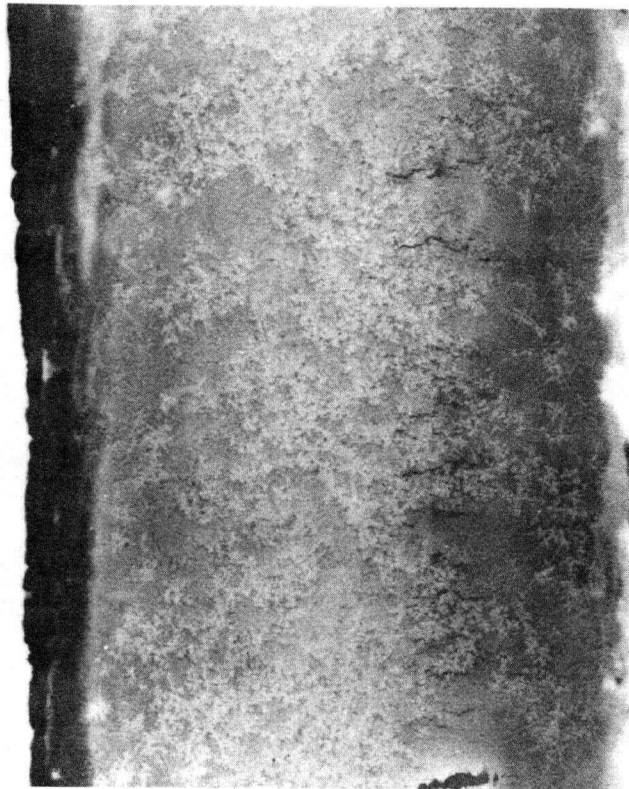


Fig. (15). Longitudinal section, taken 1 in. off the billet  
centreline. x.6

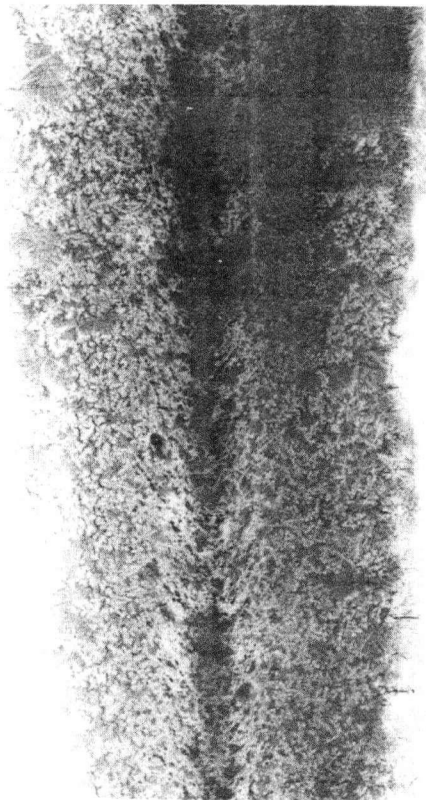


Fig. (16). Longitudinal section taken on the billet centre-  
line. x.6

Fig. (16) is included to show the large equioxed zone and the V-shaped segregation pattern on the centreline of the sections.

#### 3.1.4. Experiment #3.

Tracers: Au<sup>198</sup> added to centre and north pools.

##### 3.1.4.1. General Comments.

In the first two experiments using Au<sup>198</sup>, profiles of the liquid pool were obtained for parts of the north and centre pools. When gold was added to the north pool, it showed the profiles in the area of the meniscus for both the centre and north pools. When added to the centre pool, the gold showed the profiles in the centre pool, but not as far up as the meniscus. Therefore, in this experiment Au<sup>198</sup> was added simultaneously to both pools in order to show both pools together and to show the shell thickness in the centre pool up to the meniscus. In this way a more complete picture of the pool profile of both pools is obtained.

##### 3.1.4.2. Pool Profile.

The autoradiographs from this experiment are shown in Figs. (17) - (21). These show the distribution of Au<sup>198</sup> in a sequence of sections from the top to the bottom of the pool. The column of sections on the left are from the north strand and on the right from the corresponding centre strand.

In Fig. (17), the meniscus can be seen in the second

N

C

47



Fig. (17). Composite of autoradiographs from experiment #3, showing the sequence of sections in the north and centre pools. 0.44 X

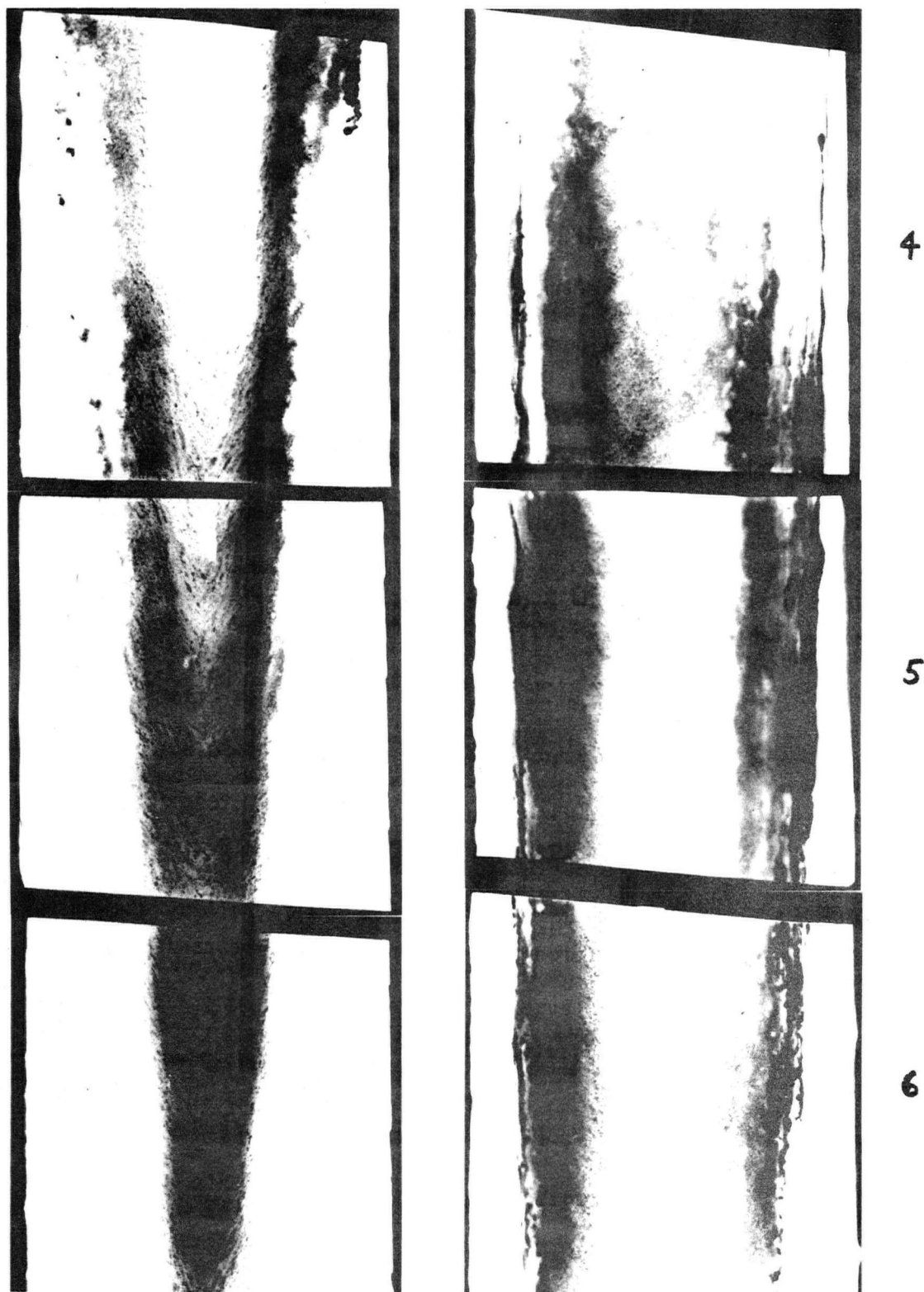


Fig. (18). Composite of autoradiographs from experiment #3. Sections 4-6 follow in sequence from Fig. (17).

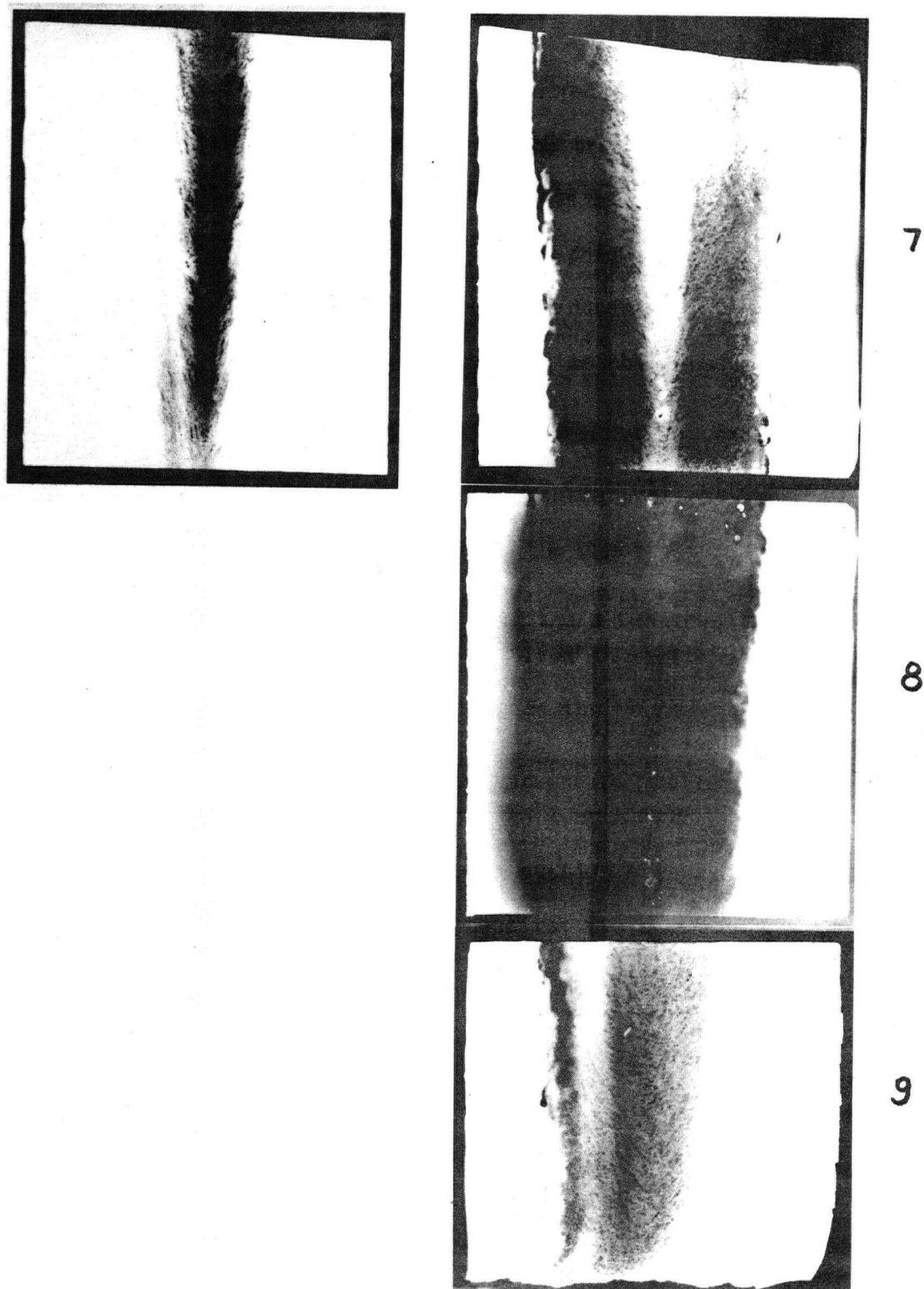


Fig. (19). Composite of autoradiographs from experiment #3. Sections 7-9 follow in sequence from those in Fig. (18).

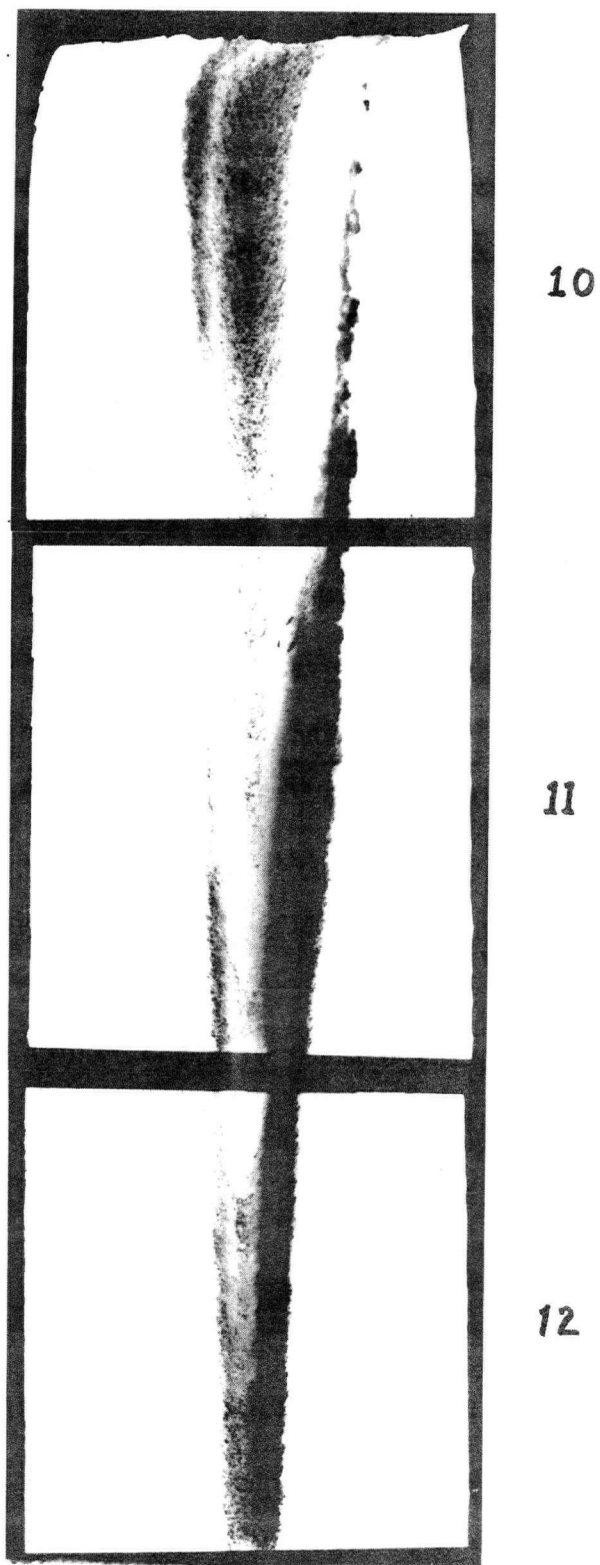


Fig. (20). Composite of autoradiographs from experiment #3. Sections 10-12 follow in sequence from those in Fig. (19).

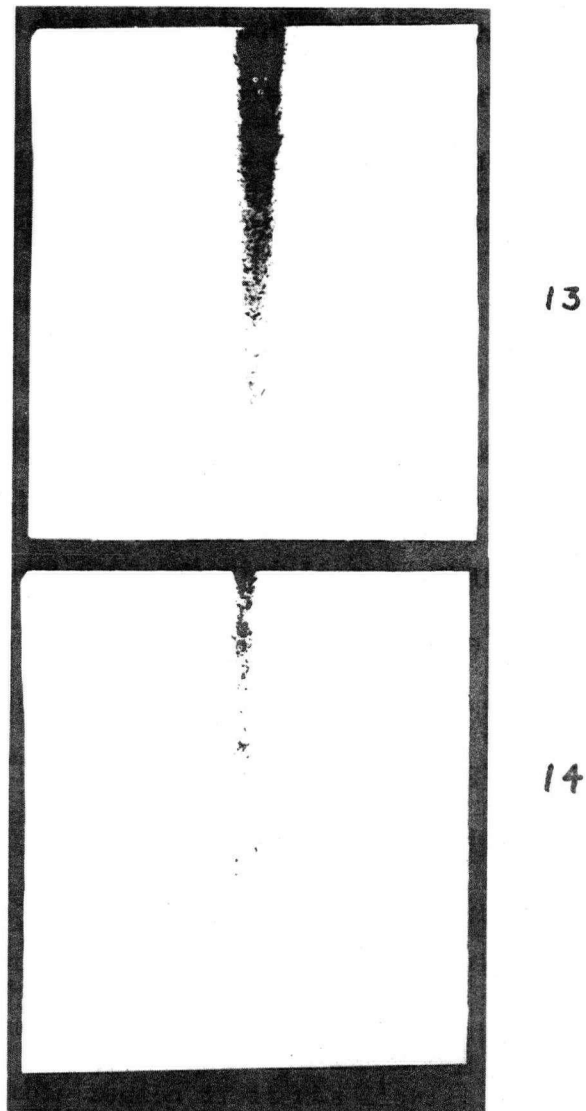


Fig. (21). Composite of autoradiographs from experiment #3. Sections 13 and 14 follow in sequence from those in Fig. (20).

sections from the top. The white wedge-shaped areas show the solid shell formed at the time of addition of the tracer. The meniscus for the north pool is seen to be about 5" higher than that of the centre pool, which could be due to several seconds difference in the addition of the two gold samples or a small difference in the rate of mixing in the two pools. The difference is not considered to be significant.

In Figs. (17) and (18), the centre pool profile is sharply delineated by a sharp boundary for a number of feet below the meniscus; in the north pool the boundary is not clear for more than a foot below the meniscus. This was observed in the first experiment on the north pool as well, but in this case the boundary is even less clear. The same short conical profile is seen in Fig. (18), as in Fig. (7), and is approximately of the same length. However, some blackened areas of the film can be found outside the narrow conical profile. These are most obvious in the first two sections in Fig. (18). This indicates that the  $\text{Au}^{198}$  is not mixing completely in the liquid in this pool, since the gold observed outside the cone could only have reached this region if it was liquid. This would suggest the conical profile outlined by the gold is a liquid-liquid interface and not a solid-liquid interface.

In Fig. (19), the autoradiographs of the centre strand continue to show a sharp boundary to the metal containing tracer, at least on one side. This indicates that the  $\text{Au}^{198}$  is marking the

solid-liquid interface and the profile is the actual liquid pool profile. The slight fogging of the interface in the second centre strand section in Fig. (19) is caused by overexposure and is not significant. The distortion in the last section is caused by the mechanical shear. Fig. (19) also shows the last autoradiograph from the north pool, which again shows the pool profile tapering to a sharp point.

The last five autoradiographs from the centre strand are shown in Figs. (20) and (21). The tracer here describes a sharply pointed cone, similar to the north pool. The boundaries here are also less sharp than that observed in the mold region, and are similar to the boundaries in the north pool. In Fig. (21), the first section appears to show the termination of the cone, which then reappears in the following section. This is a result of the plane of sectioning being slightly different in the two sections. The first section was cut slightly off the centreline.

The distribution of the tracer in the autoradiographs in Figs. (20) and (21) is not uniform, and there is a heavy concentration on one side of the billet, particularly in the sections in Fig. (20). In the sections above these, such as in Fig. (18), the  $\text{Au}^{198}$  is also not uniformly distributed. Similar to the first two experiments, the greatest concentration of  $\text{Au}^{198}$  is at the edge of the area marked by the tracer, diminishing towards the centreline of the sections. This is most apparent in the centre pool but is also apparent in the upper

parts of the north pool near the meniscus as well. This effect can be observed down the centre pool for a distance slightly shorter than the distance for which the solid-liquid interface is sharply defined.

In general, the solid liquid interface outlined by the  $\text{Au}^{198}$  near the top of the pool is quite sharp and smooth in the centre strand. However, in Fig. (18), a series of ripples can be seen on the interface. These ripples indicate that there are fluctuations in the shell thickness for some unknown reason. The fluctuations can be seen in more detail in Fig. (22) which is an autoradiograph of the same section seen in Fig. (18), made on Contrast Process Ortho film. The dendritic structure is not resolved, but the interface at the indentation is shown to be smooth, the same as the other parts of the shell.

#### 3.1.4.3. Structure.

In other respects, Fig. (22) is much like the autoradiographs from the second experiment. The columnar zone is short and most of the cross section of the billet is equiaxed in structure. The V-shaped segregation pattern is again visible down the centreline. The spots directly on the centreline are stains produced by small amounts of cutting fluid retained in centreline pores. The pores are not as large as the stain, but are visible on the ground surface.



Fig. (22). Autoradiograph of billet section 5, in Fig. (18).  
**0.75 x**

### 3.1.5. Experiments #4, 5.

Tracers: Tungsten pellets added to north and centre pools.

#### 3.1.5.1. Pool Depths.

In order to establish that the pool depth determined by the depth of penetration of Au<sup>198</sup> into the liquid pool in the first three experiments did correspond to the actual pool depth, tungsten pellets were dropped into the north and centre pools. The casting conditions for both pellet experiments were similar to those in previous tests, as listed in Table 1.

The distance between the position of the tungsten pellet and the upper liquid surface for the centre pool was found to be 14 ft., twice the depth indicated by the Au<sup>198</sup>. The corresponding distance in the north pool was 13 ft., which is very much larger than the 3 ft. pool depth indicated by the Au<sup>198</sup>. The pool depths shown in the autoradiographs do not, therefore, correspond to actual pool depths.

### 3.1.6. Experiment #6.

Tracers: Tungsten pellet and Au<sup>198</sup> added to north pool.

#### 3.1.6.1. General Comments.

To ensure that the results of pool depth determined

from the position of tungsten pellets dropped in the liquid pool, and that obtained from the autoradiographs are directly comparable. Experiment #6 was carried out in which tungsten pellets and Au<sup>198</sup> were added simultaneously to the liquid in both north and centre pools.

The high manganese content in this heat made cutting and machining of the billets slow and difficult. As a result only a few sections could be prepared in the time available before the gold decayed below a useable activity level.

#### 3.1.6.2. Pool Profile and Depth.

The composite of the autoradiographs from this heat is shown in Fig. (23). The profile is very similar to that in the first experiment and pool depths appear to be of approximately the same length as that observed previously. In this case, the lateral mixing was even less than experiment #3, and the Au<sup>198</sup> is heavily concentrated on one side of the liquid pool.

The marker inserted in the corner of the strand when the tracers were added was located 6 in. above the top section shown in Fig. (23). The tungsten pellet was found 10 ft. below the marker. The profile given by the Au<sup>198</sup> is only 3 ft. deep, indicating that the pool extends <sup>7</sup> ~~6~~ ft. below the termination of the profile in agreement with the previous results.

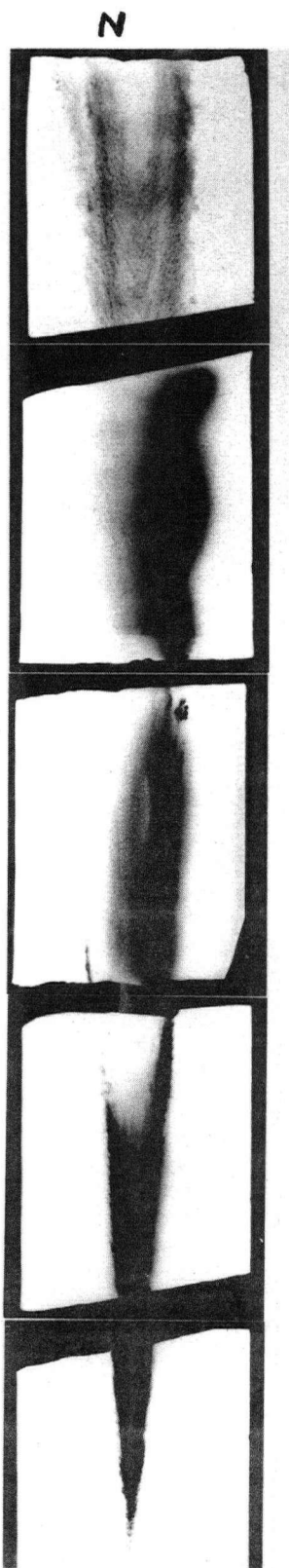


Fig. (23). Composite of autoradiographs from experiment #6. (north pool). 0.22 X

### 3.1.7. Experiment #7.

Tracers: Tungsten pellet and Au<sup>198</sup> added to north and centre pools simultaneously.

#### 3.1.7.1. General Comments.

Particular attention was directed in this experiment to the depth and thickness of the liquid layer in the web joining the billets. Au<sup>198</sup> and tungsten pellets were again used simultaneously in both the north and centre pools. As in experiment #6, the billets were difficult to cut and machine so that only transverse sections were made. These sections are suitable for an examination of the web.

#### 3.1.7.2. Pool Profile and Depth.

The set of autoradiographs obtained for this casting is shown in Figs. (24) and (25). The numbers indicate the location of each section below the meniscus marker. Part of the marker can be seen in section 1N . The pool profile outlined by these autoradiographs is consistent with those from earlier experiments. The top sections in Fig. (24) are located above the meniscus level since no solid skin is present around the edges. The solid shell starts in sections 1N and 1C and thickens progressively in the lower sections. The outline of the solid-liquid interface in the north strand in section 3 is no longer clearly indicated. Further down

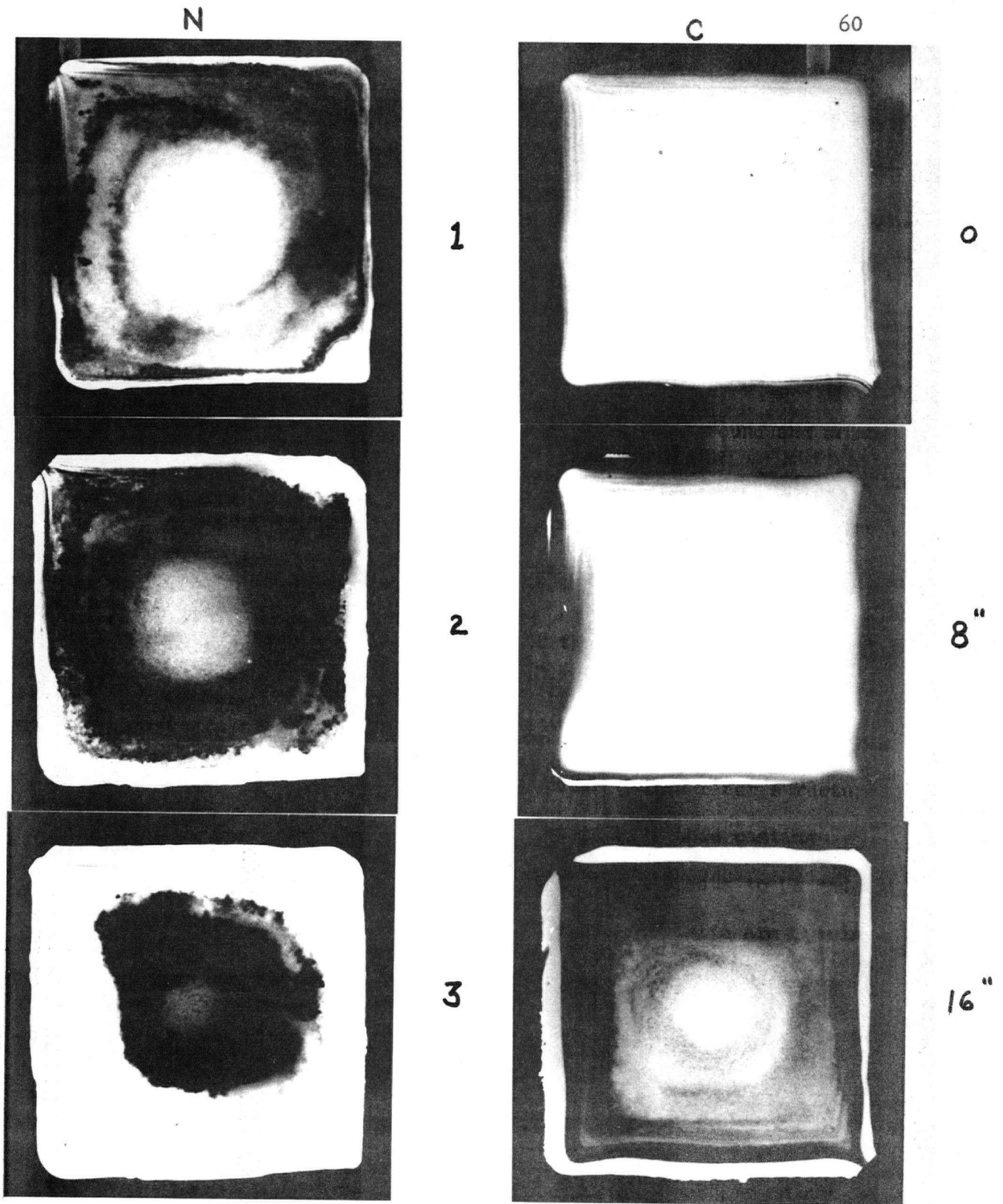
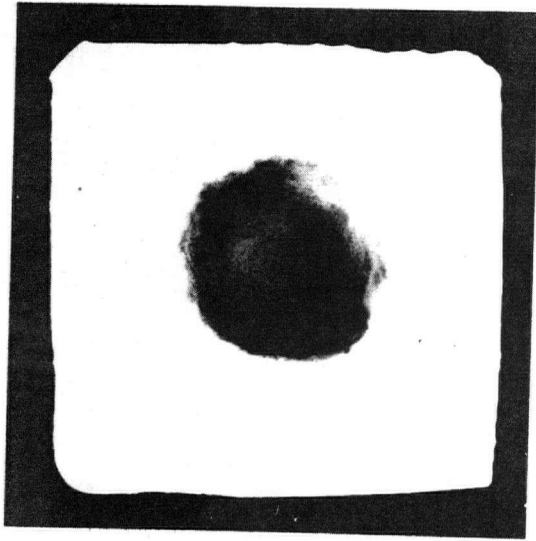
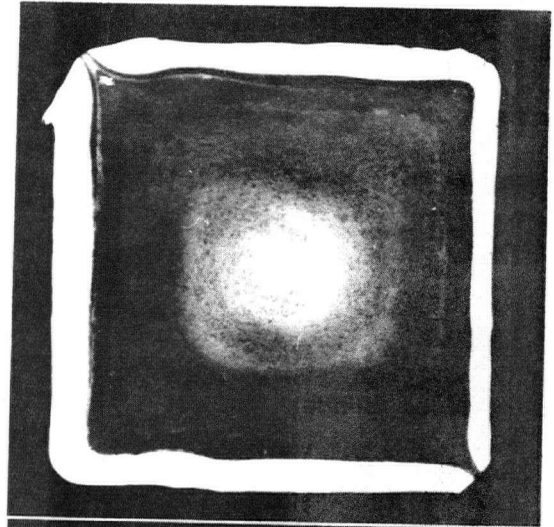


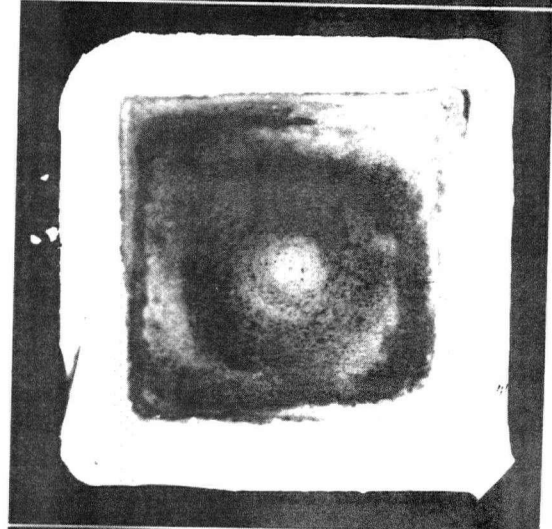
Fig. (24). Composite of autoradiographs from experiment #7. The measurements indicate the spacing of the sections. 0.4X



4

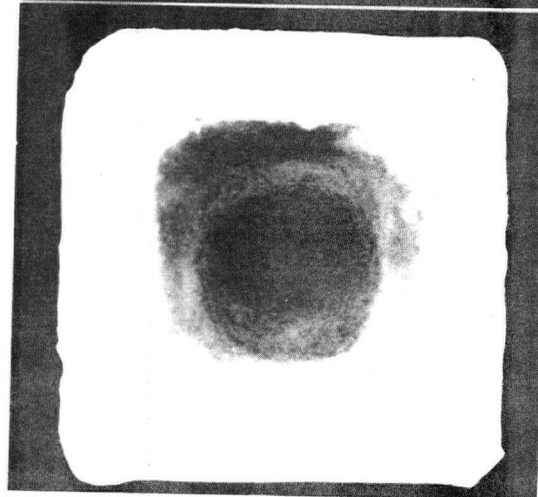


24"



5

30"



6

36"

Fig. (25). Composite of autoradiographs from experiment #7. These transverse sections follow in sequence from those in Fig. (24).

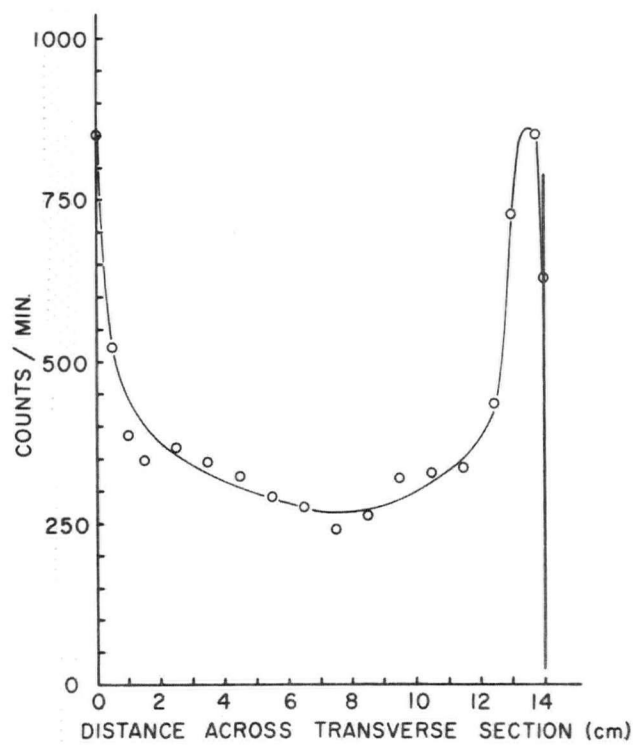
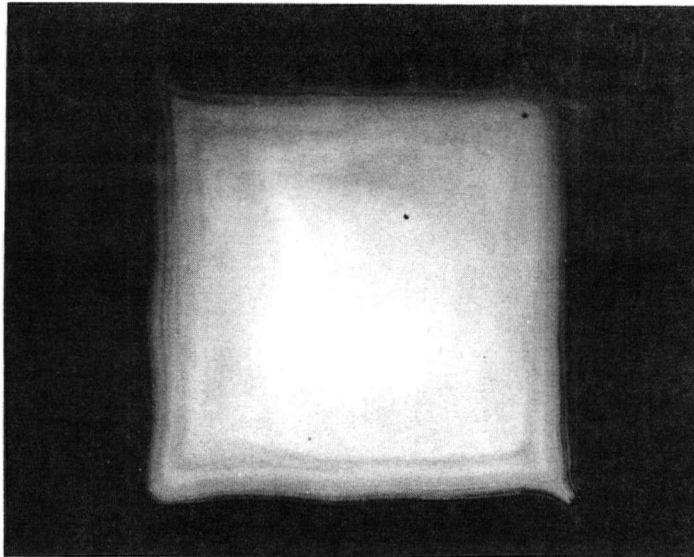


Fig. (26). Plot of counts/min. vs. distance across transverse section

1 C . Corresponding autoradiograph shown above.

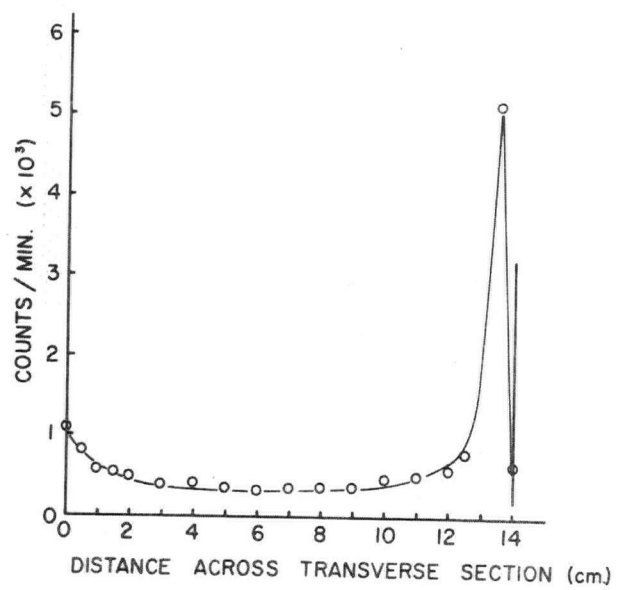
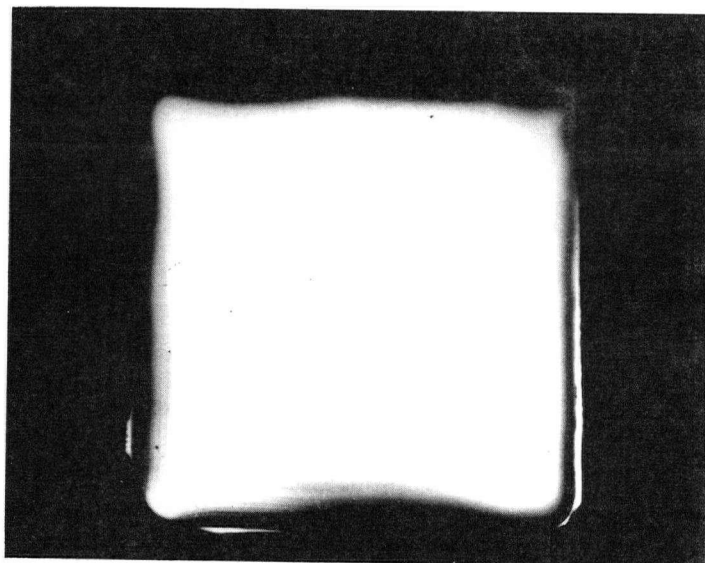


Fig. (27). Plot of counts/min. vs. distance across transverse section  
2 C . Corresponding autoradiograph shown above.

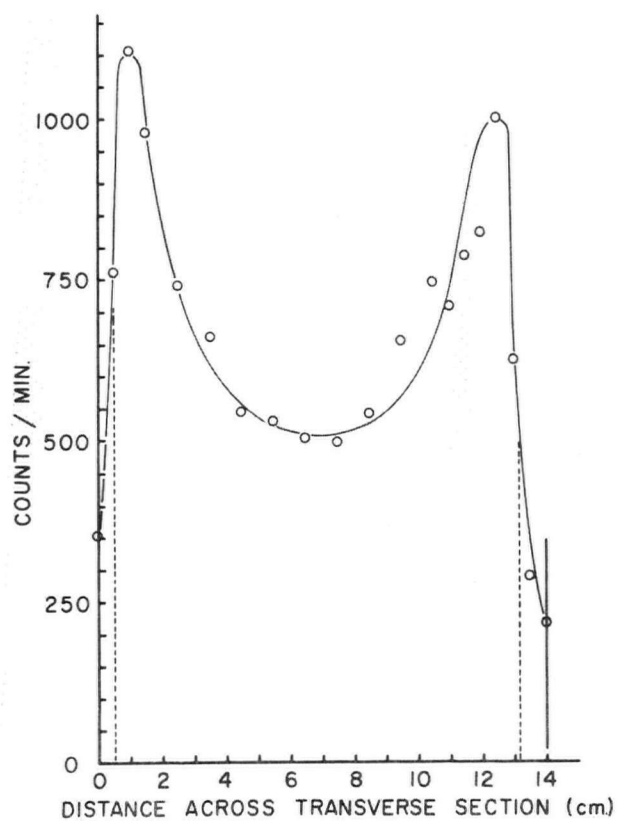
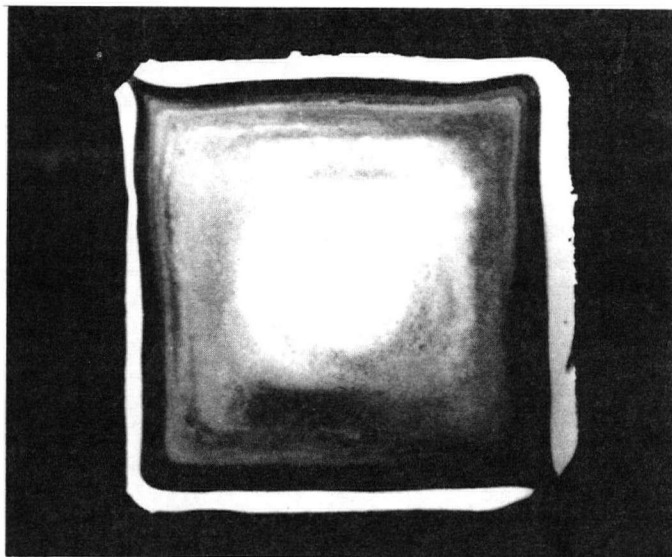


Fig. (28). Plot of counts/min. vs. distance across transverse section

**3C** . Corresponding autoradiograph shown above.

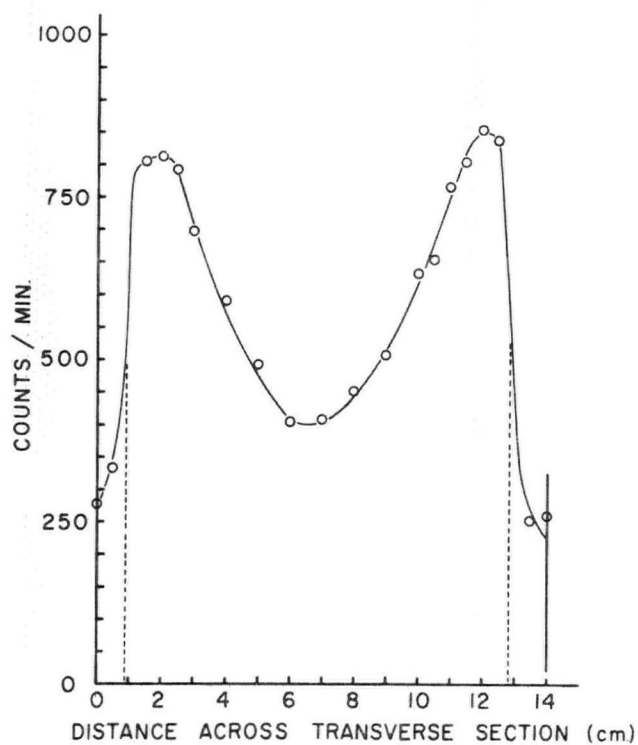
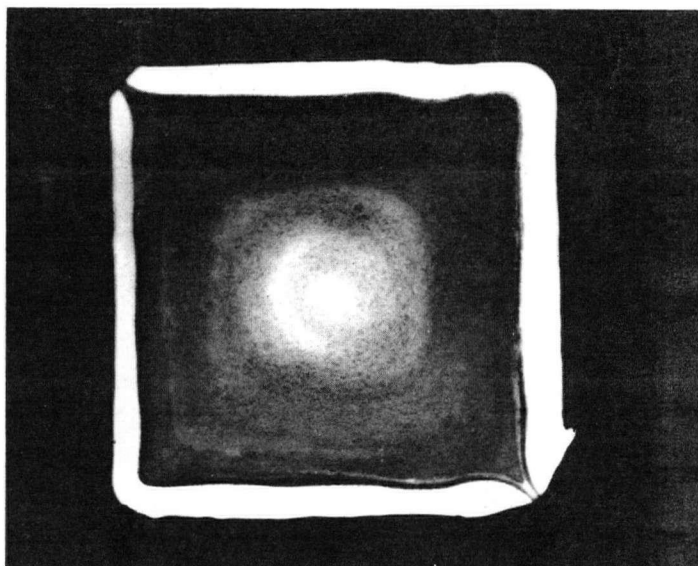


Fig. (29). Plot of counts/min. vs. distance across transverse section  
**4C** . Corresponding autoradiograph shown above.

in section 4C the solid shell is  $\frac{1}{2}$  in. thick at which point the web should be closed since it is  $\frac{5}{8}$  in. thick and solidification occurs from both sides of the web. However this is not the case as Au<sup>198</sup> was still flowing through the web.

For this particular experiment a series of scans were made of the sections which had been autoradiographed, using a scintillation counter. The plots of activity vs. distance across the sections are shown for four scans in Figs. (26) - (29). With each plot is shown the corresponding autoradiograph. The sharp boundaries to the areas containing Au<sup>198</sup> are seen in the plots as a steeply rising curve. The autoradiographs of these sections show the greatest darkening of the film at these boundaries, and the density gradually diminishes towards the centre. The plots show this effect quantitatively.

3.1.8. Experiment #8. Premier Works - Steel Company of Canada, Edmonton.

Tracers: W pellet and Au<sup>198</sup> added to the single strand.

#### 3.1.8.1. General Comments.

The eighth experiment was done at the Premier Works of the Steel Company of Canada. The section size, 6" square, and the casting speed for this heat were similar to those at Western Canada Steel. The steel cast was C1090, which is higher in carbon than any of the steels cast in the preceding Western Canada Steel experiments.

Both tungsten pellet and Au<sup>198</sup> were added to the pool simultaneously. However, the pellet was not located in the billet after it had cooled; as a result the pool depth was not measured.

### 3.1.8.2. Pool Profile.

The autoradiographs obtained are shown in the composite in Figs. (30), (31) and (32). The marker inserted at the meniscus was located in section 1 in Fig. (30). As in the Western Canada Steel experiments, the profile is clearly marked in the upper part of the pool, in sections 1 to 5. The boundaries of the areas containing Au<sup>198</sup> are sharp and the solid-liquid interface is clearly delineated. Below section 5, in Fig. (31), the interface is less sharply defined, and the tracer does not seem to have mixed completely across the full width of the pool. This is observed in section 5 where the sharp line marking the solid-liquid interface breaks down. This occurs at a depth of  $3\frac{1}{2}$  ft. below the meniscus marker. In sections 6 to 9, the tracer fills a narrow cone, tapering to a sharp point, similar to the Western Canada Steel profiles. The termination of this cone is at a depth of 5 ft. below the meniscus marker.

In the top 5 sections, the darkening of the film and therefore the concentration of Au<sup>198</sup> is greatest near the interface marked by the tracer. Toward the centre it is more dilute. This dilution is seen in the autoradiographs in Fig. (30) as a light region extending down the centreline of the sections. When it reaches

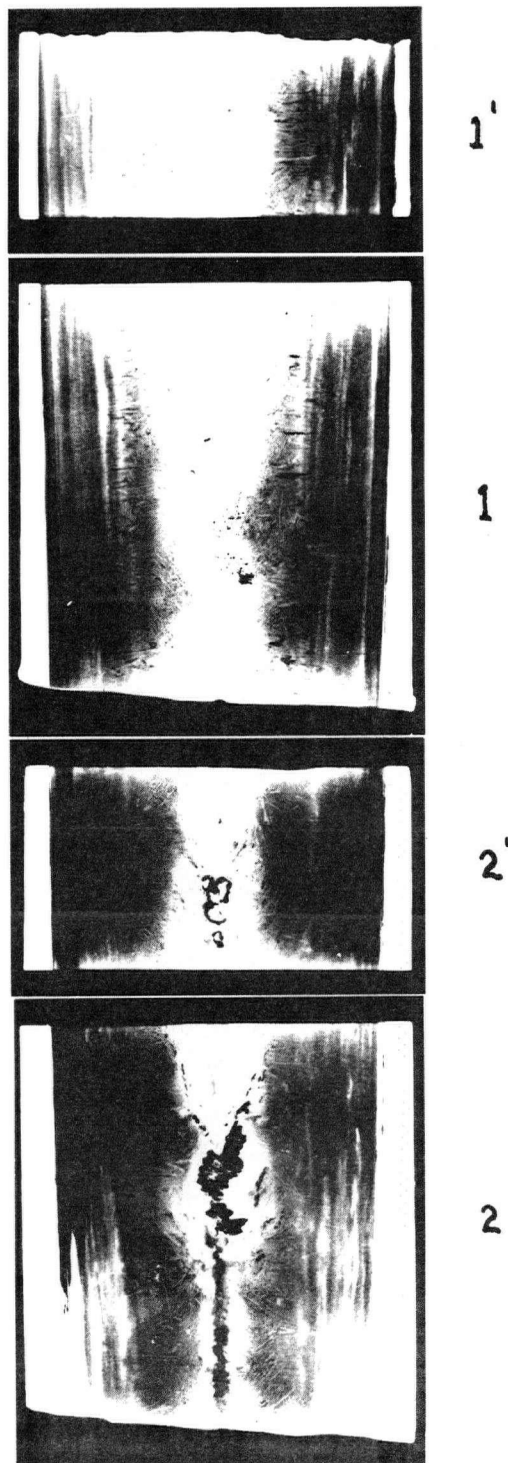


Fig. (30). Composite of autoradiographs from experiment #8. (Single strand mold, Stelco). 0.3 X

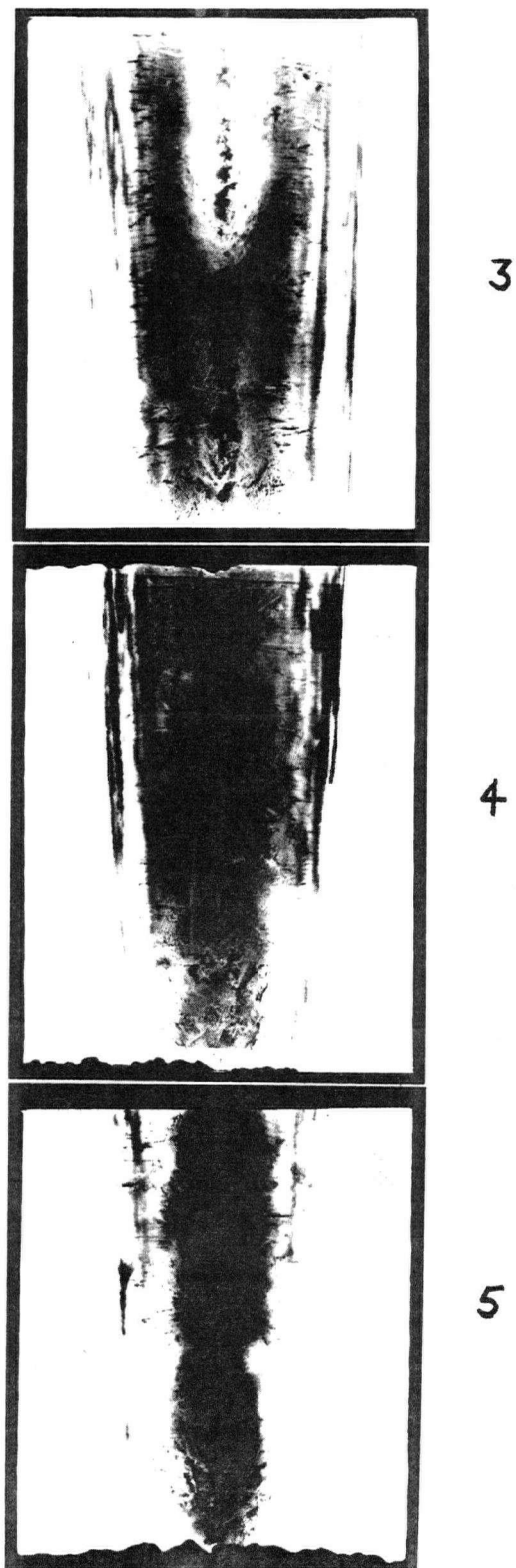


Fig. (31). Composite of autoradiographs from experiment #8. (Stelco).  
Sections 3-5 follow in sequence from those in Fig. (30).

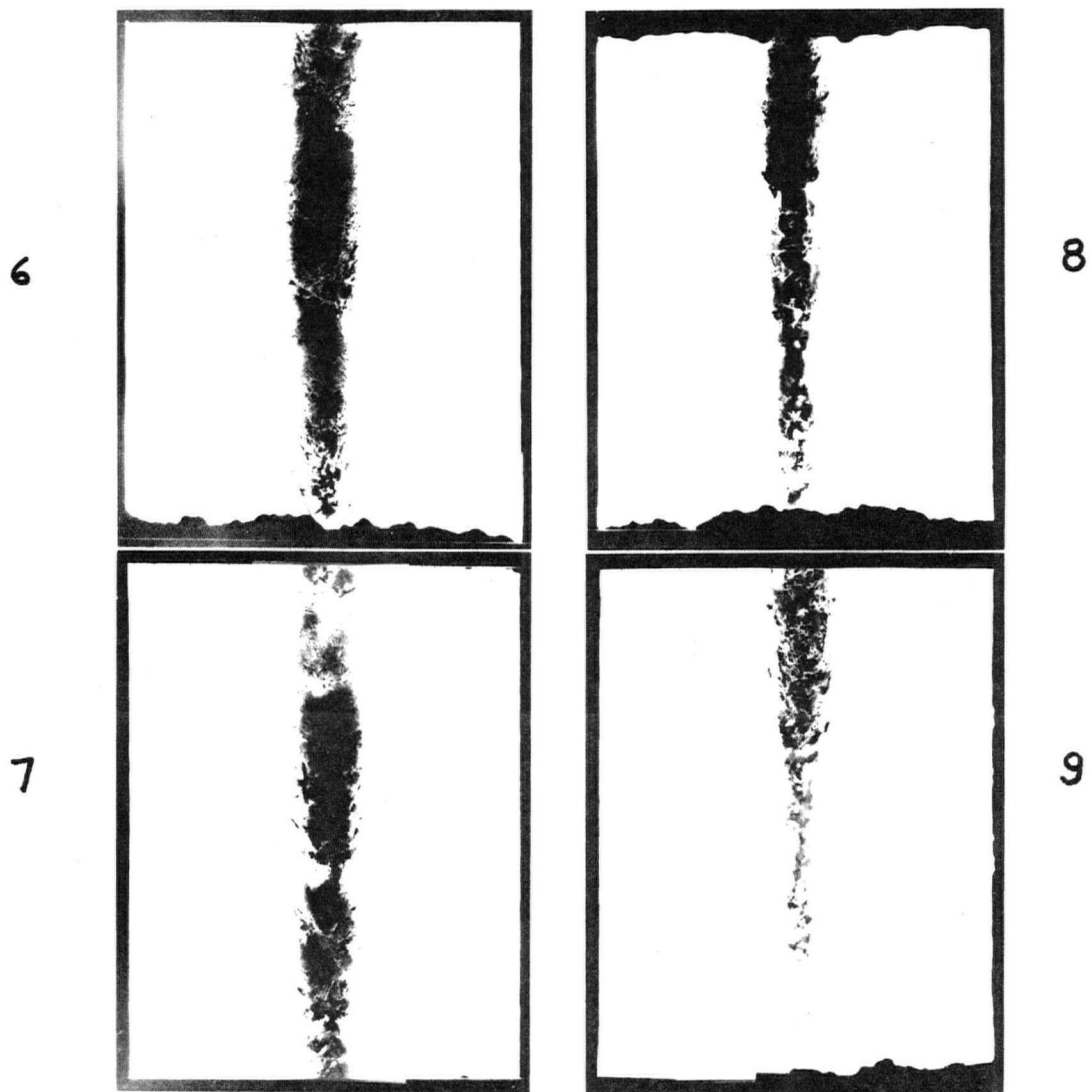


Fig. (32). Composite of autoradiographs from experiment #8. (Stelco).  
Sections 6-9 follow in sequence from those in Fig. (31).

the level of section 3, 33 to 38 in. below the meniscus, it disappears and the distribution of Au<sup>198</sup> across the sections is then more uniform.

### 3.1.8.3. Structure.

The autoradiographs in Figs. (30) - (32) were made on x-ray film. Each of these sections was also surface ground and autoradiographed on Contrast Process Ortho film. These autoradiographs, which yielded a large amount of the detail of the dendritic structure, are shown in Figs. (33) - (39).

In general, the structure of these sections is much coarser than the Western Canada Steel billets and the columnar zone is much larger. Measurements of dendrite arm spacings in billets from Western Canada Steel were not possible because of the finer structure and limited resolution. The dendritic structure in this casting was coarse enough to enable dendrite spacing measurements to be made from the autoradiographs. The value for primary dendrite arm spacing was found to be .022 in.

Fig. (33) is a transverse section from ingot section 1<sup>1</sup>. The notch in the corner is the outline of the meniscus marker. The dendritic structure here can be seen to be quite different to that observed at Western Canada Steel. The columnar dendrites are very regular and extend most of the distance to the centreline of the billet. Only about 1½" of the 6" across the section is equiaxed, and the remainder is columnar. Around the edges of this section a series

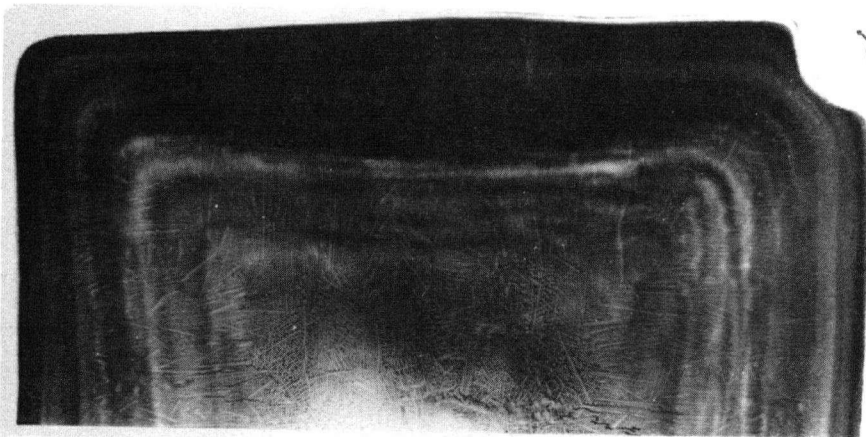


Fig. (33). Transverse section from billet section 1<sup>1</sup>.  
0.75 x

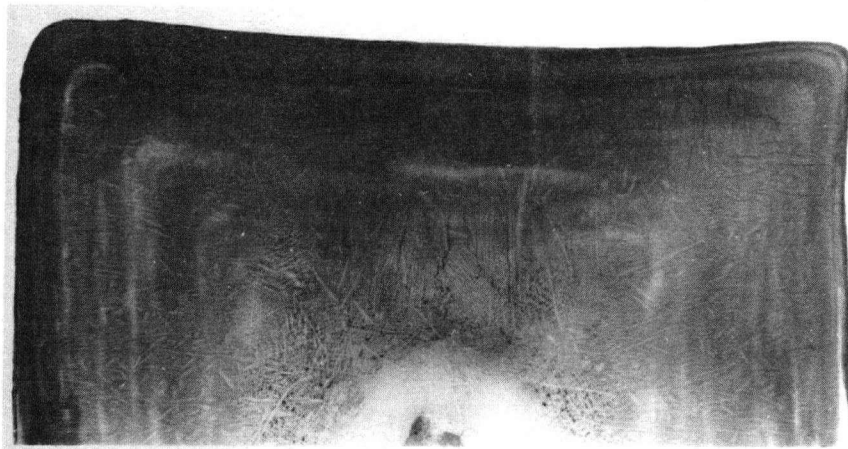


Fig. (34). Transverse section from billet section 2<sup>1</sup>.  
0.75 x

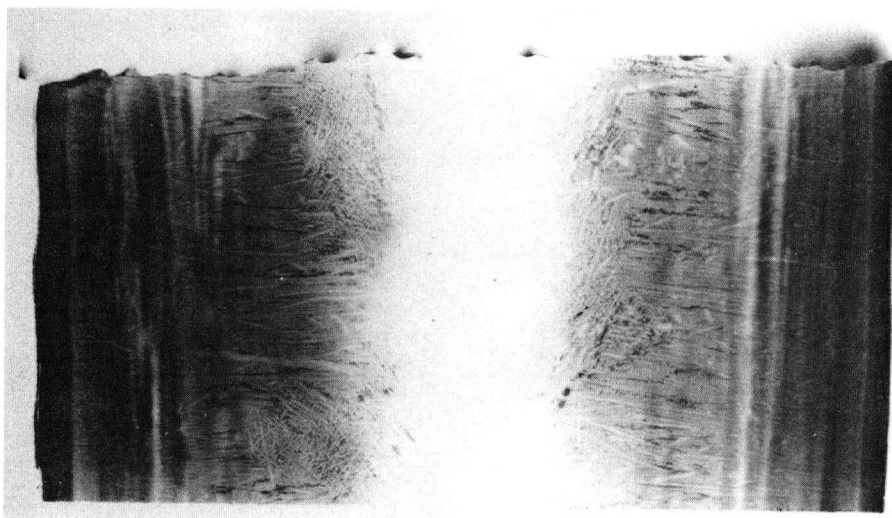


Fig. (35). Longitudinal section from billet section 1<sup>1</sup>.  
0.75 x

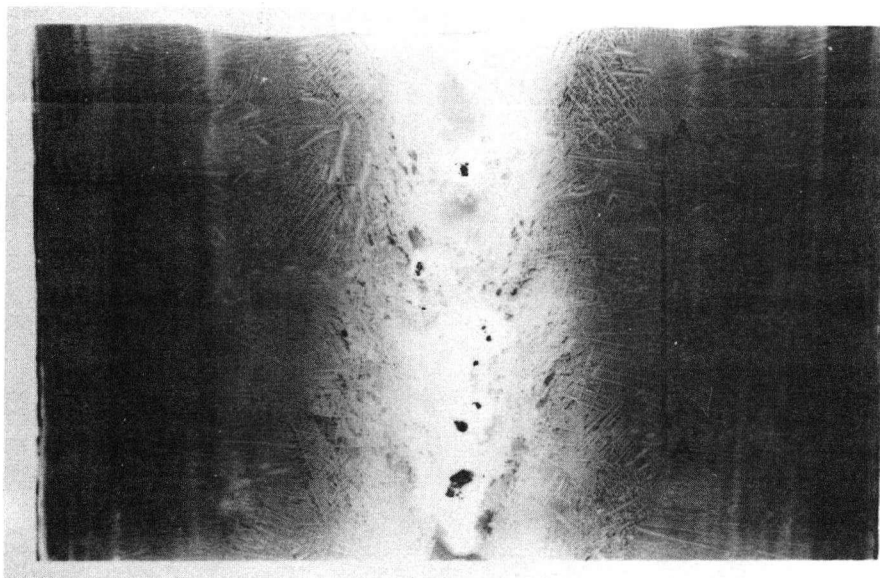


Fig. (36). Longitudinal section from billet section 2<sup>1</sup>.  
0.75 x

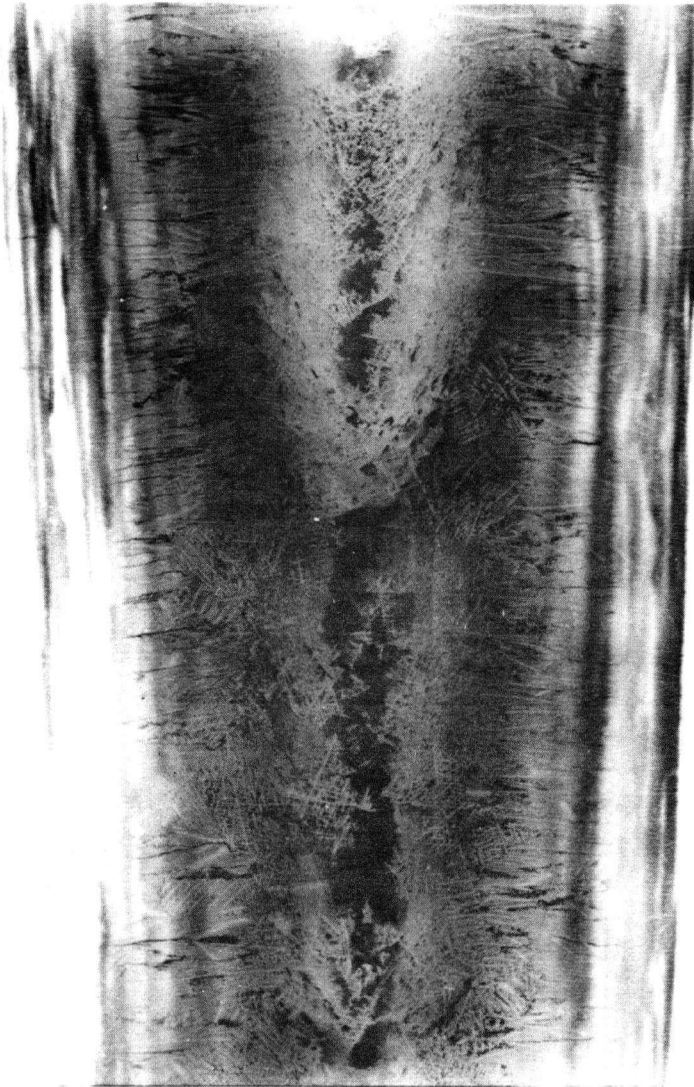


Fig. (37). Longitudinal section from billet section 3.  
0.85 x



Fig. (38). Longitudinal section from billet section 4.  
0.85x

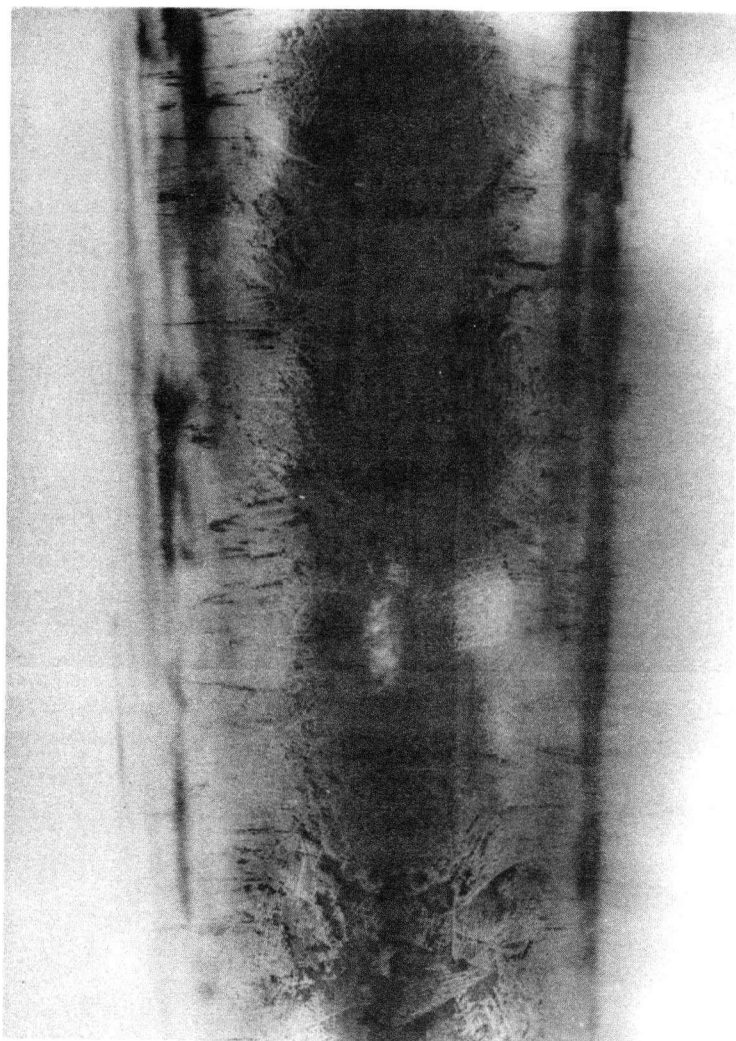


Fig. (39). Longitudinal section from billet section 5.  
0.85x

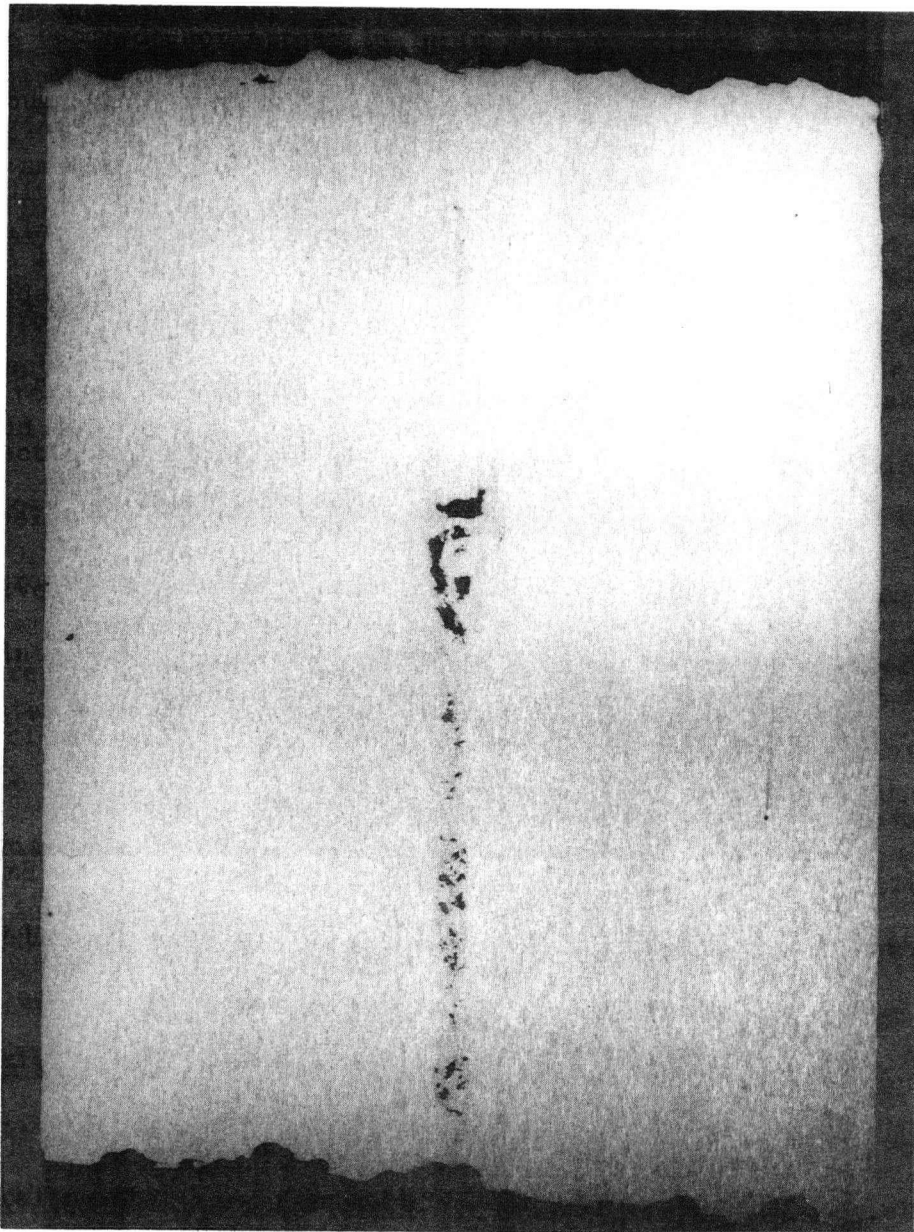


Fig. (40). Surface ground section of a billet from experiment #8.  
(sectioned on the centreline of the billet). 0.75x

of dark bands can be seen running parallel to the ingot faces. The dark bands do not appear to influence the columnar dendrites passing through them. The bands are probably due to liquid containing varying amounts of  $\text{Au}^{198}$  sweeping along the solid-liquid interface. Similar bands were observed in the autoradiographs from the Western Canada Steel billets.

Fig. (34) is similar to Fig. (33) but it is taken from a section approximately 7 in. further down the strand. This section is below the meniscus marker. The dark area near the edge of the autoradiograph where the centreline of the strand is located, is a hole. The origin of this centreline porosity will be discussed in a later section.

Figs. (35) and (36) are longitudinal sections taken from 1<sup>1</sup> and 2<sup>1</sup> respectively. These show quite clearly the transition from the columnar to the equiaxed structure. Near the transition zone and in the columnar zone, a series of transverse cracks are seen, which are present in most of the autoradiographs in this series. The cracks could not be detected on the ground surface of the section, indicating that they formed before solidification was complete and were filled by interdendritic liquid enriched with  $\text{Au}^{198}$ , as with the Western Canada Steel billets. A similar series of cracks are visible in Figs. (33) and (34), but these are closer to the outside walls of the casting.

Figs. (37), (38) and (39) show more of the longitudinal

sections obtained. In these autoradiographs the very large grain size in the equiaxed zone is evident.

A feature that does not show up well in the reproductions of the autoradiographs but is still visible in Fig. (39) is the series of narrow, dark spikes extending out from the interface marked by the  $\text{Au}^{198}$ . The interface here is smooth except for these spikes which project into the columnar dendrite zone on the solid side of the solid-liquid interface.

Figs. (37) and (38) show more of the extensive cracking observed in this steel. In Fig. (37) more cracks can be seen along the interface between the columnar and equiaxed zone, but for these particular cracks the cause is probably the settling of the dendrites in the liquid core during freezing. This settling could cause the dendrites to part from the interface, leaving a space which is filled with Au-rich interdendritic liquid.

Fig. (40) is a photograph of a surface ground section of the steel from the Premier Works. It is included to show the centre-line porosity found in this casting. The porosity does not show up as such on the autoradiographs. In most of the autoradiographs the pores result in stains on the film from the cutting fluid retained in the holes.

### 3.1.9. Experiment #9.

Tracers: W pellet added to centre pool,  $\text{Au}^{198}$  to centre and north pools.

### 3.1.9.1. General Comments.

This experiment, done at Western Canada Steel, was originally intended to be a C1090 steel to be compared to the heat of C1090 done at Stelco. This grade was not available at the time, so a low carbon steel was taken. Both pools had Au<sup>198</sup> added so that the pool profile in the mold would be obtained. The tungsten pellet was dropped in the centre pool only.

### 3.1.9.2. Pool Profile.

Figs. (41) - (43) show the autoradiographs taken from the centre and north strands. The meniscus and solid shell profile are clearly shown and are similar to the results of the previous experiments. However, one feature that was observed before but not as noticeably as in this heat is the marked variations of the shell thickness with position in the mold. This is most prominent in sections 2, 3 and 4 in Fig. (41). The variations in thickness seem to originate near the meniscus, and persist as the shell thickens. The variations are similar on both sides of the billet indicating that they are not due to local effects on the mold surface, but do not correlate across the north and centre strands. Associated with each thin section in the shell is a small indentation on the outer surface of the billet where the billet has separated locally from the mold.

These fluctuations in shell thickness may be an indication

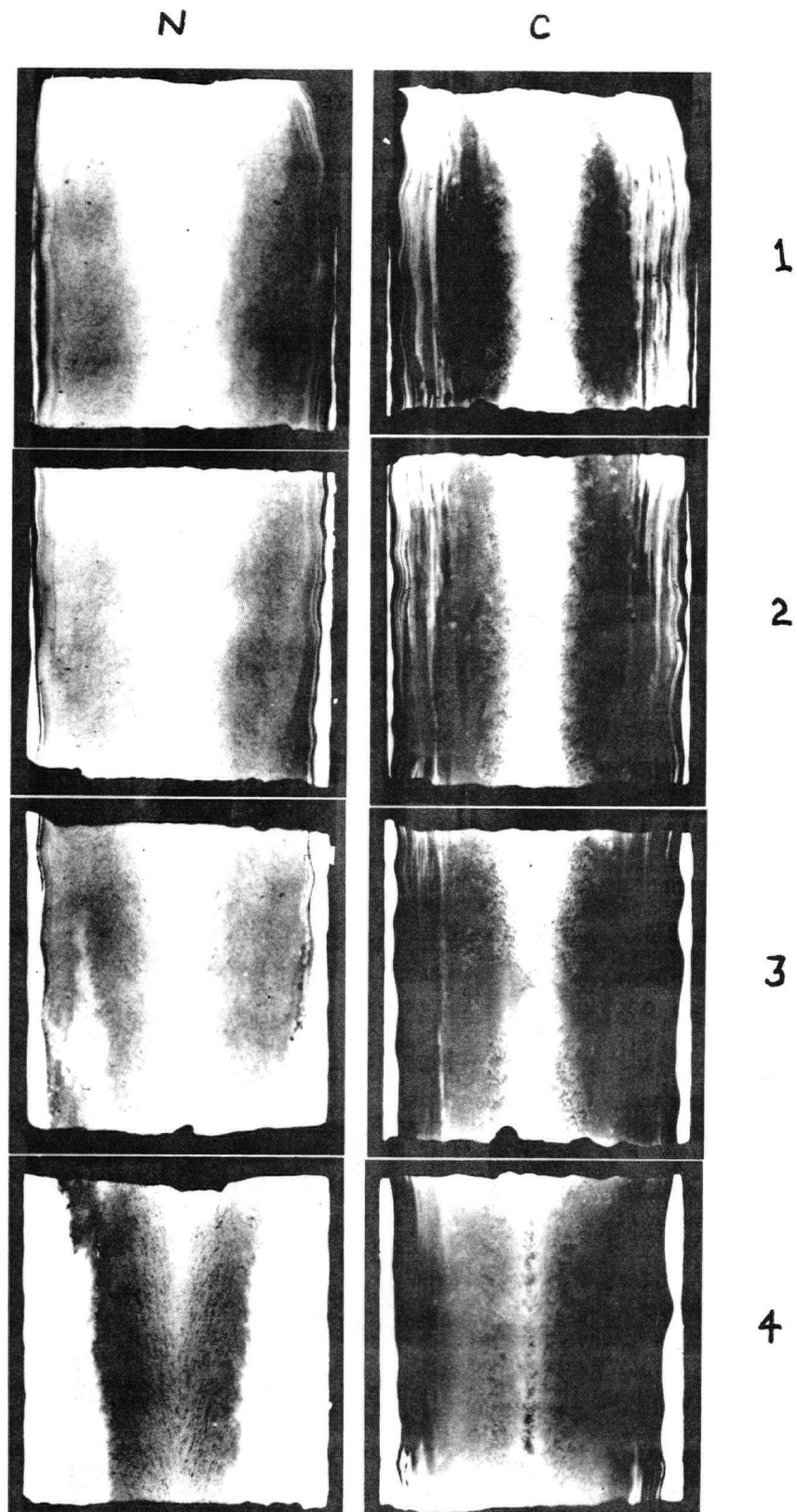


Fig. (41). Composite of autoradiographs from experiment #9, showing the sequence of sections for the north and centre pools.  
0.3 x

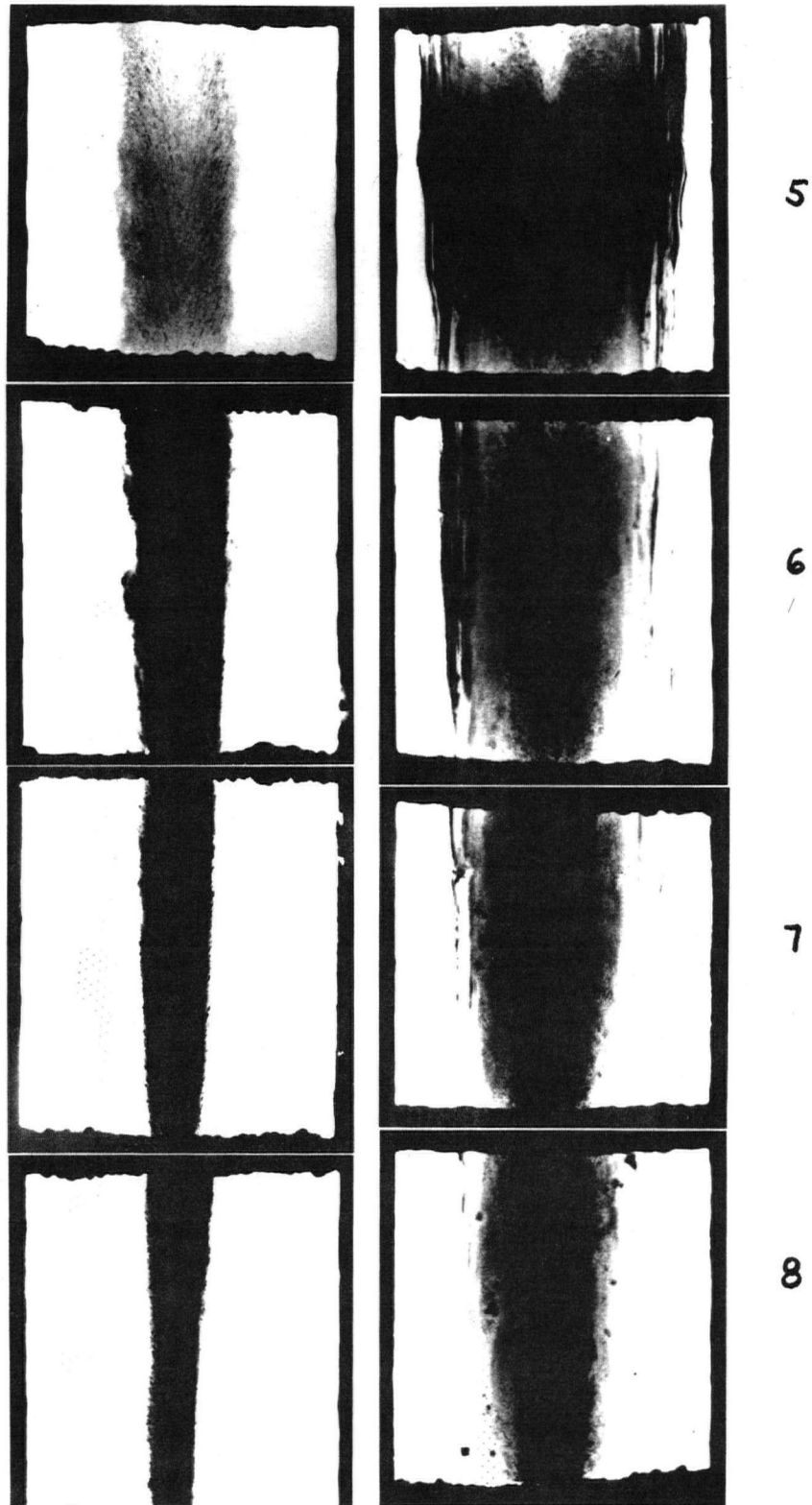


Fig. (42). Composite of autoradiographs from experiment #9. Sections 5-8 follow in sequence from Fig. (41).

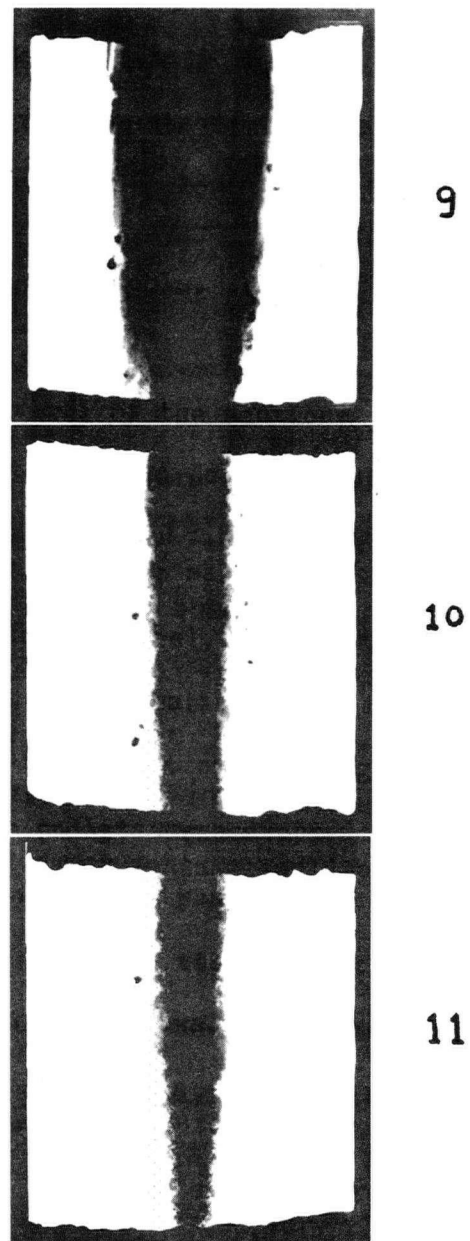


Fig. (43). Composite of autoradiographs from experiment #9. Sections 9-11 follow in sequence from those in Fig. (42).

of the origin of the liquid metal breakouts that occasionally occur for no apparent reason. Although the shell is, on the average, of sufficient thickness to support the ferrostatic head of the liquid core, the thickness of metal at certain parts of the shell may be too thin to support this pressure and a breakout occurs, particularly if interdendritic cracking is present.

### 3.1.10. Experiment #10.

Tracers: Three W pellets added to the centre pool at casting speeds of 40, 55, and 70 in./min.

#### 3.1.10.1. General Comments.

In order to determine the effect of changing the casting speed on pool depth, three tungsten pellets were dropped in the centre pool at three different casting rates. This was done on a single heat. The rates used were 40, 55, and 70 in./min. After each pellet was dropped into the liquid pool, the withdrawal rate was changed and the pool allowed to stabilize at the new speed for 5 min.

#### 3.1.10.2. Pool Depths.

The depths measured are shown in Table 1. At 55 and 70 in./min., the pool depths are almost the same, being <sup>14.5</sup>~~15~~ ft. and <sup>15</sup>~~14.5~~ ft. respectively. At the lower speed of 40 in./min. the depth measured was 5 ft. These values are considered to be good estimates of the

depth because the pellets were found aligned along the longitudinal axis of the billet in each case, indicating that they had not frozen to the walls in the pool.

### 3.1.11. Experiment #11.

Tracers: Au<sup>198</sup> added to north and centre pools. W pellet dropped in centre pool.

#### 3.1.11.1. General Comments.

This last experiment was done to make a comparison between the Weybridge mold used at Western Canada Steel, and the single strand mold used at Stelco. A heat of C1090 steel was used, similar in composition to that used in the Premier Works. Au<sup>198</sup> was added to the north and centre pools; one tungsten pellet was added to the centre pool.

#### 3.1.11.2. Pool Profile.

Fig. (44) is a composite of the autoradiographs of the centre pool. The mixing of the Au<sup>198</sup> was limited to the region of the mold and the profile is very short. The meniscus is located at the top of section 1. The solid liquid interface is well marked to a depth of about 17 in., which is 3 in. less than the effective mold length. In section 3, the sharpness of the interface marked by the tracer breaks down, and in subsequent sections it is not clear. Be-

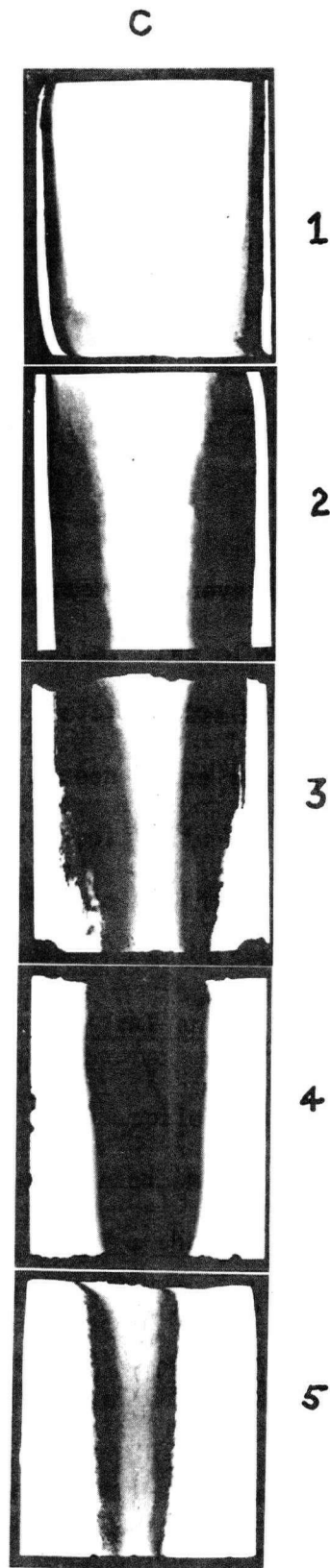


Fig. (44). Composite of autoradiographs from experiment #11. Centre pool only. 0.22 x

ginning at this level in section 3, the profile marked by the tracer narrows more quickly, and tapers down apparently in the same way as in previous experiments. The same dilution in the centre of the sections seen in previous autoradiographs is found in sections 1, 2, and 3.

### 3.1.11.3. Structure.

Autoradiographs of several of the sections were made on Contrast Process Ortho film. Two of these are shown in Fig. (45) and Fig. (46). The dendritic structure of these sections is not clearly resolved, but it can be seen to be much finer than that observed in the C1090 steel from Stelco. This is obvious in Fig. (46) which is taken from the equiaxed zone in the centre of the strand.

### 3.2. Comparison of theoretical and experimental liquid pool profiles.

<sup>13</sup>  
Brimacombe has applied the analytical heat transfer model of Hills and the numerical model of Mizikar to three of the Au<sup>198</sup> tracer experiments. The theoretical and experimental plots of solid shell thickness vs. depth in the mold are shown in Figs. (47) - (49). It can be seen that the profiles correspond very closely in each of the three cases, except near the bottom of the mold, where the strand enters the secondary cooling zone and the rate of heat transfer changes. The Hills<sup>4</sup> model is applicable only in the mold and the part of the Mizikar model used is also restricted to the mold region. The experimental plot in Fig. (49) does not show points up

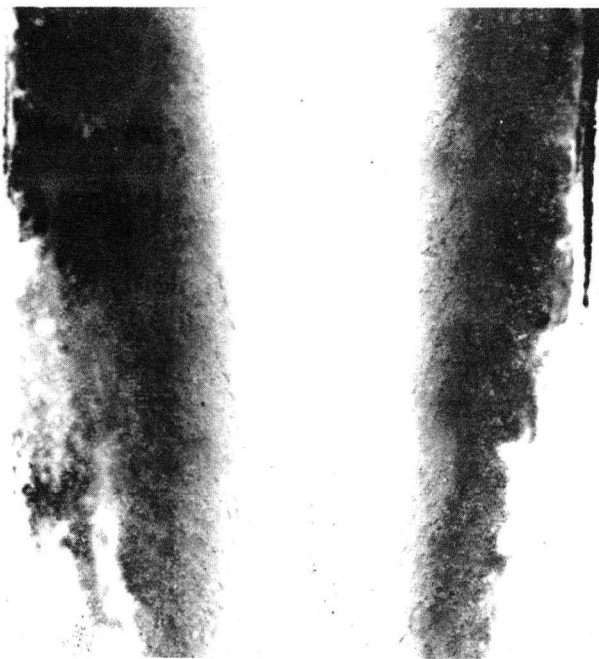


Fig. (45). Longitudinal section from billet section 3 (Fig. 44).  
0.66x

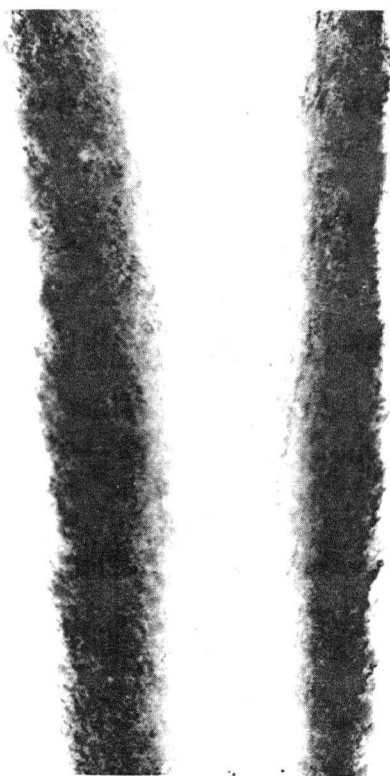


Fig. (46). Longitudinal section from billet section 4 (Fig. 44).  
0.66x

to the meniscus because the autoradiographs of this part of the strand were incomplete.

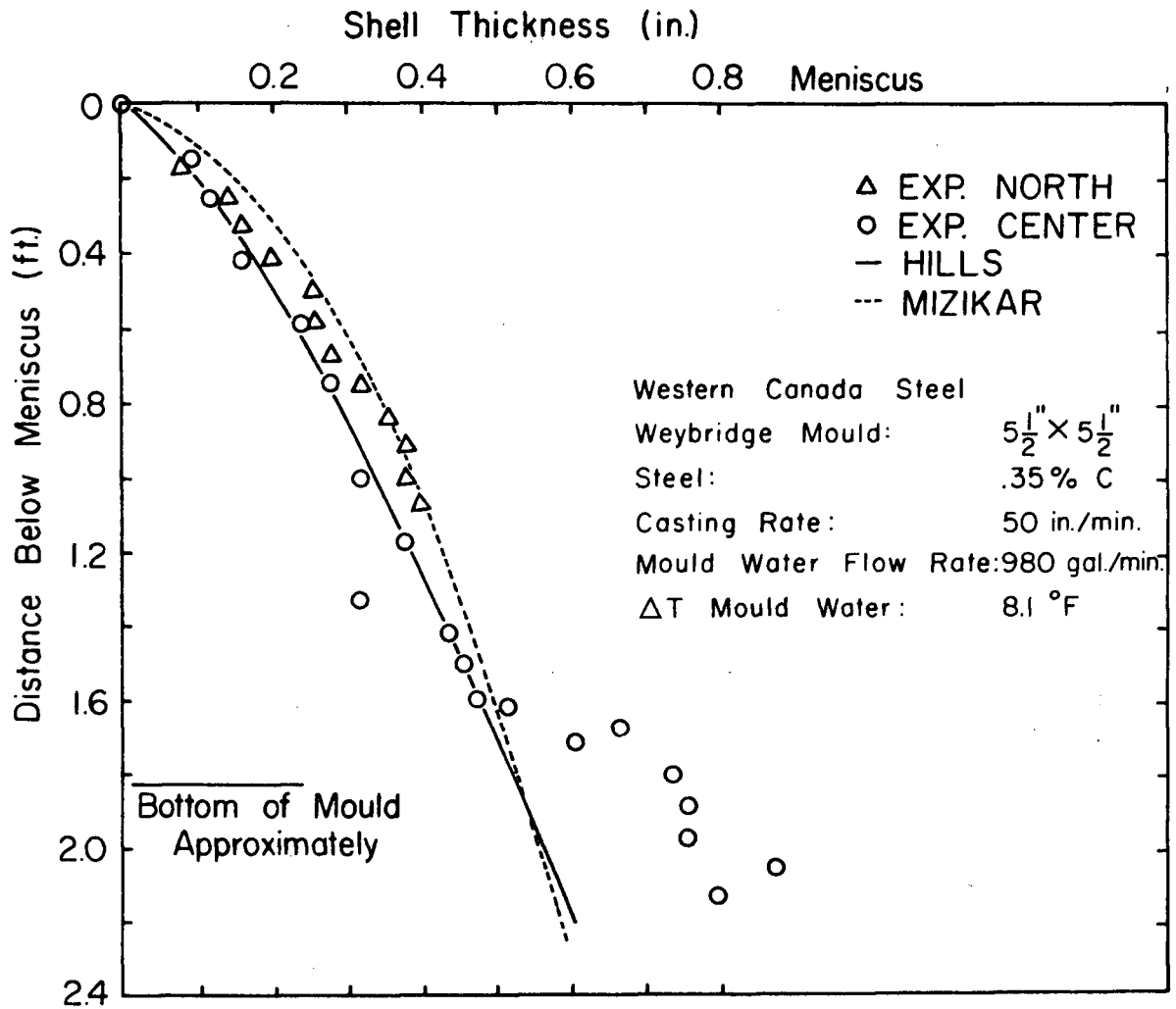


Fig. (47). Theoretical and experimental pool profiles for experiment #3. Theoretical profiles calculated from Hills and Mizikar models.

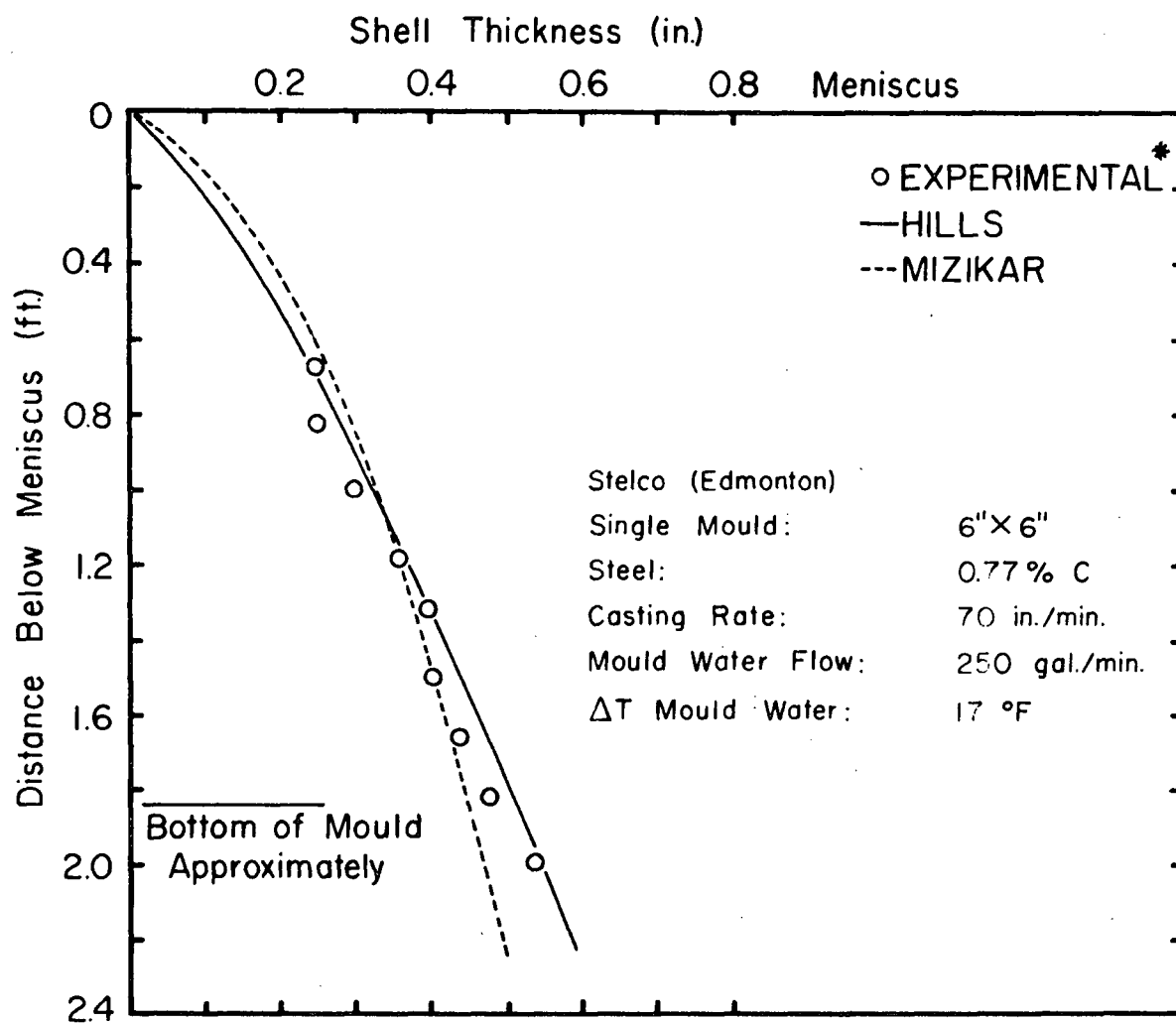


Fig. (48). Theoretical and experimental pool profiles for experiment #8. Theoretical profiles calculated from Hills and Mizikar models.

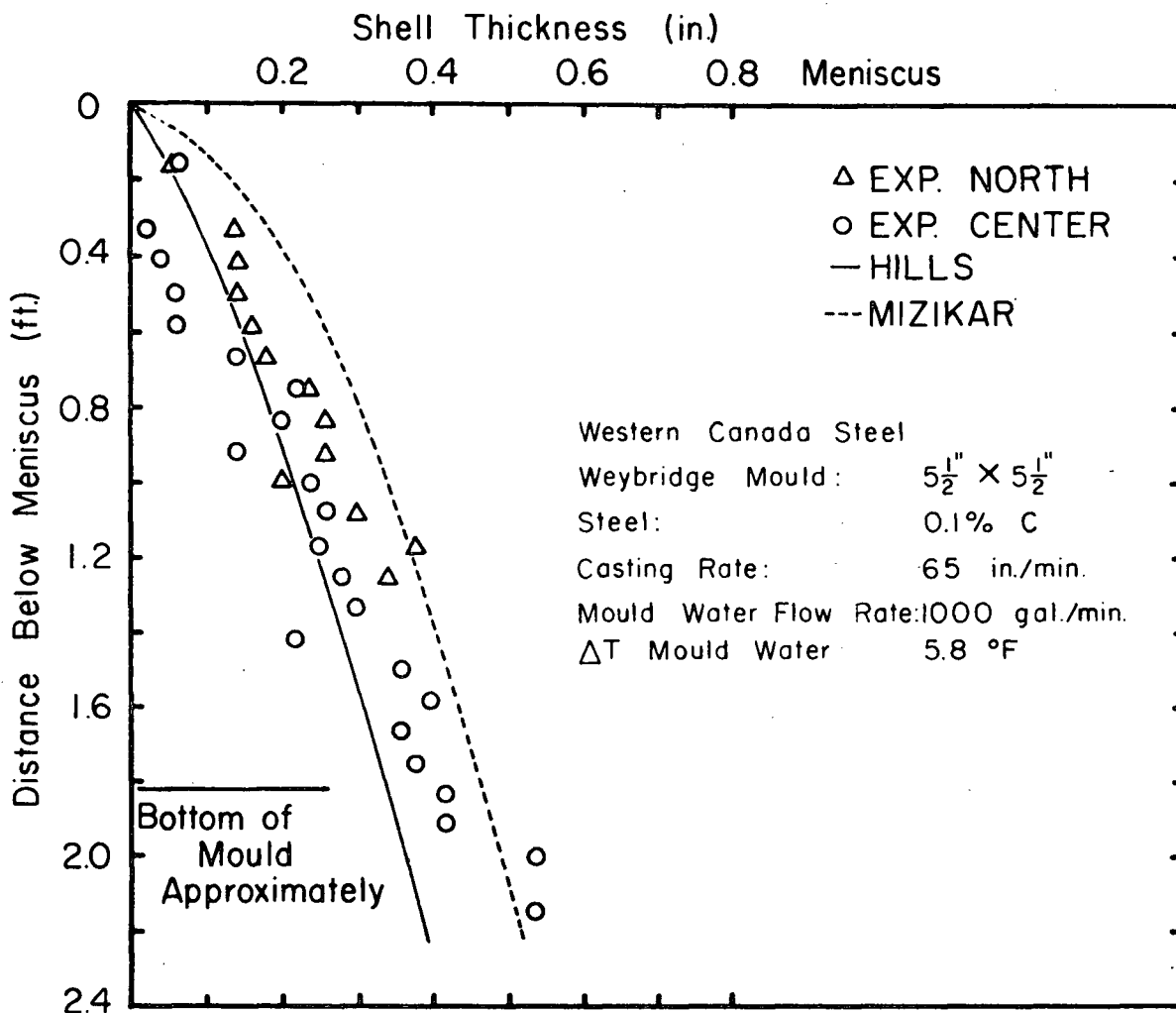


Fig. (49). Theoretical and experimental pool profiles for experiment #9. Theoretical profiles calculated from Hills and Mizikar models.

#### 4. Discussion

##### 4.1. Pool Depths.

##### 4.1.1. From Au<sup>198</sup> profiles.

The experiments in which a tungsten pellet was added with the Au<sup>198</sup> show that the pool depths indicated by the Au<sup>198</sup> profiles clearly cannot be interpreted as being directly related to the actual pool depth. In the upper 2 to 3 ft. of the pool, the gold delineates the solid-liquid interface sharply, outlining the liquid pool. Below the maximum depth of penetration of the inlet stream, the mixing is apparently much slower and less complete, and the tracer does not mix rapidly enough or deep enough to show the bottom of the pool. The maximum depth reached by the Au<sup>198</sup> in any of the experiments was 7 ft. below the meniscus. Kohn,<sup>11</sup> on the other hand, found that the Au<sup>198</sup> in his experiments mixed to a depth of 16 ft. It is not clear why the present experiments differ from the Kohn results.

#### 4.1.2. From tungsten pellets.

The tungsten pellets have given more consistent measurements of the pool depth than the gold profiles, and are considered to be a reliable estimate of the depth. In the normal range of casting speeds, between 50 and 65 in./min., the depths obtained were from 10 ft. to 15 ft. The centre and north pool depths seem to be comparable, and for all practical purposes, are the same.

The depth measurement made with these pellets does not indicate the level at which solidification is complete. The depth measured is the distance that the  $\frac{1}{2}$ " pellet can fall in the liquid, and is therefore limited, at a maximum, to the point where the liquid pool is  $\frac{1}{2}$ " in diameter.

The pellet might be prevented from reaching the maximum depth by obstructions in the pool. The liquid in the lower parts of the pool will certainly contain many dendrites that are forming the equiaxed zone of the casting. However, these dendrites are still free and suspended in the liquid; the heavy tungsten pellet might be expected to fall more or less unobstructed through this material. The solid walls that finally restrict the motion of the pellet are formed of the equiaxed dendrites from the core that have become attached to the advancing solid-liquid interface and are no longer free to move. Some liquid still exists in the interdendritic spaces behind this interface, but as far as the pellet is concerned these

dendrites form solid walls that taper down and eventually prevent the pellet from falling further. A short distance below the final position of the pellet, the liquid core is finally bridged over by the dendrites, and the solid network is continuous across the strand. Liquid still exists in the interdendritic spaces for some distance below the pellet, but the bottom of the pool, as such, is a short distance below the pellet.

The depths obtained in this way from the tungsten pellets are similar to the values reported by Kohn.<sup>11</sup> For example, on a single strand casting machine, casting sections 4.13 in. and 4.72 in. square at ~~22~~<sup>89</sup> in./min., the depths Kohn measured with W<sup>184</sup> pellets were in the range of 16 ft. This can be compared with 15 ft. at 60 in./min. for Western Canada Steel.

The pool depth appears to be relatively insensitive to withdrawal rate at high rates as shown in experiment #10 where the pool depth was measured as ~~12~~<sup>14.5</sup> ft. and ~~12~~<sup>15</sup> ft. for 55 in./min. and 70 in./min. respectively. The depth decreases rapidly at slow withdrawal rates - 5 ft. depth for 45 in./min. This agrees with Kohn's<sup>11</sup> results which showed a 14% decrease in going from 89 in./min. to 68 in./min.

## 4.2. Pool Geometry.

### 4.2.1. Inside the mold.

#### 4.2.1.1. The centre pool.

The profile of the solid shell formed in the mold has been observed in several of the experiments. The solid-liquid interface is marked in this region by a sharp boundary to the areas containing the Au<sup>198</sup> tracer, and it shows the profile from the meniscus to a depth of from 2 to 3 ft. Below this level, the tracer apparently does not show the location of the interface. This is a result of liquid mixing, which is different in these two zones. In the upper 2 or 3 ft., the strong mixing effect of the inlet stream is felt and the dissolved tracer is rapidly mixed and distributed throughout the liquid. Below the depth of the maximum penetration of the inlet stream, the mixing is much less vigorous and the tracer never delineates the solid-liquid interface completely in this zone. The mixing time for the Au<sup>198</sup> in the mold region has been estimated to be approximately 5 sec. This was determined by measuring the distance between the meniscus marker and the meniscus marked by the gold. The distance is from 5 to 6 in. at a withdrawal rate of 60 in./min., so the time delay in mixing is about 5 sec.

#### 4.2.1.2. The north pool.

The solid-liquid interface in the north pool is not delineated as sharply as the centre pool, and the profiles that have been formed are not clear for more than 1 ft. This is a result of the fluid flow and mixing conditions in this pool, which does not have the strong influence of the inlet stream as the centre pool does. However, the small part of the solid shell profile that has been ob-

served indicates that it is similar to the centre pool profile and thickens at the same rate. Other than this short section at the top of the pool, the Au<sup>198</sup> does not give any indication of the actual pool profile. It has been shown that the tracer does not mix completely to the outside of the liquid core, but is confined to a narrow cone down the centre, which is surrounded by liquid containing little or no radioactive material.

#### 4.2.2. Below the mold.

Once the strand is outside the mold, the thermal conditions in the liquid pool change abruptly. The liquid metal stream in the centre pool apparently penetrates only about 1 foot or less below the bottom of the mold, and the liquid mixing below this level is decreased to the extent that the true pool profile cannot be seen in the autoradiographs. In the north pool, where there is no inlet stream, the mixing is even less, and no Au<sup>198</sup> is detected farther than 20 in. below the mold bottom. In the centre pool, the Au<sup>198</sup> penetrates up to 5½ ft. below the mold bottom but this profile is useful mainly in observing the dendritic structure, segregation, and mixing in this region, and not the solid shell profile. Although only a short length of the shell has been delineated below the mold, in experiment #3, this was sufficient to see that the freezing rate increases abruptly when the strand emerges from the mold.

#### 4.2.3. Fluctuations in wall thickness.

In experiment #9, a series of ripples were observed in the solid shell of the steel in the mold. These were apparently formed near the meniscus and persisted as the shell thickened, forming local thin areas in the casting. It was noted that these thin sections showed a correspondence across the width of the strand and were associated with small indentations on the outer surface of the strand. This suggests a possible mechanism for the formation of the fluctuations. If pouring is interrupted for a short time, perhaps only 1 or 2 seconds, the solid formed at the meniscus may be able to freeze more rapidly than if metal was continuously added. If this rim of solid at the meniscus cools more rapidly, it will shrink away slightly from the mold, and the good thermal contact between the shell and mold will then be broken. When pouring is resumed, the fresh metal will then start to form the solid shell again, but the indentation on the outer surface may remain. If it does, the local rate of heat transfer at this part of the strand will be reduced, and the shell here will thicken at a slower rate, producing an indentation in the otherwise smooth solid-liquid interface. This mechanism accounts for the correspondence across the billet section and the indentations on the outer surface. Also, because the throttling of the stream is irregular, the fluctuations produced in this way would be irregular, as observed. It is possible that this effect could be produced by some other disturbance of the liquid in the mold, such as the shaking sometimes caused by the reciprocation mechanism, but such disturbance would form a more regular

series of ripples on the interface.

The occurrence of these fluctuations may explain the liquid metal breakouts that occasionally happen for no apparent reason. When the strand emerges from the mold, the shell may be  $\frac{1}{2}$ " thick and more than sufficient to maintain the ferrostatic head of metal, but if there are thin areas such as those observed, parts of the shell may be only  $\frac{1}{2}$  or  $\frac{1}{3}$  as thick, and are prone to rupture.

#### 4.2.4. Web Depth.

It has been observed that the narrow web joining the centre and outside strands of the Weybridge mold may be open for at least 5 in. below the mold. This web is therefore the thinnest and weakest part of the strand. If it is open for a sufficient distance below the mold, the ferrostatic head may be large enough to force the web apart and bulge out the strand. These bulges, which are peculiar to the Weybridge mold, seem to originate at the web, suggesting that this is, in fact, the mechanism. Fig. (50) shows a photograph of a strand that has had a bulge and a liquid metal breakout. The inner surface of the web is visible from the meniscus to a depth of 6 ft. and does not seem to have been frozen over at any time. The surface is smooth all the way down. When the bulge occurred, the web was parted and the north and centre strands bowed outward, hinging on the web. When this happened, a crack opened up at the corner of the north strand and the liquid drained from the shell, leaving the hollow casting shown in Fig. (50).



Fig. (50). Bulged strand from Western Canada Steel (Weybridge mold), showing the part of the web that has separated.

### 4.3. Liquid Mixing (mixing geometry).

#### 4.3.1. Between pools in the Weybridge mold.

In the first experiment it was demonstrated that liquid mixing takes place between the three liquid pools in the Weybridge mold. This flow is not only from the centre to the outside pools, which are filled from the centre, but occurs in the opposite direction as well. Au<sup>198</sup> tracer added to the north pool was mixed in the centre and south pools, apparently in opposition to the flow of metal through the web from the centre pool. The time of mixing was estimated to be on the order of 5 sec. or less. This was determined by comparing the profiles and the location of the meniscus in each strand. The correspondence between the three strands was within  $\frac{1}{2}$  ft. and at the casting speed 60 in./min. this represents a delay of about 6 sec.

The mixing observed between the north and centre pools was not expected because it was thought that the flow of metal through the web would be in one direction only. However, if the web is open to depths such as those found in experiment #7, the flow between the pools may be much more complex than anticipated and mixing from the north to centre may occur somewhere deeper in the mold region.

#### 4.3.2. In the north pool.

The tracer profiles in the north pool are much shorter than the actual pool depths, as measured by the tungsten pellets. Generally, the tracer is confined to the upper 3 ft. of the pool and

it does not mix completely even in this zone. This was shown in Fig. (18). For a short distance, the solid-liquid interface is marked, but beyond 1 ft. the interface is no longer shown clearly in the autoradiographs, and the tracer profile narrows down to a point. More liquid exists outside this profile as evidenced by the small patches of film exposed in sections 4 and 5 in Fig. (18). Depth measurements with tungsten pellets confirmed that the actual pool depth is at least 10 ft. in this pool, so the liquid extends a minimum of 6 ft. below the bottom of the tracer profile. This leads to the conclusions that mixing in the north pool is limited to the upper 3 ft. of the pool and is probably a result of flow of metal from the centre pool. Most of the mixing was observed in the region where the web is open and this flow is possible, ie. in the mold. Below the mold, all the north pool profiles show only a narrow, short cone and this may be produced by the volume shrinkage of the metal on freezing. As the steel in the north pool freezes, the shrinkage will draw liquid metal down to compensate for the volume change. Then, the tracer in the mold region may gradually be drawn down and form the conical profile observed. Liquid convective flow could not produce, by itself, a sharp point at the bottom of the pool.

#### 4.3.3. In the centre pool.

In the centre pool of the Weybridge mold, the mixing geometry can be considered in two sections: in the mold, and below the mold. In the mold, the inlet stream produces strong forced convection

and rapid mixing. Flow of metal through the web from the outside pool contributes significantly to this mixing and is demonstrated by the fact that it is necessary to add Au<sup>198</sup> to the north pool to get a good profile of the centre pool in the mold. An estimate of the depth of penetration of the inlet stream can be made from the autoradiograph. In the centre pool profiles it was noted that a relatively gold-free zone was present for a distance of about 36 in. below the meniscus. This zone is visible as a light area down the centreline of the sections in Figs. (18) and (19) from experiment #3 and Fig. (30) from experiment #8. It is suggested that this region in which the Au<sup>198</sup> is depleted is formed by the inlet stream. When the Au<sup>198</sup> is added, the concentration in the liquid will be a maximum when it first dissolves and mixes. At this time the profiles in the mold are formed and show the highest concentration of Au at the edge of the profile. After this, the concentration is steadily decreased by the addition of fresh Au-free metal in the inlet stream. The dilution effect will be greatest in the part of the strand where the stream is actually flowing, and this is down the middle of the strand. If the dilution in the centre persists until freezing is complete, and this is possible in view of the limited mixing observed in the lower parts of the pool below the mold, then the position and depth of the inlet stream will be visible in the autoradiographs. This effect holds not only for the Weybridge mold, but for the single strand mold as well, and is seen in Fig. (30). The termination of the stream is marked A. In the Weybridge mold this depth of penetration of the inlet stream is estimated at between 2 and 3 ft., and in the single strand mold the distance estimated is 2 ft.

These depths are comparable to the effective mold length.

Below the mold, or below the depth to which the stream of metal from the tundish flows, the mixing changes. The transition from the upper zone around the inlet stream to the lower zone beneath the stream is gradual. The change begins at the level when the stream terminates. It is here that part of the liquid from the stream begins to move back up the walls of the casting, while the remainder moves downward, mixing in some complex pattern. In Fig. (30), the transition can be observed. Section 5 shows the end of the inlet stream at A. Below this point, the pool profile is still well marked for a distance of 7 to 8 in., but the distribution of  $\text{Au}^{198}$  across the sections is more uniform. About 7 in. below A, the definition of the solid-liquid interface starts to break down. This is considered to reflect the reduction in the amount of mixing and fluid flow taking place in the pool from this level down. Gradually, the interface disappears and eventually all that remains of the tracer profile is a narrow channel down the centreline that does not show the true liquid pool profile. The same observations can be made in Figs. (17), (18), and (19) from experiment #3. Below the point B, corresponding to point A in Fig. (30), the  $\text{Au}^{198}$  mixes only 4 ft. further, and yet the pool extends possibly 7 to 12 ft. deeper. The mixing is, therefore, relatively slow and incomplete in this region below the transition zone.

Fig. (2) is a flow pattern suggested by Kohn,<sup>11</sup> from his observations of the tracer distribution. The geometry he proposes is

similar to that derived in this work, and the dimensions for the strand, pool depths, and inlet stream penetration are also very much the same. However there is no evidence that upward flow occurs in small sections along the solid-liquid interface since this should carry  $\text{Au}^{198}$  from the centre region along the interface, which does not occur.

In experiment #2, a certain characteristic of the mixing in the Weybridge mold was observed. In this particular experiment, the  $\text{Au}^{198}$  was added to the centre pool only and was contained in a steel capsule that was connected to a steel rod with an aluminum rod. The purpose of the aluminum section in the rod was to allow the tracer to be carried down deep in the pool to be dissolved and mixed. But, in the autoradiographs, the profile was found only part way up to the meniscus. The  $\text{Au}^{198}$  mixed back up to the meniscus, but did not show the profile in the mold.

This effect is thought to be caused by the liquid mixing between the centre and north pools and may be explained as follows. When the  $\text{Au}^{198}$  is carried down and dissolved in the stream, some is mixed in the lower parts of the pool, and some is carried back up with the flow of liquid. As this liquid flows back toward the meniscus it marks the solid-liquid interface with  $\text{Au}^{198}$  as it sweeps over it. This produces the greatest blackening of the film at the interface, as is observed in sections 1 to 4 in Fig. (11). As the liquid flows toward the meniscus, it approaches the region in which the web is open, and mixing with the north pool occurs. It has been observed that a considerable flow of metal is passing through the web from the north

pool to the centre pool. In this particular case, this liquid will not contain any Au<sup>198</sup>. If this flow from the north pool passes through the web and then sweeps over the walls of the centre strand, it will, in effect, intercept the flow of Au-containing liquid from below, either diluting the Au in it, or diverting the flow. The result may then be that the solid profile is not marked by the Au<sup>198</sup> and will therefore not show up in the autoradiographs.

#### 4.3.4. Comparison of theoretical and experimental tracer concentration profiles.

In experiment #7, a series of scans were made of the transverse faces of the billets with a scintillation counter. Plots of the counts/min. against distance were shown in Figs. (26) - (29). These curves show general similarities with some of those predicted by Szekely and Stanek.<sup>10</sup> Fig. (51), taken from Szekely and Stanek,<sup>10</sup> shows the predicted distribution of tracer for the case of complete mixing in the liquid. The ordinate is the dimensionless tracer concentration and the abscissa the dimensionless distance from the billet centreline, ie.  $x = 0$  corresponds to the billet centreline and  $x = 1$  is the outer surface of the billet. The profiles at  $t = 2, 3,$  and  $4$  may be compared to the plots in Figs. (26) - (29). At the boundary of the tracer in the experimental curves, the concentration rises steeply from zero to a maximum and then decreases again toward the centre. The curves from Figs. (26) - (29) behave in a similar way. However, the autoradiographs indicate that the concentration

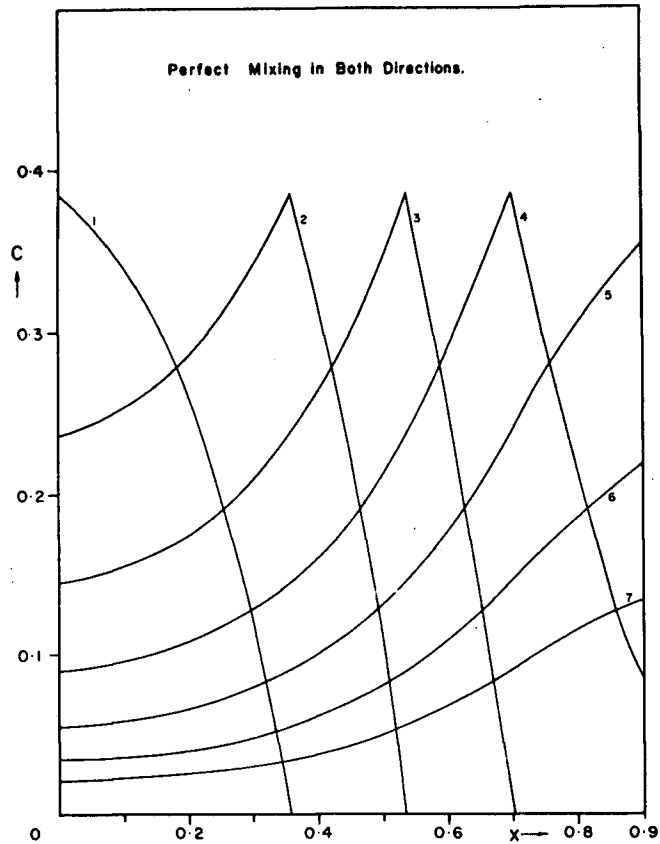


Fig. (51). Predicted tracer distribution in the cast billet for the case of complete mixing in the liquid pool, from Szekely and Stanek.<sup>10</sup>  $x$  = dimensionless horizontal coordinate ( $x = 0$  corresponds to billet centreline and  $x = 1$  corresponds to outer surface),  $c$  = dimensionless tracer concentration,  $t$  = dimensionless time. Concentration profiles are shown for various times at point at which solidification is complete.

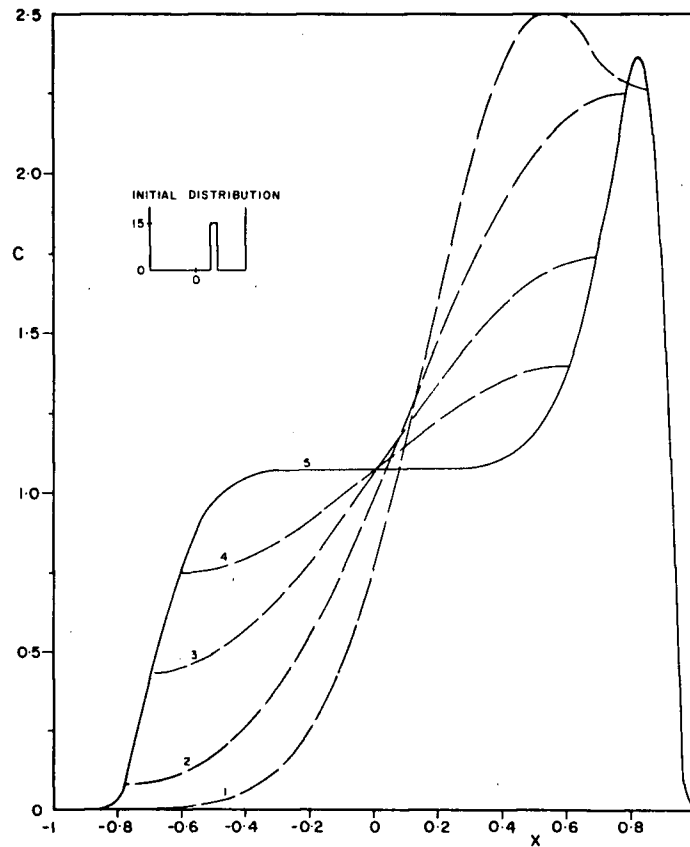


Fig. (52). Predicted tracer distribution in the solidified billet for the case of eddy diffusion, from Szekely and Stanek.<sup>10</sup> The continuous line shows the final distribution.  $c$  = dimensionless concentration,  $x$  = dimensionless horizontal coordinate ( $x = 0$  is the billet centreline and  $x = 1$  is the outer surface).

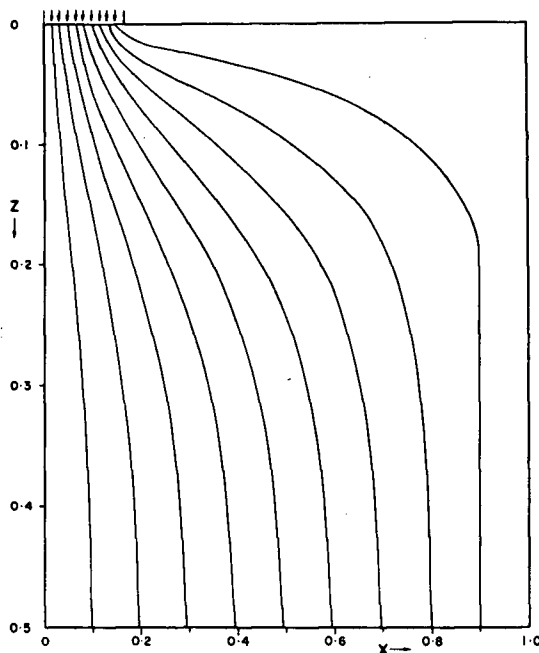


Fig. (53). Streamlines in the liquid pool under conditions of potential flow, from Szekely and Stanek.<sup>10</sup>  $Z$  = dimensionless vertical coordinate below meniscus.  $x$  = dimensionless horizontal coordinate from the centreline.

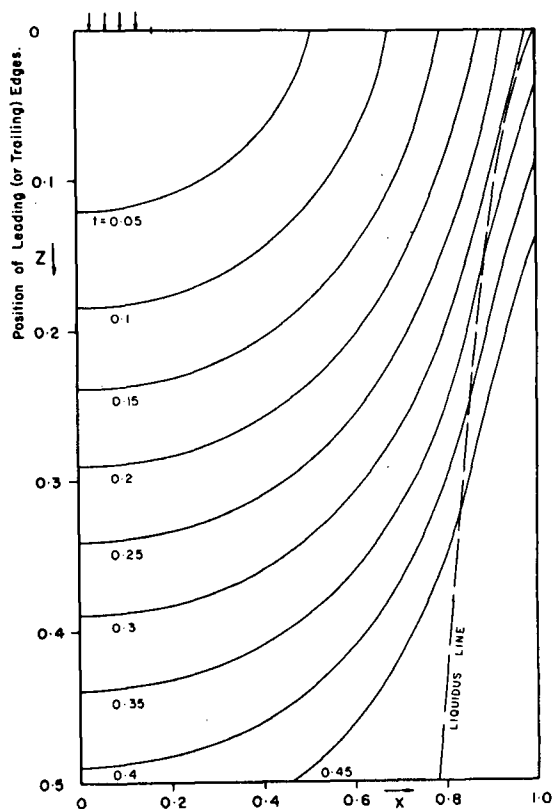


Fig. (54). Tracer distribution in the liquid under conditions of potential flow, from Szekely and Stanek.<sup>10</sup> Pattern shows the leading and/or trailing edge as a function of time.

of tracer is a maximum right at the boundary, and the steep initial rise of the experimental curve can be attributed to the slit geometry. A 1/16" slit was used, and this is wide enough for the detector to subtend an angle of several degrees, which is enough to show a less sharply defined interface on the plots. The steepness of the initial rise is then a function of the width of the slit, and does not show the actual tracer distribution right at the boundary.

One of Szekely's<sup>10</sup> predicted profiles from the eddy diffusion model also shows some similarities with the curves from the scans. Fig. (52) shows Szekely's<sup>10</sup> predicted profile for the case of a tracer added at a point between the centreline and the edge of the billet. The right hand side of the predicted curve is much like the corresponding half of the experimental curves, but again, the experimental curves are affected by the slit geometry and do not show the actual concentration profile near the boundary.

The condition of potential flow assumed by Szekely and Stanek<sup>10</sup> does not, in general, appear applicable to the fluid flow considered here, but it was found that the north pool of the Weybridge mold may, in fact, approach this condition of flow. This pool does not have a vertical inlet stream and the only apparent driving force for mixing is the flow through the web and the volume shrinkage on freezing. The profiles obtained from the north pool in most cases had a relatively sharp boundary to the regions containing tracer, and there was little or no mixing outside the boundary. Fig. (7) is a good example of this. The tracer profiles do not outline the pool

and the observed profile is similar to what may be expected for conditions of potential flow. Figs. (53) and (54), taken from Szekely and Stanek<sup>10</sup> show, respectively, the streamlines and tracer profiles in the liquid for potential flow.

#### 4.4. Structure.

The dendritic structure of the billets autoradiographed shows three sections: (i) an unresolved structural area near the billet surface. (ii) a columnar zone that extends inward nearly horizontally. (iii) a central equiaxed zone.

##### 4.4.1. Columnar zone.

###### 4.4.1.1. Weybridge mold.

The columnar dendrite structure in the Weybridge mold billets is very short. The columnar dendrites extend only about <sup>1.4</sup>~~1.5~~ in. in from the billet surface out of a total of 2.75 in. from the surface to the centreline (ie. 50% of the distance). The remainder of the section is equiaxed.

###### 4.4.1.2. Single strand mold (Stelco).

The billets cast in the single strand machine showed a structure which differed from that in the Weybridge mold. The columnar zone is much longer and extends for 2 in. (or 67% of the

distance) from the billet surface. It is too fine to resolve near the surface, at distances comparable to the columnar zone in the Western Canada Steel billets, but near the end of the columnar zone the dendrites become very coarse and measurements of primary dendrite arm spacings were made along AA<sup>1</sup> in Fig. (36). The value obtained for the average primary dendrite arm spacing was .022 in.

The steel used in the tracer work on the single strand machine was a C1090 grade and it was thought that the high carbon concentration might account for the different structure, as compared to Western Canada Steel billet structures. However the experiment done on a C1090 steel at Western Canada Steel showed that this was not the case. The billet structure at Western Canada Steel for the high carbon content was similar to that observed in low and medium carbon steels. This was true not only for the columnar zone but the equiaxed zone as well.

The autoradiographs in Fig. (38) were observed to show a series of dark spikes projecting from the solid-liquid interface into the columnar dendrites. It is suggested that this indicates the flow of liquid back into grain boundary cusps at the solid-liquid interface. This may be caused by the mechanisms that produce the classical inverse segregation, ie. the volume shrinkage of the metal on freezing and density differences in the liquid. This effect was observed only in this one experiment in which the carbon content was high. The most probable reason for this is that the structure was coarser, and

the high carbon concentration increased the segregation and the spikes were therefore larger and resolveable in the autoradiographs.

#### 4.4.2. Equiaxed zone.

##### 4.4.2.1. Weybridge mold.

In the Weybridge mold, the equiaxed zone constituted most of the cross section of the billets, the columnar zone being very short. The equiaxed zone accounts for approximately 4 in. of the  $5\frac{1}{2}$  in. of the width of the billets. The dendrites in this region are very fine and are just resolved in the autoradiographs, such as Fig. (45).

##### 4.4.2.2. Single strand mold (Stelco).

In the billets from the single strand mold, the equiaxed zone is much narrower than in the Western Canada Steel billets. The zone is, on the average, only about  $1\frac{1}{2}$  to 2" wide in a 6 in. square billet. The dendrites are large by comparison to those in the equiaxed zone in the Western Canada Steel billets.

##### 4.4.3. Origin of the equiaxed zone.

The equiaxed dendrites in the continuously cast billets may originate in several ways: (1) by nucleation in the constitutionally supercooled liquid ahead of the interface; (2) by accumulation of nuclei that have formed at the surface of the pool in the mold, ie. Southin's mechanism; and (3) by remelting of dendrite tips in the

columnar zone, producing new nuclei in the liquid. Considering the structure observed in the single strand and Weybridge molds, the third mechanism is the most attractive because it incorporates the basic difference found in the two molds that may cause the difference in structures. This difference is in the fluid flow. In the single strand mold, only  $1/3$  as much metal is poured into the pot as in the Weybridge mold, and as a result, the inlet stream will be less powerful and the fluid flow less vigorous. Consequently, the remelting of dendrites in the single strand may be less extensive than in the Weybridge mold, and as a result of this, fewer nuclei are produced. If there are fewer nuclei, they will be able to grow larger and produce a coarse equiaxed dendritic structure. If many nuclei are formed, as is suggested occurs in the Weybridge mold, the nuclei will not be able to grow as large, and the equiaxed dendrites will be finer. Also, if there are many nuclei, they may rapidly provide a barrier to the growth of the columnar dendrites, and so the equiaxed zone will in this case be wider and the columnar zone narrower. These results are observed in the autoradiographs.

The coarseness of the single strand billets and the relatively fine structure of the Western Canada Steel billets were originally suspected to be at least partly a result of compositional differences, but the C1090 steel from Western Canada Steel showed the same fine dendritic structure as in the lower carbon steels.

#### 4.4.4. V-segregation pattern.

In the autoradiographs and etched surfaces of the billets, a V-shaped pattern was observed. The autoradiographs revealed that the pattern was composition of pockets of interdendritic material segregated during freezing of the equiaxed zone. It is suggested that the V-shape of the pattern is caused by the settling of the liquid and dendrites in the centre of the strand. The settling may be caused by the shrinkage that occurs on freezing. As the "mush" of dendrites settles down, the greatest movement will be at the centre, where the largest fraction of liquid will exist.

#### 4.4.5. Porosity.

In all of the continuously cast steel examined, a certain amount of centreline porosity was found. In the Western Canada Steel billets, it was generally small and sometimes was not seen until stains were produced on the autoradiographic films. In the Stelco billets the porosity was quite large. The relative sizes of the porosity is considered to be a reflection of the grain size in the respective castings. In the Western Canada Steel billets, the equiaxed grain size was small, so interdendritic spaces were small, and the voids formed by shrinkage must also be small. In the Stelco billets, the equiaxed grains were very large, and as a result, the porosity was also found to be large.

#### 4.4.6. Cracking.

It has been determined that the dark lines observed in certain sections of the autoradiographs are cracks. These cracks existed only during the solidification process, and as they opened up they are filled with Au-rich interdendritic liquid. This produces the lines on the autoradiographs that show the existence of the cracks. Ultrasonic testing and dye-check reveals no evidence of the existence of the cracks in the final casting.

In the Stelco casting, the cracks were observed in the columnar dendrites, running between the primary stalks. Some were also seen between the columnar and equiaxed zones. In the Western Canada Steel billets, the cracks were all in the equiaxed zone. The cause of these cracks is not known. They might be due to stresses in the billet introduced by the water chills below the mold.

#### 4.5. Theoretical and experimental pool profiles.

It was found that for the mold region the solid shell profiles predicted by the Hills and Mizikar heat transfer models corresponded very closely to the experimentally determined profiles. In general, the experimental profiles lie in between the two predicted profiles. The experimental profiles, and experiment #9 in particular, show some scatter which is attributed to local variations in shell thickness.

## SUGGESTED FUTURE WORK

1. In order to obtain a better evaluation of the theoretical heat transfer models, more Au<sup>198</sup> tracer experiments should be carried out. Only three experimental profiles have been used in this work, and this is not sufficient for a reliable comparison with the theoretical profiles.
2. Using the tungsten pellets, it should be possible to determine more quantitatively the effects of the process variables, such as casting speed and pouring temperature, on the liquid pool depth.
3. Measurements of surface temperatures of the strand in the secondary cooling zone could be used to calculate heat transfer and solidification rates in this region.
4. Tracer experiments could be carried out on several continuous casting machines. The Weybridge mold used in ten of the eleven experiments done is not typical, and data for other types of molds would be useful.

## REFERENCES

1. H. Krainer and B. Tarmann: Metal Treatment and Drop Forging 17 (1950) p. 3.
2. J. Savage and W.H. Pritchard: JISI 178 (1954) p. 269.
3. J. Savage: JISI 200 (1962) p. 41.
4. A.W.D. Hills: JISI 203 (1965) p. 18.
5. R.D. Pehlke: Metals Eng. Quart. 4 no. 2 (1964) p. 42.
6. T.Z. Fahidy: JISI 207 (1969) p. 1373.
7. E.A. Mizikar: Trans. of Met. Soc. of AIME 239 (1967) p. 1747.
8. J.W. Donaldson and M. Hess: "Continuous Processing and Process Control", Proceedings of a Symposium sponsored by the Met. Soc. of AIME, Philadelphia, Dec. 5-8, 1966, p. 299.
9. J.J. Gautier et al: JISI 208 (1970) p. 1053.
10. J. Szekely and V. Stanek: Metallurgical Transactions 1 (1970) p. 119.
11. J. Arnoult, A. Kohn, J.P. Plumensi: Revue de Metallurgie 66 (1969) p. 585.
12. J. Fodor and C. Varga: International Conference on the Peaceful Uses of Atomic Energy (1964).
13. J.K. Brimacombe: University of British Columbia, private communication (1971).